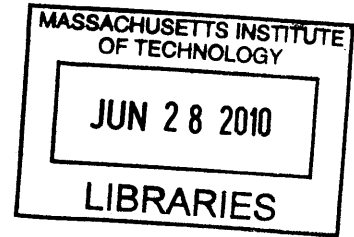


**Transit Timing with Fast Cameras on Large
Telescopes**

by

Elisabeth Rose Adams



Submitted to the Department of Earth, Atmospheric, and Planetary
Sciences

in partial fulfillment of the requirements for the degree of

Doctor of Philosophy

ARCHIVES

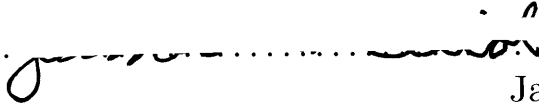
at the

MASSACHUSETTS INSTITUTE OF TECHNOLOGY

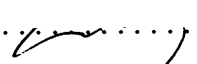
June 2010

© Massachusetts Institute of Technology 2010. All rights reserved.

Author
Department of Earth, Atmospheric, and Planetary Sciences
April 28, 2010

Certified by

James L. Elliot
Professor of Planetary Astronomy and Physics
Thesis Supervisor

Certified by
Sara Seager
Ellen Swallow Richards Professor of Planetary Science
Thesis Supervisor

Accepted by

Maria Zuber
E. A. Griswold Professor of Geophysics and Head of the Department
of Earth, Atmospheric, and Planetary Sciences

Transit Timing with Fast Cameras on Large Telescopes

by

Elisabeth Rose Adams

Submitted to the Department of Earth, Atmospheric, and Planetary Sciences
on April 28, 2010, in partial fulfillment of the
requirements for the degree of
Doctor of Philosophy

Abstract

Timing and system parameters were measured for seven transiting exoplanets: OGLE-TR-56b (11 transits), OGLE-TR-132b (7), OGLE-TR-111b (6), OGLE-TR-113b (6), CoRoT-2b (3), OGLE-TR-10b (3), and XO-2b (2). Ground-based observations of 38 transits were made using three new frame-transfer instruments: POETS and MagIC-e2v on the 6.5m Magellan telescopes, and MORIS on the 3m IRTF. For each planet, all transit light curves including available literature data were jointly fit using a Monte Carlo Markov Chain method, providing accurate new values for the planetary radius and other parameters. Transit ephemerides have been updated and transit mid-times have been investigated for potential transit timing variations (TTVs) caused by other planets or moons. Our transit midtime analysis contradicts a claimed TTV for OGLE-TR-111b (Díaz et al., 2008), finding no evidence in data from 2005-2009. The radius, $1.019 \pm 0.026 R_J$, is intermediate to previous values (Winn et al., 2007; Díaz et al., 2008). We confirm the radius of OGLE-TR-56b, which previously had only one light curve (Pont et al., 2007), as $1.332 \pm 0.063 R_J$, but find a longer duration by 15 minutes, while the orbital period, 1.2119094 ± 0.0000024 , is unchanged. Times for OGLE-TR-10b are consistent with the ephemeris of Holman et al. (2007), though two literature transits show large deviations (586 ± 86 s; Pont et al., 2007) and (-612 ± 26 s; Bentley et al., 2009). Times for four planets (OGLE-TR-113b, OGLE-TR-132b, CoRoT-2b, and XO-2b), with midtime errors as small as 9 s, agree with published ephemerides and show no signs of TTVs. The orbital period of OGLE-TR-113b derived from new data from 2007-2009, however, is shorter by 0.24 ± 0.12 s compared to the period calculated for literature data from 2002 and 2005. If confirmed, this would be the first detection of a change in the orbital period of an exoplanet, which could be caused by orbital decay as the planet falls onto its star.

Thesis Supervisor: James L. Elliot

Title: Professor of Planetary Astronomy and Physics

Thesis Supervisor: Sara Seager

Title: Ellen Swallow Richards Professor of Planetary Science

Acknowledgments

I would like to thank my advisor, Jim Elliot, for taking a chance on a new project, even though neither of us quite knew where it was going to lead at the time. His tireless commitment to properly acquiring and analyzing good data, and his dogged perseverance in the face of obstacles, have taught me much about being a scientist. I would also like to thank my advisor, Sara Seager, for teaching to me to be ruthless with my own ideas and to make sure I don't lose sight of the big picture.

My co-workers and collaborators have been invaluable. I would particularly like to thank Mercedes Lopez-Morales for all that observing and pushing and shoving around of data. Thanks also go to Dave Osip, for keeping me from breaking the instruments at Magellan, and to the other astronomers and support staff that I met at Las Campanas, too numerous to name here, for equal parts science and camaraderie. Amanda Gulbis has been both a mentor and a friend, and I thank her for advice on all areas of research and life. A big thanks to Carlos Zuluaga, for always bringing dark chocolate when he needs a big favor, and to Mike Person, for being unfailingly helpful and for keeping the group from descending into chaos. Thanks to Matt Lockhart for those nights spent observing, not all of which were plagued by clouds or telescope failures. I would also like to thank past members of the group, Susan (Kern) Benecchi and Julie Kane Akhter; it wouldn't have been the same without you.

My fellow graduate students and partners in crime deserve special thanks, particularly Cristina Thomas, who got there first, and Jenny Meyer, who will follow soon. Thank you both for all the great discussions about science and distractions from the same (perhaps not in that order), and for making the fourth floor an awesome place to work. Thanks also are due to Andy Lutomirski, Kaisey Mandel, Leo Stein, Angela Zalucha, Amanda Zangari, and everyone else I'm forgetting, for making sure my life outside of work was filled with good food, books, trips, conversation, and fun.

I would like to thank my family for their support, even if they didn't always understand why. I particularly thank my brother, Chris Adams, for all the many years of big brotherly advice, which have been (mostly) appreciated.

Finally, I would like to thank the love of my life, Jonathan Foster, for everything. His love, humor, patience, and support have meant the world to me, and there is no one else with whom I would rather explore space and time and life. It is to him that I dedicate this thesis.

Contents

1	Introduction	15
1.1	Exoplanets: a brief history	15
1.1.1	How we detect exoplanets, and what we can learn	16
1.2	On the timing of transits	20
1.3	Our observational project	21
1.3.1	Improved radii	22
1.3.2	Transit timing	22
1.3.3	Targets for observation	22
1.3.4	Choice of instrument	24
1.3.5	Other instruments	27
1.4	Outline	27
2	Claimed TTV for OGLE-TR-111b Not Confirmed with Six New Transits	29
2.1	Abstract	29
2.2	Introduction	30
2.3	Observations and data analysis	33
2.3.1	Data analysis	34
2.4	Transit fitting results	39
2.4.1	Model	39
2.4.2	Light curve fits	40
2.4.3	Systematic errors and correlated noise	42
2.5	Results	46

2.5.1	Timing	46
2.5.2	Parameter variation	49
2.5.3	Limits on perturber mass	52
2.6	Conclusions	53
2.7	Acknowledgements	55
3	Eleven New Transits of OGLE-TR-56b	57
3.1	Abstract	57
3.2	Introduction	58
3.3	Observations and data analysis	60
3.3.1	Data analysis	63
3.4	Transit fitting results	69
3.4.1	Model	69
3.4.2	Light curve fits	70
3.4.3	Discrepancy in shape of 20060720 transit	73
3.4.4	Timing	76
3.4.5	Limits on perturber mass	79
3.5	Conclusions	80
3.6	Acknowledgements	81
4	Bright, Active Stars and High-Precision Transits: OGLE-TR-113b and CoRoT-2b	83
4.1	Introduction	83
4.2	OGLE-TR-113b	84
4.2.1	Observations	86
4.3	Transit fitting results	89
4.3.1	Model and light curve fits	89
4.3.2	Stellar variability	94
4.3.3	Systematic errors and correlated noise	94
4.3.4	Timing	95
4.3.5	Limits on perturber mass	97

4.4	CoRoT-2b	100
4.4.1	Observations	100
4.4.2	Model and light curve fits	103
4.4.3	Timing	105
4.5	Conclusions	107
4.6	Acknowledgements	108
5	Other Planets: OGLE-TR-132b, OGLE-TR-10b, XO-2b	109
5.1	Additional planets	109
5.2	OGLE-TR-132b	109
5.2.1	Observations	110
5.2.2	Model and light curve fits	114
5.2.3	Timing	116
5.3	OGLE-TR-10b	120
5.3.1	Observations	122
5.3.2	Model and light curve fits	125
5.4	XO-2b	132
5.4.1	Observations	132
5.4.2	Model and light curve fits	135
5.4.3	Timing	137
5.5	Conclusions	139
5.6	Acknowledgements	140
6	Conclusions	141
6.1	Improved system parameters	142
6.2	Transit timing	143
6.2.1	Placing limits on perturbers	143
6.2.2	Orbital decay	144
6.3	Anomalies and future work	146

A	Observation Details	149
A.1	Finder charts	149
A.2	All full or partial transits observed	155
A.3	Gallery of regrettable data	158
B	Actual vs. predicted precision	161
B.1	Predicted precision	161
B.1.1	Photometric error	161
B.1.2	Errors on transit parameters	162
B.2	Actual achieved precision	164
C	Accurate timing	165
C.1	Accurate UTC times	165
C.2	BJD and HJD	165
C.3	Converting UTC to BJD	166

List of Figures

2-1	Eleven transits of OGLE-TR-111b	38
2-2	Parameter distributions for joint fit to eleven transits of OGLE-TR-111b	43
2-3	Observed minus calculated midtimes for OGLE-TR-111b	48
2-4	Parameter variation of individual transits of OGLE-TR-111b	50
2-5	Upper mass limit on companions to OGLE-TR-111b	53
3-1	Twelve transits of OGLE-TR-56b (full data with residuals)	64
3-2	Twelve transits of OGLE-TR-56b (data binned to two minutes)	66
3-3	Parameter distributions for joint fit to twelve transits of OGLE-TR-56b	71
3-4	Parameter variation of individual transits of OGLE-TR-56b	73
3-5	Transit of OGLE-TR-56b on 20060720	75
3-6	Observed minus calculated midtimes for OGLE-TR-56b.	78
3-7	Upper mass limit on companions to OGLE-TR-56b.	80
4-1	Nine transits of OGLE-TR-113b.	85
4-2	Long-term variability of OGLE-TR-113b	89
4-3	Potential starspot on transit of OGLE-TR-113b on 20080514	90
4-4	Parameter distributions for joint fit to nine transits of OGLE-TR-113b	91
4-5	Parameter variation of individual transits of OGLE-TR-113b	92
4-6	Observed minus calculated midtimes for OGLE-TR-113b	98
4-7	Upper mass limit on potential companion planets to OGLE-TR-113b	99
4-8	Three transits of CoRoT-2b	101
4-9	Parameter distributions for joint fit to three transits of CoRoT-2b . .	104
4-10	Observed minus calculated midtimes for CoRoT-2b	106

5-1	Nine transits of OGLE-TR-132b	113
5-2	Parameter distributions for joint fit to nine transits of OGLE-TR-132b	115
5-3	Parameter variation of individual transits of OGLE-TR-132b	117
5-4	Observed minus calculated midtimes for OGLE-TR-132b	118
5-5	Variability of OGLE-TR-10b	121
5-6	Three transits of OGLE-TR-10b	123
5-7	Parameter variation of individual transits of OGLE-TR-10b	126
5-8	Observed minus calculated midtimes for OGLE-TR-10b	130
5-9	Two transits of XO-2b	133
5-10	Parameter distributions for joint fit to nine transits of XO-2b	136
5-11	Observed minus calculated midtimes for XO-2b	139
A-1	Finder chart for OGLE-TR-10 on MagIC-e2v	149
A-2	Finder chart for OGLE-TR-56 on MagIC-e2v	150
A-3	Finder chart for OGLE-TR-111 on MagIC-e2v	150
A-4	Finder chart for OGLE-TR-113 on MagIC-e2v	151
A-5	Finder chart for OGLE-TR-132 on MagIC-e2v	151
A-6	Finder chart for CoRoT-2 on MagIC-e2v	152
A-7	Finder chart for CoRoT-2 on MORIS	153
A-8	Finder chart for XO-2 on MORIS	154
A-9	Attempted transit of OGLE-TR-56b on 20060720 using POETS	158
A-10	Attempted transit of OGLE-TR-10b on 20080514 using MagIC-e2v	159
A-11	The shutter monster	159
B-1	Predicted RMS error vs. <i>I</i> magnitude for 100 s integrations	163

List of Tables

1.1	Target planets	23
2.1	Constraints on maximum perturber mass (M_{\oplus}) from the literature . .	31
2.2	Selected parameters from the literature for OGLE-TR-111b	32
2.3	Observational and photometry parameters for OGLE-TR-111b	35
2.4	Flux values for new transits of OGLE-TR-111b	36
2.5	Transit parameters for OGLE-TR-111b (jointly fit)	42
2.6	Timing residuals for OGLE-TR-111b	49
2.7	Individual transit parameters for OGLE-TR-111b (independently fit)	51
3.1	Observational and photometry parameters for OGLE-TR-56b	62
3.2	Flux values for new transits of OGLE-TR-56b	65
3.3	Transit parameters for OGLE-TR-56b (jointly fit)	72
3.4	Individual transit parameters for OGLE-TR-56b (independently fit) .	74
3.5	Timing residuals for OGLE-TR-56b	79
4.1	Observational and photometry parameters for OGLE-TR-113b	87
4.2	Flux values for new transits of OGLE-TR-113b	88
4.3	Transit parameters for OGLE-TR-113b (jointly fit)	93
4.4	Individual transit parameters for OGLE-TR-113b (independently fit)	93
4.5	Timing residuals for OGLE-TR-113b	97
4.6	Observational and photometry parameters for CoRoT-2	100
4.7	Flux values for new transits of CoRoT-2b	102
4.8	Transit parameters for CoRoT-2b (jointly fit)	104

4.9	Timing residuals for CoRoT-2b	107
5.1	Observational and photometry parameters for OGLE-TR-132b	110
5.2	Flux values for new transits of OGLE-TR-132b	114
5.3	Transit parameters for OGLE-TR-132b (jointly fit)	116
5.4	Individual transit parameters for OGLE-TR-132b (independently fit)	117
5.5	Timing residuals for OGLE-TR-132b	119
5.6	Observational and photometry parameters for OGLE-TR-10b	122
5.7	Transit parameters for OGLE-TR-10b (jointly fit)	128
5.8	Individual transit parameters for OGLE-TR-10b (independently fit)	128
5.9	Timing residuals for OGLE-TR-10b	131
5.10	Observational and photometry parameters for XO-2	134
5.11	Transit parameters for XO-2b (jointly fit)	135
5.12	Timing residuals for XO-2b	138
6.1	New light curve parameters for seven transiting planets	143
6.2	New transit ephemerides	145
6.3	Constraints on maximum perturber mass (M_{\oplus}) from this work	145
A.1	All attempted transit observations for seven systems	156
A.1	All attempted transit observations for seven systems	157
B.1	Predicted vs. actual performance for three planets	164

Chapter 1

Introduction

1.1 Exoplanets: a brief history

Although we now recognize a few earlier detections (Latham et al., 1989; Wolszczan & Frail, 1992), the first planet around another star to be widely accepted, 51 Peg b, was discovered only fifteen years ago (Mayor & Queloz, 1995). Since then, the number and kinds of known exoplanets have exploded: 453 planets have been discovered as of 2010 April 28¹. Exoplanets have been found by at least six different methods: radial velocity, transit photometry, gravitational microlensing, direct imaging, astrometry, and timing of stellar pulsations. They have been found around A stars and M dwarfs and everything in between; the closest known planet-hosting star is a mere 3.2 pc away (Epsilon Eridani), while the furthest is more than 6000 pc distant. The planets discovered come in all sizes: the largest exoplanets are many times the mass of Jupiter and blend somewhat uncertainly with the smallest brown dwarfs, while the smallest confirmed exoplanet, PSR 1257+12b, is about twice the mass of the Moon and orbits a pulsar (Wolszczan, 1994; Wolszczan & Frail, 1992). (The lowest mass exoplanet around a solar type star, GJ 581e, is about twice the mass of the Earth; Mayor et al., 2009). Although most extrasolar planets are the only objects we know in their stellar systems, there are almost 50 systems with multiple exoplanets, the most being around 55 Cancri, which has five planets (Fischer et al., 2008). Most planets are in systems

¹<http://exoplanet.eu>

that little resemble our own solar system. Hot, bloated gas giants orbit their stars in only a few days, far closer than the planet Mercury, and highly eccentric orbits are common. Some planets orbit binary stars or even triple stars (e.g., Mugrauer et al., 2007), despite the challenges this poses to theorists trying to explain how they formed (Xie & Zhou, 2009). For some planets, we can measure the temperature and composition of the atmosphere and can estimate the bulk composition, and again we are finding that exoplanets differ wildly both from our own solar system and from each other. Perhaps the main lesson of the last fifteen years is not that there are so many planets, but that they are all so very odd.

Through the study of extrasolar planets, we can examine models of planet formation developed for our solar system and determine how typical our experience was (or, commonly, how incorrect our initial models were). By examining hundreds of planets of different types and ages and in different environments, we can learn how planets form, migrate, evolve, and die. Planets are currently the only places we know life exists, so by discovering new planets we find new places to look for life. We might even be detecting destinations for our distant descendants to travel to and live on some day.

1.1.1 How we detect exoplanets, and what we can learn

The most straightforward way to find an exoplanet is to directly observe it in orbit around its star, with either an image or a spectrum. This is quite difficult because most planets are too close to their much brighter host stars; the contrast ratio makes it extremely challenging to resolve planets directly with current technology. There have been many proposals to somehow block out the starlight so that the planet can be observed, such as using a coronagraph (e.g., Yamamoto et al., 2009) or even the darkened limb of the moon (Elliot, 1978), but the only discoveries so far have been of widely-separated planets, such as Fomalhaut b at 115 AU (Kalas et al., 2008). Direct imaging detections without coronagraphs have been made in a few cases with favorable contrast ratios, mostly around young stars where the planets are still hot and bright. The stars themselves also tend to extremes: the first imaged exoplanets

were around low mass stars or brown dwarfs (e.g., 2M1207b Chauvin et al., 2005), which have the most favorable contrast ratios. More recently planets have been found in wide orbits around A stars, such as or HR 8799 b,c,d, at 24-68 AU (Marois et al., 2008); planets are thought to exist at those distances because A stars can have larger accretion disks than solar type stars. The planets that can currently be detected by direct imaging have very different properties than those detectable by other means and are like nothing in our solar system.

A second class of detection methods looks for wobbles in the stellar position due to a perturbing planet. Generally only some components of the stellar motion can be detected: either the radial velocity of the star, seen through shifts in spectral lines, or the transverse velocity, detected through astrometric measurements of the star's center of light. By far the most success has been seen with the radial velocity method, which has been used to discover the vast majority of exoplanets, including the first ones that are still accepted today (e.g., Mayor & Queloz, 1995; Marcy & Butler, 1996; Latham et al., 1989). Although astrometry was the first method used to look for exoplanets, precise measurements are difficult to achieve; very early claims of exoplanets had to be retracted (van de Kamp, 1963; Gatewood & Eichhorn, 1973), while more recent discovery claims have been disputed (Pravdo & Shaklan, 2009; Bean et al., 2010). Several close planetary systems have been detected astrometrically using the Hubble Space Telescope (e.g., Epsilon Eridani by Benedict et al., 2006).

A third method is to look for planets that happen to transit their star. During a transit, the planet will block a small fraction of the starlight, producing a distinctive photometric light curve. Only a small subset of planets are geometrically positioned to cross in front of their star from our vantage point on Earth, but those that do can be studied in exquisite detail. Ten years ago the first planet observed to transit, HD 209458b, was announced, after having previously been detected using radial velocity measurements (Charbonneau et al., 2000; Henry et al., 2000). Since then, most of the 71 planets known to transit have been found through dedicated photometric surveys (e.g., Udalski et al., 2002a). In addition to the technical difficulties of maintaining photometric precision of better than 1% over many days or years, a huge challenge

with transit surveys is to eliminate false positives, such as a grazing binary star, that can mimic the shape and depth of a planetary transit. For that reason radial velocity measurements must be taken of the most promising candidates to determine whether they are in fact caused by objects of planetary mass.

Additional methods to look for planets include gravitational microlensing surveys, which monitor large sections of the sky for serendipitous alignments of a foreground star and planet system with a background lens; the planet can be detected from distinctive features on the brightening curve (e.g., Bond et al., 2004). Such planets typically cannot be followed up after the microlensing event, however, because in most cases the host star is too faint to be detected. Thus, planets discovered through this method are most useful for statistical claims about the frequency of certain classes of exoplanets. One final method is to examine non-main-sequence stars, such as pulsars (Wolszczan & Frail, 1992) or other pulsating variable stars (e.g., Silvotti et al., 2007), and to search for deviations in the timing of these pulsations that might be periodic planetary perturbations.

We will now focus on the two most productive detection methods, radial velocity and transit photometry. Although both methods detect periodic signals from a planet, they produce complementary data. With radial velocity, we can determine the mass of the planet times a factor of $\sin(i)$, since we do not know the relative inclination of the planetary system to our line of sight; a face-on planetary orbit ($i = 0^\circ$) would be undetectable since the planet would induce no radial velocity motion in the star. A transiting planet, however, by its very nature must be oriented so that the system is more or less edge on ($i = 90^\circ$). Most radial velocity planets are not observed to transit, but all transiting planets have radial velocity measurements, so they are the only planets for which precise masses are known. The shape of the planetary transit light curve provides additional information: the ratio between the planetary and stellar radius, the semimajor axis of the planet in units of stellar radii, and the stellar limb darkening parameters.

Transiting planets are also the only planets we can estimate the composition of, using the relationship between the mass and radius and the equation of state of the

planetary constituents (Zapolsky & Salpeter, 1969). A number of known transiting planets have such high radius values that it is difficult for theories to account for them (e.g. TrES-4, Mandushev et al., 2007), although some progress has been made using models that couple orbital evolution, tidal heating, stellar irradiation, and planetary atmospheric models (e.g., Ibgui & Burrows, 2009). For smaller, potentially Earth-like exoplanets, even with current measurement precision we can identify if a planet is mostly rocky-iron or if it must also have a water or gas layer (e.g., Seager et al., 2007). Due to degeneracies in the models and assumptions, additional information besides the mass and radius may be needed to distinguish between, for example, a small rocky planet with a thick atmosphere or a water-rich world (e.g., Adams et al., 2008).

Fortunately, due to their geometry, transiting planets are uniquely situated for many other measurements of physical properties, which will allow us to begin studying them as individual worlds. By observing the distortion of the radial velocity of the planet during the time of transit, called the Rossiter-McLaughlin effect (Rossiter, 1924; McLaughlin, 1924; Ohta et al., 2005), we can determine whether the planetary orbit is aligned (e.g., Queloz et al., 2000) with the stellar rotation axis or not (e.g., Winn et al., 2009a), or possibly even in a retrograde orbit (e.g., Narita et al., 2009; Winn et al., 2009b), which will help study how these objects migrated close to their stars. If the planet has an atmosphere, this will increase its apparent radius in wavebands where the atmosphere is optically thick, and spectroscopic observations during transit can detect species in the atmosphere (e.g., Charbonneau et al., 2002). Hot short-period planets emit enough radiation in the infrared that light from the planet itself can be detected due to its absence when the planet passes behind the star (e.g., Charbonneau et al., 2005; Deming et al., 2005). Most (but not all) transiting planets are also aligned so that we can observe this disappearance, called variously the planetary occultation or secondary eclipse. By comparing the flux during the planetary occultation to the flux just before the planet disappears, we can estimate the temperature of the planet. Most such thermal measurements have been made from space using the Spitzer telescope (e.g., Knutson et al., 2007a), but recently

detections of both thermal emission and reflected optical light have also been made from the ground (e.g., Snellen & Covino, 2007; Sing & López-Morales, 2009).

1.2 On the timing of transits

One of the most basic things to determine about a transit is its midtime. The precision with which we can determine the midtime of the transit scales with the photometric precision of the light curve, so high-quality transit light curves can have very small midtime errors (e.g., 7 s for WASP-10b; Johnson et al., 2009), although more typically errors in ground based observations are of order 30-60 s. If the errors on the midtimes are low enough, we can start to look for variations that might be caused by a third body in the system, such as another planet or a moon (Holman & Murray, 2005; Agol et al., 2005; Heyl & Gladman, 2007; Ford & Holman, 2007; Simon et al., 2007; Kipping, 2009; Kipping et al., 2009). The presence of a third body will perturb the orbit of the transiting planet, producing transit timing variations (TTVs) or transit duration variations (TDVs). Theoretical estimates of the magnitude and pattern of timing variations caused by third bodies vary widely, because the perturbing objects could occupy a large parameter space of masses and orbits, and the size of the TTV scales with the period of the known planet as well as with the mass of the perturber. Some of the strongest signals would be produced by objects in close mean-motion resonances, so that the periods of the two planets were related by a smaller integer ratio. Although several examples are known of exoplanetary systems in 2:1 mean-motion resonances (e.g., Mayor et al., 2004), most are further from their stars than the known transiting planets. Estimates from Holman & Murray (2005) for a typical transiting hot Jupiter, HD 209458b, with close, resonant companions, place the potential TTVs at the 10-20s level, which is about the level of timing precision reachable with the best light curves today. It is an open question how likely close resonant companions to short period planets are. However, given the history of surprises in the study of exoplanets, our approach has been to work to identify a timing anomaly first and then to figure out whether the object causing it could exist.

In addition to quasi-periodic variations such as TTVs and TDVs, careful timing could potentially identify small secular changes in the orbital period due to tidal decay (e.g., Sasselov, 2003; Pätzold et al., 2004; Carone & Pätzold, 2007; Levrard et al., 2009). OGLE-TR-56b in particular has been the subject of much discussion on the potential observability of its period changing, as discussed in more detail in the introduction to Chapter 3. Generally the size of the period change is expected to be detectable only over timescales of many years or decades, so it is important to regularly monitor the most promising systems with high quality transit timing.

Most planetary surveys do not produce individual transits with adequate sampling to be useful for transit timing studies. Typically, only one or two high quality light curves will be observed for each new planet, which is not enough to constrain a timing variation; depending on the TTV pattern, five or ten light curves might be needed to identify a variation, and even more to accurately characterize it and, more difficultly, determine what caused it. There is a real need for multiple high-quality light curves of each planet, ideally observed with the same instrument and telescope to minimize systematic errors. We therefore developed a project to observe five light curves each of five targets, with two goals: (1) improve the planetary radius and other system parameters, and (2) achieve timing precision within 10-20 s on each transit to begin searching for timing variations.

1.3 Our observational project

Although the best platform for a transit timing study would be a dedicated space telescope that would achieve high precision on many consecutive transits of the targeted planets, ground-based telescopes have an important role, particularly for fainter objects ($I \sim 15$) for which the increased number of photons collected by a larger mirror outweighs the gains of moving to space. Ground based photometry must deal with high levels of correlated noise, mostly from atmospheric effects, but if we can properly account for that noise it offers the potential for acquiring much cheaper light curves. We have chosen to focus on five relatively faint planets from the OGLE survey, with

stars of I magnitudes from 14.4-15.7; these planets have been somewhat overlooked as brighter, easier targets have been discovered.

1.3.1 Improved radii

High photometric precision is needed to reduce the ambiguity between correlated parameters (notably the orbital inclination, radius ratio, and stellar limb darkening). Determining accurate radii for extrasolar planets will help address whether hot Jupiters have massive cores, and perhaps why some of the closest planets have highly inflated radii compared to theoretical models, while others do not. Although there have been notable improvements in the radius values in recent years, the OGLE planets still tend to have fairly large errors on the measured planetary radii, around 5%, due to uncertainties in stellar radius models and errors in the observed planet-star radius ratio. By systematically combining multiple (3-5) high quality transit light curves, our goal was to measure the radius ratio to within 1% or better, which will leave the stellar radius as the dominant source of uncertainty.

1.3.2 Transit timing

The main focus of the project will be on precisely timing each transit. We expected to achieve timing precision for single transits of 10-20 s (see Appendix B), which was comparable to the best timing available (14 s on HD 209458b using HST; Knutson et al., 2007b, which was limited by systematic errors despite high photometric precision). Since we do not know a priori what kind of timing variations we might find, it is important to build a library of many well-timed transits that we can search for deviations and patterns.

1.3.3 Targets for observation

When this project was first proposed in spring 2006, only ten planets were known to transit, five of which were visible in the southern hemisphere from Las Campanas Observatory. All of these planets were discovered by the Optical Gravitational Lens-

Table 1.1. Target planets

Planet	RA	Dec	Mag. (<i>I</i>)	M_P (M_J)	R_P (R_J)	P (d) ^a	Source ^b
OGLE-TR-10b	17:51:28.25	-29:52:34.9	14.93	0.57 ± 0.12	1.056 ± 0.069	3.101274 (4)	1
OGLE-TR-56b	17:56:35.51	-29:32:21.2	15.3	1.29 ± 0.11	1.30 ± 0.05	1.211909 (1)	2
OGLE-TR-111b	10:53:17.91	-61:24:20.3	15.55	0.52 ± 0.13	1.067 ± 0.054	4.0144479 (41)	3
OGLE-TR-113b	10:52:24.40	-61:26:48.5	14.42	1.32 ± 0.19	1.09 ± 0.03	1.4324757 (13)	4
OGLE-TR-132b	10:50:34.72	-61:57:25.9	15.72	1.14 ± 0.12	1.18 ± 0.07	1.689868 (3)	5
CoRoT-2b	19:27:06.50	+01:23:01.5	11.49	3.31 ± 0.16	1.465 ± 0.029	1.7429964 (17)	6
XO-2b	07:48:06.47	+50:13:33.0	10.3	0.57 ± 0.06	0.98 ± 0.03	2.615857 (5)	7

^aError is on the last digits quoted.

^b[1] Holman et al. (2007); [2] Pont et al. (2007); [3] Winn et al. (2007); [4] Gillon et al. (2006); [5] Gillon et al. (2007); [6] Alonso et al. (2008); [7] Burke et al. (2007)

ing Experiment, or OGLE (Udalski et al., 2002a,c,b), and despite the survey name they were found using the transit method. Starting in 2008, other photometric surveys began to operate in the southern hemisphere, such as SuperWASP (Wide Angle Search for Planets, Cameron et al., 2007) and HAT-South (Hungarian Automated Telescope, Bakos et al., 2009). Additionally, the CoRoT space mission (Convection Rotation and planetary Transits, e.g., Barge et al., 2008) searched for planets in fields that are visible from both hemispheres. We added CoRoT-2b to our survey in 2008 soon after its coordinates were released. A critical feature of all of our targets is that they have at least one bright comparison star within the field of view of the instrument, and preferably several; the precision of a photometric light curve should ideally not be limited by photon noise from the comparison star(s).

Also in 2008 we began work on a new instrument, now called MORIS², on the IRTF; MORIS is described in more detail in Section 1.3.4. We were able to obtain time on this instrument, which is still under development, to observe planetary transits of four targets (CoRoT-2b, XO-2b, TrES-3b, and TrES-1b; results for the first two systems are presented in this thesis). These stars were selected because they have at least one bright companion star within the 60'' x 60'' field of view.

²<http://occult.mit.edu/instrumentation/POETS/IRTF/>

1.3.4 Choice of instrument

Measuring midtimes to better than 30 s precision requires millimagnitude-level photometry sustained over several hours. Thus the choice of instrument is important. Ideally, the instrument should have low read-noise per pixel, uniform flat field response, few bad pixels or other cosmetic defects, and short readout times to maximize the time coverage during transit. A large telescope aperture is also helpful to overcome read noise with many photons. To minimize flat-fielding errors and differential pixel response, the light from the stars should be spread over many pixels. This can be achieved either by designing an instrument to have a small pixel scale, so that the full-width-half-maximum (FWHM) of the star under typical seeing conditions is many pixels, or by deliberately defocusing the telescope to the desired FWHM. Given the crowded conditions of the OGLE fields and the desire to avoid blending with nearby stars, defocusing is not a good option. We have opted for frame-transfer CCDs where possible, which combine low read-noise with fast readout times (a few milliseconds) between frames. The tradeoff of small chip sizes and hence small field of view is acceptable, although it does limit the target choice for brighter stars which are not in crowded fields.

A second important factor in good transit observations is to select a good site. Many of the best-quality light curves have been taken with space-based instruments (e.g., HST, Spitzer, CoRoT, Kepler) because they can avoid all the woes attendant to changing atmospheric conditions. However, space missions are expensive, have limited time available, and have smaller mirrors and older instruments than the best ground-based observatories offer. We selected the 6.5m twin Magellan telescopes, Baade and Clay, due to their superior site conditions (average seeing is 0."7) and their support for installing a new instrument to be used partly for exoplanet transits.

A third important factor is to make sure the transits are accurately timed. The best option is to have each exposure triggered by a GPS receiver (as we do for POETS and MORIS, described below), but careful syncing of the control computer times can also lead to the desired accuracy. In the future, as we push the error on the midtimes

down to the level of a few seconds or better, controlling for instrumental effects will become even more important.

POETS

Our first pilot transits of OGLE-TR-56b were taken in 2006 June-July with a visiting instrument POETS (Portable Occultation, Eclipse, and Transit System, Souza et al., 2006). We used POETS-Blue, an Andor iXon DU-897-BV frame-transfer camera with 512x512 16-micron square pixels. We used the 1 MHz Conventional mode and the 1x gain setting, which has a read noise of 6 e- per pixel and gain of 3.7e-/ADU. The field of view was 23" x 23" and a plate scale of 0.0"45 per pixel unbinned. The photometric accuracy we achieved with POETS on Magellan was 5.4 mmag in 2 s on an $I = 15.3$ source, which in principle would bin into 0.7 mmag in 2 min for a single transit (in practice, for the transit in question, 20060622, it binned to 1 mmag in 2 min; see Chapter 3). All POETS transit observations were triggered by an external GPS, so the recorded times should be accurate at the microsecond level.

MagIC-e2v

In order to have a frame-transfer camera at Magellan available full-time for transit and occultation observations, we upgraded the existing instrument MagIC (Magellan Instant Camera) to contain dual CCDs, which share a common dewar, shutter and filter wheel (Osip et al., 2008). I worked on upgrading the instrument control software to work with both CCDs and performed extensive debugging of the system, since the transit observations presented in this thesis were the first to regularly use the new instrument. The new CCD, MagIC-e2v, is identical to the red CCD on HIPO (Dunham et al., 2004), a fast read-out direct imaging camera and one of the first generation instruments to be flown on SOFIA (Stratospheric Observatory for Infrared Astronomy); both cameras use the LOIS control software (Taylor et al., 2004). MagIC-e2v has 1024x1024 pixels, each 13 micron square, and on Magellan has a field of view of 38" x 38" and a plate scale of 0."037 per pixel unbinned.

When MagIC-e2v was first operational, in 2008 April, only the single-frame mode

was available, which while not frame transfer still had a low readout time of 5 s. Since 2009 February, the frame transfer mode for the MagIC-e2v CCD has been operational, with $> 99\%$ duty cycle possible for long sequences of exposures.

For the 2008 transits, the start times for each image were recorded from a network time server, which was verified by eye to be synchronized within less than a second with the observatory's GPS clocks at the beginning of each night; this error is well below the midtime precision of all transits. For the 2009 observations, the times came from a small embedded control computer (a PC104), which received unlabeled GPS pulses every second, and was synchronized with the observatory's GPS before each transit observation.

MORIS

Our newest instrument, MORIS (MIT Optical Rapid Imaging System; the PI is A. Gulbis), is co-mounted with the infrared spectrograph SpEX on the IRTF (Infrared Telescope Facility) on Mauna Kea³. MORIS is a similar model of camera (Andor Ixon DU-897-BV) to POETS, although it also has a set of 3:1 reducing optics to accommodate being co-mounted with another instrument. Like POETS, MORIS uses an external GPS to trigger each exposure.

Data quality for transits observed with MORIS has been more variable than for data from Magellan, partly due to poor weather but mostly because of problems with the new instrument, which were first characterized during the course of our transit observations. (Our transit observations were one of the first programs to use MORIS regularly, and subsequent engineering runs were planned to correct the problems we identified.) The most serious problem has been the uneven illumination pattern. Because the telescope was optimized for infrared and not visible light, there have been additional (and variable) sources of scattered light, which were not accounted for in the original optical design, resulting in the center of the CCD being about twice as bright as the edges (see Figure A-7 and Figure A-8). Furthermore, the illumination pattern has been observed to change during the night, so that it cannot be removed

³<http://occult.mit.edu/instrumentation/POETS/IRTF/>

with flat-field calibration data. However, in spite of the optical problems we have obtained several of our highest-quality light curves with MORIS.

1.3.5 Other instruments

During 2007 and 2008, while waiting for MagIC-e2v to be installed, we observed a few transits using other instruments on Magellan: the original MagIC-SiTe CCD, and IMACS. Both have small pixel scales ($0.''069$ per pixel and $0.''11$ per pixel, respectively), so defocusing was unnecessary, though their readout times are much longer (23 s and 35 s in subraster mode, respectively). Although they did not produce our very best light curves, the photometry from these instruments was also quite good, partly due to sharing the same excellent site and telescopes. (See Chapter 3 for the IMACS transit and Chapter 4 for two SiTe transits.)

1.4 Outline

In this thesis, we examine the photometry and timing results for seven planetary systems. In Chapter 2 we examine six new light curves of OGLE-TR-111b, the only system for which transit timing variations (TTVs) have been claimed (Díaz et al., 2008), and find that our data contradicts that finding. We find no evidence for TTVs, and can exclude potential companion planets with masses as small as Earth in a 2:1 mean-motion resonance. In Chapter 3, we provide eleven new light curves for OGLE-TR-56b, which previously only had one high-quality light curve available (Pont et al., 2007). We find no evidence of timing variations within our light curves, although we note a five minute discrepancy with the published transit ephemeris. We also note a disagreement in the shapes of the light curves we measured compared with the literature, most notably in the form of a duration that differs by 15 minutes. In Chapter 4, we examine two systems, OGLE-TR-113b with six transits and CoRoT-2b with three transits. Both systems have high timing precision (our best light curve of OGLE-TR-113b has a midtime error of only 9 s). We find that although there are no signs of TTVs, the orbital period of OGLE-TR-113b is shorter by 0.24 ± 0.12 s in

the new data from 2007-2009 compared to the period determined in the literature for 2002-2005. If confirmed, this is the first detection of the orbital decay of an extrasolar planet. In Chapter 5 we discuss the final three systems: OGLE-TR-132b, for which we have seven light curves and see no signs of timing variations; OGLE-TR-10b, a system that has radius estimates in the literature that differ by a factor of 2, and for which we have three light curves, and also note a curious deviance of previously published midtimes; and XO-2b, a bright binary star for which we have obtained two well-timed light curves, which are completely consistent with other published midtimes.

Chapter 2

Claimed TTV for OGLE-TR-111b Not Confirmed with Six New Transits

A version of this chapter will be published in ApJ as "Lack of Transit Timing Variations of OGLE-TR-111b: A re-analysis with six new epochs", Adams, E. R., Lopez-Morales, M., Elliot, J. L., Seager, S., & Osip, D. J., 2010

2.1 Abstract

We present six new transits of the exoplanet OGLE-TR-111b observed with the Magellan Telescopes in Chile between 2008 April and 2009 March. We combine these new transits with five previously published transit epochs for this planet between 2005 and 2006 to extend the analysis of transit timing variations reported for this system. We derive a new planetary radius value of $1.019 \pm 0.026 R_J$, which is intermediate to the previously reported radii of $1.067 \pm 0.054 R_J$ (Winn et al., 2007) and $0.922 \pm 0.057 R_J$ (Díaz et al., 2008). We also examine the transit timing variation and duration change claims of Díaz et al. (2008). Our analysis of all eleven transit epochs does not reveal any points with deviations larger than 2σ , and most points are well within 1σ . Although the transit duration nominally decreases over the four year span of the data,

systematic errors in the photometry can account for this result. Therefore, there is no compelling evidence for either a timing or a duration variation in this system. Numerical integrations place an upper limit of about $1 M_{\oplus}$ on the mass of a potential second planet in a 2:1 mean-motion resonance with OGLE-TR-111b.

2.2 Introduction

Transiting exoplanets provide a wealth of information for studies of the physical parameters of planets and their environments. For example, the combination of several accurately timed transits of a known transiting exoplanet can be used not only to improve estimates of the planetary radius and orbital parameters of the star-planet system, but also to detect additional objects. Detecting potential variations of parameters such as the inclination and duration of the transits would indicate a precessing planetary orbit, potentially caused by another planet (Miralda-Escudé, 2002). We can also use transit timing to search for additional planets or moons, as discussed in several recent theory papers (Holman & Murray, 2005; Agol et al., 2005; Heyl & Gladman, 2007; Ford & Holman, 2007; Simon et al., 2007; Kipping, 2009; Kipping et al., 2009). The idea is that the presence of additional objects will perturb the orbit of the transiting planet, producing transit timing variations (TTVs) or transit duration variations (TDVs). Those TTVs and TDVs can be detected by monitoring transits over many orbital periods. The absence of such variations can be also used to place limits on the mass and orbital parameters of additional objects in those planetary systems and to gain insight into the systems' architectures.

Recent observations show hints of timing variations for some transiting planets, but no definitive detection of additional planets or satellites has been reported using this technique. The most interesting results so far are (1) the absence of TTVs in several systems, which do not host planets more massive than several Earth masses in low-order resonant orbits (see a summary of constraints that can be placed in Table 2.1); (2) the tentative detection of TDVs in GJ436, roughly 3 minutes per year (Coughlin et al., 2008), a trend consistent with the presence of a low-mass companion

Table 2.1. Constraints on maximum perturber mass (M_{\oplus}) from the literature

System	Max O-C (sec)	1:2 ^a	2:3	Interior (non-resonant)	3:2	2:1	Exterior (non resonant)	Source ^b
CoRoT-1	78 ± 24	unstable	unstable	unstable	–	4	200 ($P < 4d$)	1
	< 60	–	–	–	–	1	10 ($P < 3.5d$), 100 ($P < 5d$)	2
GJ 436	< 60	–	–	–	–	–	8 ($P < 5d$)	3
	< 120	10	2	–	2	20	20 ($P < 5d$)	4
HAT-P-3	< 60	0.7-1.0	–	–	–	30-40	–	5
HD 189733	< 45	4	1	–	8	20	32 ($P < 5d$)	6
HD 209458	70 ± 50	0.3	–	20	0.3	0.3	–	7
		–	–	–	–	–	17 ($P < 7d$), 100 ($P < 10d$)	8
TrES-1	107 ± 17	1	2	3	2	1	100 ($P < 6d$)	9, 10
TrES-2	257 ± 27	2	15	30	–	1	50 ($P < 7d$)	10
TrES-3	70 ± 30	3-4	–	–	–	10-15	–	11

^aA perturber in an n:m resonance completes m orbits while the known planet completes n .

^b[1] Bean (2009); [2] Csizmadia et al. (2009); [3] Bean & Seifahrt (2008); [4] Ballard et al. (2009); [5] Gibson et al. (2010); [6] Miller-Ricci et al. (2008b); [7] Miller-Ricci et al. (2008a); [8] Agol & Steffen (2007); [9] Steffen & Agol (2005); [10] Rabus et al. (2009); [11] Gibson et al. (2009).

($< 12 M_{\oplus}$) in a close exterior but non-resonant orbit; this result is consistent with the $8 M_{\oplus}$ limit placed by transit timing (Bean & Seifahrt, 2008); and (3) the preliminary detection of TTVs with a maximum residual of 156 ± 48 sec (3.3σ) over a period of 2 years reported by Díaz et al. (2008) for OGLE-TR-111b, the subject of this paper.

OGLE-TR-111b is a $0.5M_J$ hot Jupiter orbiting its host star, a faint ($I = 15.5$) K dwarf, every 4.01 days. This object was first announced as a transiting planet candidate by Udalski et al. (2002b), and was confirmed to have planetary mass by Pont et al. (2004). The physical parameters of the planet were refined over the next two years, with several new radial velocity measurements (Gallardo et al., 2005; Silva & Cruz, 2006; Santos et al., 2006). The first high precision transit photometry was provided by Winn et al. (2007), with two I -band transits of the planet on 2006 Feb 21 and Mar 5. Shortly after, Minniti et al. (2007) published a V -band transit from 2005 April 9 and noted that the midtime occurred 5 minutes earlier than expected from the ephemeris in Winn et al. (2007), although with only three epochs they could draw no firm conclusions. A follow-up paper by Díaz et al. (2008) reported two consecutive I -band transits of OGLE-TR-111b on 2006 Dec 19 and 23. Combining all five epochs, they concluded that the previously claimed TTVs were real, with the

Table 2.2. Selected parameters from the literature for OGLE-TR-111b

Radius ^a (R_J)	Midtime (JD)	Duration (hours)	Impact parameter	Filter	Source ^b
0.97 ± 0.06	24552330.44867 (fixed)	–	$0 - 0.68$	<i>I</i>	1, 2
1.01 ± 0.06	$24553470.56389 \pm 0.00055$	2.9 ± 0.1	$0 - 0.65$	<i>V</i>	3, 4
1.067 ± 0.054	$24553787.70854 \pm 0.00035$	2.743 ± 0.033	$0.25 - 0.55$	<i>I</i>	5
1.067 ± 0.054	$24553799.75138 \pm 0.00032$	2.743 ± 0.033	$0.25 - 0.55$	<i>I</i>	5
0.922 ± 0.057^c	$24554088.79145 \pm 0.00045$	2.67 ± 0.014	0.38 ± 0.2	<i>I</i>	4
0.922 ± 0.057^c	$24554092.80493 \pm 0.00045$	2.67 ± 0.014	0.38 ± 0.2	<i>I</i>	4
1.025 ± 0.047	$24553470.56385 \pm 0.00100$	2.75 ± 0.11	0.39 ± 0.28	<i>V</i>	6
1.066 ± 0.038	$24553787.70860 \pm 0.00076$	2.73 ± 0.047	0.30 ± 0.14	<i>I</i>	6
1.062 ± 0.051	$24553799.75135 \pm 0.00090$	2.76 ± 0.065	0.39 ± 0.16	<i>I</i>	6
0.952 ± 0.076	$24554088.79118 \pm 0.00138$	2.62 ± 0.060	0.38 ± 0.12	<i>I</i>	6
0.968 ± 0.064	$24554092.80494 \pm 0.00129$	2.66 ± 0.071	0.35 ± 0.15	<i>I</i>	6
1.045 ± 0.036	$24554574.54805 \pm 0.00078$	2.40 ± 0.393^d	0.51 ± 0.27	<i>i'</i>	6
1.030 ± 0.029	$24554578.55395 \pm 0.00061$	2.73 ± 0.062	0.36 ± 0.19	<i>i'</i>	6
0.996 ± 0.022	$24554598.62680 \pm 0.00047$	2.63 ± 0.037	0.22 ± 0.11	<i>i'</i>	6
1.028 ± 0.021	$24554602.64098 \pm 0.00053$	2.69 ± 0.051	0.30 ± 0.12	<i>i'</i>	6
1.006 ± 0.025	$24554879.63787 \pm 0.00056$	2.68 ± 0.054	0.28 ± 0.12	<i>i'</i>	6
1.025 ± 0.022	$24554903.72515 \pm 0.00039$	2.61 ± 0.058	0.16 ± 0.11	<i>i'</i>	6

^aExcept as noted, assuming $R_* = 0.83R_\odot$

^b[1] Pont et al. (2004); [2] Santos et al. (2006); [3] Minniti et al. (2007); [4] Díaz et al. (2008); [5] Winn et al. (2007); [6] This work; all values are taken from individual MCMC fits to each light curve, with with errors inflated to account for correlated noise, as discussed in § 2.4.3.

^cUsing $R_* = 0.811R_\odot$; if $R_* = 0.83R_\odot$ is used, the radius is $R_P = 0.944R_J$

^dHalf-transit

residuals spanning -156 ± 48 to $+98 \pm 39$ seconds. Among other scenarios, they noted that if OGLE-TR-111b were in an eccentric orbit with $e \sim 0.3$, the observed TTVs would be consistent with the presence of an Earth-mass planet near an exterior 4:1 resonant orbit. Additionally, Díaz et al. (2008) noted two parameters with marginally discrepant values across the five transits (see Table 2.2). Compared to the results from Winn et al. (2007), the Díaz et al. (2008) values for the planetary radius disagreed at the 10% level, or 1.3σ , and the total transit duration differed by 1.6σ . The radius ratio discrepancy was suggested to be the result of the parameters chosen for the image subtraction photometry, which focused on precise timing rather than on an accurate transit depth determination. The duration variation, if real, could be due to a perturber decreasing the orbital inclination, which would offer another way of determining the properties of the third body in the system suggested by their TTVs.

Here we present six new transits observed during 2008 and 2009, which double the

number of high-quality transit light curves available for OGLE-TR-111b. In § 2.3 we describe the collection and analysis of the new data. In § 2.4 we describe the transit model fitting, and discuss additional sources of error not included in the formal fit. In § 2.5 we combine the six new transits with the five previously published observations and provide a new analysis of parameter variation in the OGLE-TR-111 system. In § 2.6 we discuss the implications of our results.

2.3 Observations and data analysis

All six new transits were observed between April 2008 and March 2009 in the Sloan *i'* filter with the new MagIC-e2v camera¹ on Magellan. The MagIC-e2v camera has a field of view of 38" x 38" and a plate scale of 0."037 per pixel unbinned. With such high resolution and good average seeing at the site, blends are minimized and aperture photometry can be successfully applied even in fairly crowded fields. The camera can be operated in two different modes: single exposure mode, with a readout time of about 5 seconds per exposure, and frame transfer mode, with a readout time of only 3 milliseconds between frames in an image cube. Our first four transits were observed in single exposure mode. The frame transfer mode first became available after engineering in July 2008, and was used for the last two transits of OGLE-TR-111b. The gain and read noise of the first four transits were 2.4 e-/ADU and 5.5 e- per pixel, respectively; after engineering, these values were changed to the current values of 0.54 e-/ADU and 5 e- per pixel.

The exposure times during each transit were adjusted to maintain a minimum count level of about 10^6 integrated photons, both for the target and multiple nearby comparison stars. For the 2008 transits, we collected unbinned (1x1) data with exposure times between 30 and 120 sec, depending on the observing conditions, with an additional readout overhead per exposure of 5 seconds per frame. The 2009 data

¹The MagIC-e2v detector, which shares a dewar with the older SiTe CCD, is identical to the red CCD on HIPO, a fast read-out direct imaging camera and one of the first generation instruments to be flown on SOFIA; both cameras use the LOIS control software (Dunham et al., 2004; Taylor et al., 2004; Osip et al., 2008).

were collected in frame-transfer mode with the camera binned 2x2, which yielded an improved sampling rate of 15-30 sec per frame. Details of the observing settings are noted in Table 2.3.

Accurate timing is of the utmost importance for this project, so special care was taken to ensure that the correct times were recorded in the image headers. For the 2008 transits, the start times for each image were recorded from a network time server, which was verified by eye to be synchronized with the observatory's GPS clocks at the beginning of each night. For the 2009 observations, the times came from a PC104 (a small embedded control computer), which received unlabeled GPS pulses every second. As with the network time server, the PC104 was synchronized with the observatory's GPS before each transit observation. In both cases the time signals written to the image headers agree within one second with the GPS time. During both 2009 transits, a software failure caused the times for a few image cubes to not be recorded in the headers of the images, but we were able to reconstruct the observation times with precisions better than a second from detailed system logs. One second is a conservative estimate of the intrinsic error for the start time for each frame, and is significantly smaller than the mid-transit times errors.

2.3.1 Data analysis

All data were overscan corrected and flattened using IRAF.² The photometry was performed using the IRAF routine *phot*, part of the *apphot* package. Depending on the binning applied and the seeing during each transit, a subset of apertures between 6-25 pixels in radius were examined for the target star and each comparison star. Between one and seven stars were selected as comparisons from the list of 10-20 field stars present in each frame. The comparison stars had to pass several selection criteria: to be similar in brightness to the target, to not be blended, and to not be variable. The best apertures were identified as the ones which yielded the smallest

²IRAF is distributed by the National Optical Astronomy Observatories, which are operated by the Association of Universities for Research in Astronomy, Inc., under cooperative agreement with the National Science Foundation.

Table 2.3. Observational and photometry parameters for OGLE-TR-111b

Transit (UT)	Frames used (discarded)	Exp. Time (sec)	Binning	Readout (sec)	N_C	Aperture ^a (pixels)	Sky radius, width (pixels)	Scatter ^b (mmag)
20080418	178 (0)	30-60	1x1	5	3	12.8	35, 15	1.3
20080422	110 (21) ^c	120	1x1	5	4	16.4	30, 10	2.0
20080512	241 (20) ^d	60	1x1	5	3	19.2	30, 15	1.5
20080516	276 (4) ^e	30-100	1x1	5	7	17.4	30, 10	1.5
20090217	800 (0)	30	2x2	0.003 ^f	6	19.2	25, 20	1.2
20090313	600 (42) ^g	15-30	2x2	0.003 ^f	1	9.6	20, 30	1.5

^aRadius around star.

^bStandard deviation of the residuals on data binned to 120 s.

^cInsufficient counts on target.

^dElongated images due to tracking failure.

^eInitial telescope focus not yet settled (3 points) and strongly aberrant ratio (1 point).

^fFrame transfer mode.

^gComparison star saturated.

scatter in the out-of-transit flux. The choice of position of the sky background annulus also influenced which stars could be used for comparison; see § 2.4.3 for a discussion of systematic errors resulting from aperture settings. We explored sky regions with inner radii from 20-40 pixels and 10-30 pixels width, and selected the one which (a) provided several comparison stars of suitable brightness that were not variable, and (b) produced the lowest noise in the out-of-transit baseline while not introducing spikes or other obvious problems in the transit light curve.

In each of the resultant light curves, the out-of-transit baseline was examined for linear correlations with several variables: airmass, seeing, telescope azimuth, (x,y) pixel location, and time since beginning of transit. The parameters chosen are either directly correlated with physical phenomena that affect photon rates (e.g., seeing, airmass), or are proxies for other effects (e.g., the telescope azimuth is correlated with the de-rotator rates, which were not recorded for several transits). Only the 2009 transits exhibited significant trends, against telescope azimuth (both) and seeing (20090313). For each transit, we corrected those trends by successively subtracting linear fits to each variable. Detrending was critical in producing usable light curves for these two transits, but may also have introduced smaller-order systematic effects,

Table 2.4. Flux values for new transits of OGLE-TR-111b

Mid-exposure time (BJD) ^a	Flux	Error
2454574.520046	0.9820188	0.00153
2454574.522041	0.9797899	0.00153
2454574.522868	0.9824249	0.00153
2454574.523734	0.9802172	0.00153
2454574.524134	0.9828871	0.00153
...		

^aFull table available on request.

particularly in the transit depth (see also § 2.4.3).

We now briefly describe the observations and the photometric reduction of each transit dataset. All transit fluxes and times are available on request; an excerpt is shown in Table 2.4. See Appendix ?? for an image showing the regions used for aperture photometry on a sample night.

20080418

Transit 20080418 was observed during engineering time just after the e2v CCD was first installed on the telescope; due to engineering constraints, only the second half of the transit was observed. The field was repositioned before egress to eliminate diffraction spikes from a nearby bright star by moving it further off-chip. The airmass was low and fairly constant (1.2-1.3) and the seeing was good, increasing slightly from 0."4 to 0."5 during the transit. The out-of-transit data showed no apparent trends.

20080422

Transit 20080422 was observed on an intermittently cloudy night with highly variable transparency, with counts on the target star varying by a factor of 6 within a few frames. We found that eliminating the lowest count frames, those with fewer than 300,000 counts on the target star, significantly decreased the scatter of the light curve. The seeing ranged from 0."5-0."6, and the airmass was low and fairly constant (1.2-1.3). The out-of-transit data showed no apparent trends.

20080512

Transit 20080512 had stable photometric conditions for the entire pre-transit baseline. During the transit there were two drops in target counts (by a factor of 2) that coincided with sudden seeing jumps (0."4 spiking to 0."6). The field also drifted substantially (by ~ 100 rows and ~ 100 columns) due to tracking problems; about 30 minutes of post-transit baseline had to be discarded because of strong image elongation. The airmass ranged from 1.2 to 1.7. The out-of-transit data showed no apparent trends.

20080516

Transit 20080516 had very stable photometric conditions for most of the transit. The seeing gradually increased from 0."4 to 0."6, and the airmass ranged from 1.2 to 2.0. The star also drifted substantially toward the end of transit (by ~ 200 rows and ~ 200 columns) for unknown reasons. The out-of-transit data showed no apparent trends.

20090217

Transit 20090217 was the first of OGLE-TR-111b to be observed with the new frame transfer mode. The seeing fluctuated from 0."7-1."1, while the airmass decreased from 1.8 to 1.2. This transit was detrended for a slope correlated with the telescope azimuth.

20090313

Observations for transit 20090313 began late due to telescope problems and thus there is no pre-transit baseline. Seeing conditions were initially very poor, spiking to 2", but improved substantially during the second half of the transit, to around 0."6. The airmass ranged from 1.2 to 1.5. The huge disparity in seeing made photometry on this transit challenging, and the best light curve resulted from using a small aperture around the target and only the brightest single comparison star, which saturated for a

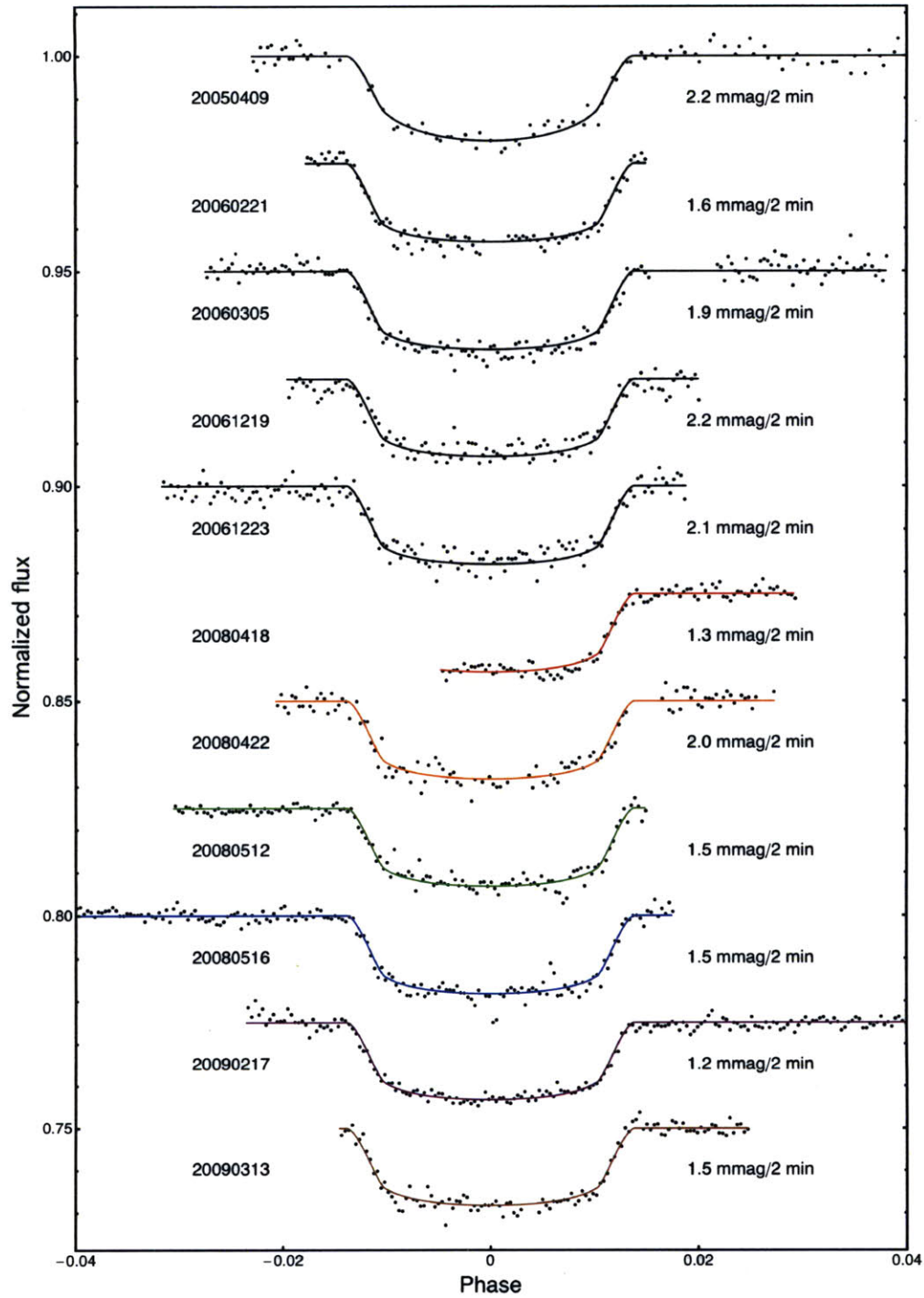


Figure 2-1 Eleven transits of OGLE-TR-111b. All available high-quality light curves are plotted vs. orbital phase, with the data binned to 2 minutes to aid comparison. The joint model fit (solid lines) were calculated using the parameter values in Table 2.5; the stated standard deviation is the residuals from the joint model fit. Table 2.4 shows the unbinned data; a full table can be provided on request.

few frames that had to be discarded. This transit was detrended for slopes correlated with the seeing and the telescope azimuth.

Literature light curves

To eliminate any uncertainty in comparing our transits to previously published transits, which might result from different models, fitting procedures, or fixed parameter values, we have obtained tables of the times and fluxes for each of the five transits drawn from the literature: 20050409 (Minniti et al., 2007), 20060221 and 20060305 (Winn et al., 2007), and 20061219 and 20061223 (Díaz et al., 2008). We have used the original photometry, except for converting from magnitudes into fluxes (where applicable) and converting the mid-exposure times from Heliocentric Julian Day, or HJD, into Barycentric Julian Day, or BJD, to be consistent with the rest of our analysis; the difference between the two time systems is much smaller than our errors, though, a few seconds at most. All values presented for the literature light curves are taken from our re-analysis of the published photometry using our model and fitting, unless otherwise noted.

The light curves for all six new transits and the five literature transits are shown in Figure 2-1, together with the best joint model fit, which will be described in detail in § 2.4.

2.4 Transit fitting results

2.4.1 Model

Each light curve was fitted with the Mandel & Agol (2002) algorithm to generate analytical models, using the basic optimized model-fitting code described in Carter & Winn (2009), but without the wavelet analysis. In the models we assumed that OGLE-TR-111b has zero obliquity, oblateness and orbital eccentricity. We used a

quadratic limb darkening law of the form

$$I(r) = 1 - u_1(1 - \sqrt{1 - r^2}) - u_2(1 - \sqrt{1 - r^2})^2, \quad (2.1)$$

with the initial parameters for u_1 and u_2 set to the values for the appropriate filter (Claret, 2000, 2004). Although analyses of different limb darkening laws have shown that using a non-linear limb darkening law is important (Southworth, 2008), it is generally not possible to fit both quadratic limb-darkening coefficients except on the highest quality, typically space-based, data. We thus fixed the quadratic term u_2 and only fit for the linear term, u_1 . (We also fixed u_1 for the sparsely-sampled transit on 20050409, the only one observed in V band.) The values for u_1 and u_2 are calculated using the *jktld* program by Southworth (2008)³, assuming $T = 5044$ K, $\log g = 4.25$, $[M/H] = 0$, and $V_{micro} = 2$ km/s. We used the limb darkening values corresponding to the Sloan i' filter for the new data, the V_C filter for the transit from Minniti et al. (2007), and the I_C filter for the transits from Winn et al. (2007) and Díaz et al. (2008), as listed in Table 2.5 (though we note for completeness that the actual filters used in the literature light curves, Mould V , CTIO I and Bessel I , respectively, do not correspond precisely to the Cousins V and I filter parameters that were available). We fixed the orbital period to $P = 4.01445$ days; later experiments with slightly different values had little effect. The other free parameters in the model are the radius ratio, k , inclination, i , semimajor axis in stellar radii, a/R_* , out-of-transit flux, F_{OOT} and transit midtime, T_C . We assume throughout the fits that $M_* = 0.81 M_\odot$, $R_* = 0.83 R_\odot$, and $M_p = 0.52 M_J$, based on the spectroscopic work of Santos et al. (2006).

2.4.2 Light curve fits

To determine the best fit value and error of each model parameter, we used a Monte Carlo Markov Chain (MCMC) method, as described in Carter & Winn (2009). The initial values for each parameter were computed by a joint least squares fit to each

³<http://www.astro.keele.ac.uk/jkt/codes/jktld.html>

light curve independently. We then weighted each light curve by the reduced χ^2 of this fit so that the new reduced $\chi^2 = 1$. (By doing this we are assuming the transit model is correct in order to determine the error on each transit, rather than assuming a noise model, e.g., photon noise, in order to test the transit model.) A joint least squares fit of all weighted transits had a reduced $\chi^2 = 1.05$. Starting from the initial least squares values, we constructed chains of 1,000,000 links, where the acceptance rate for each parameter is between 20-60%. We fit all eleven transits simultaneously, assuming common values for k , i , a/R_* , and $u_{1,x}$ (where x is the appropriate filter), with $u_{2,x}$ fixed, but fitting each transit for its own F_{OOT} and T_C . We did not fit for an airmass slope (see § 2.4.3). The first 50,000 points of the MCMC were discarded to eliminate bias toward the initial conditions. We created three independent MCMC chains, checked that the Gelman-Rubin statistic (Gelman & Rubin, 1992) is close to 1 to ensure convergence, and then combined the chains to determine the distribution of all parameters, including the total duration of the transit, T_{14} (the time from first to fourth, or final, contact), and the impact parameter, b , which are derived from fitted parameters. We plot the best model fit with the data in Figure 2-1 and tabulate the fit results in Table 2.5, where we report for each parameter the median value and the 68.3% credible interval (the equivalent to a 1σ standard deviation if the distribution is Gaussian). The distributions for each parameter are shown in Figure 2-2.

The new radius ratio for OGLE-TR-111b based on an analysis of all eleven light curves yields a planetary radius $R_p = 1.019 \pm 0.007 R_J$, if we consider only the formal fit errors; accounting for the error on the stellar radius, which is now the dominant source of error, we find a more realistic error bar is $R_p = 1.019 \pm 0.026 R_J$. Note that if we only use the six new light curves, which have more consistent radii, the value for the radius ratio is very similar (formal fit $R_p = 1.015 \pm 0.009 R_J$, or $R_p = 1.015 \pm 0.026 R_J$ with stellar errors).

As a test of the robustness of our parameter determination, we also ran additional MCMC fits for each transit independently, with results in Table 2.7. Although most of the parameters agree within the formal 1σ errors between the individual and joint fits, there are some notable exceptions. In § 2.5.2 we investigate variability Díaz et al.

Table 2.5. Transit parameters for OGLE-TR-111b (jointly fit)

	Median value	Formal Error ^a	Adopted Error ^b
<i>Fitted Parameters</i>			
k	0.1261	+0.0008, -0.0009	+0.0010, -0.0011
a/R_*	12.3	0.2	0.2
i	88.3	+0.3, -0.2	+0.3, -0.2
$u_{1,i'}$	0.32	0.03	0.04
$u_{2,i'}$	0.252	(fixed)	...
$u_{1,I}$	0.30	0.04	0.05
$u_{2,I}$	0.2582	(fixed)	...
$u_{1,V}$	0.6228	(fixed)	...
$u_{2,V}$	0.1587	(fixed)	...
$T_C - 2453470$	0.56486	+0.00065, -0.00067	+0.00098, -0.00089
$T_C - 2453787$	0.70934	+0.00043, -0.00044	+0.00131, -0.00137
$T_C - 2453799$	0.75212	0.00044	+0.00117, -0.00129
$T_C - 2454088$	0.79197	0.00028	+0.00071, -0.00077
$T_C - 2454092$	0.80573	0.00032	+0.00080, -0.00097
$T_C - 2454574$	0.54282	+0.00040, -0.00039	+0.00103, -0.00068
$T_C - 2454578$	0.55469	+0.00044, -0.00045	+0.00061, -0.00061
$T_C - 2454598$	0.62752	0.00029	+0.00055, -0.00047
$T_C - 2454602$	0.64170	0.00025	+0.00044, -0.00046
$T_C - 2454879$	0.63864	0.00022	+0.00044, -0.00035
$T_C - 2454903$	0.72565	0.00025	+0.00029, -0.00042
<i>Derived Parameters</i>			
b	0.35	+0.04, -0.06	+0.04, -0.06
T_{14} (sec)	9647	+47, -48	+57, -60
$R_p (R_J)^c$	1.019	0.025	0.026
a (AU) ^c	0.0473	+0.0015, -0.0014	+0.0015, -0.0014

^aFormal 68.3% credible interval from MCMC fit of all 11 light curves jointly.

^bAdopted error from residual permutation method, if greater than the formal error; see § 2.4.3.

^cAssuming $R_* = 0.83 \pm 0.02 R_\odot$ (Santos et al., 2006) and using $R_J = 71,492$ km.

(previously noted by 2008) in both the radius ratio, k , and the total transit duration, T_{14} .

2.4.3 Systematic errors and correlated noise

One of the most apparent results from the fits to individual light curves was that the radius ratios are similar for transits observed on the same instrument and reduced by the same group. This may indicate a degree of subjectivity in the light curve generation process, both from the choice of photometry method (e.g., aperture, image subtraction, deconvolution, etc.) and from the specific choice of reduction parameters (e.g., aperture size and sky region for aperture photometry). These choices can result in systematic errors in the transit depth, particularly when comparing transits

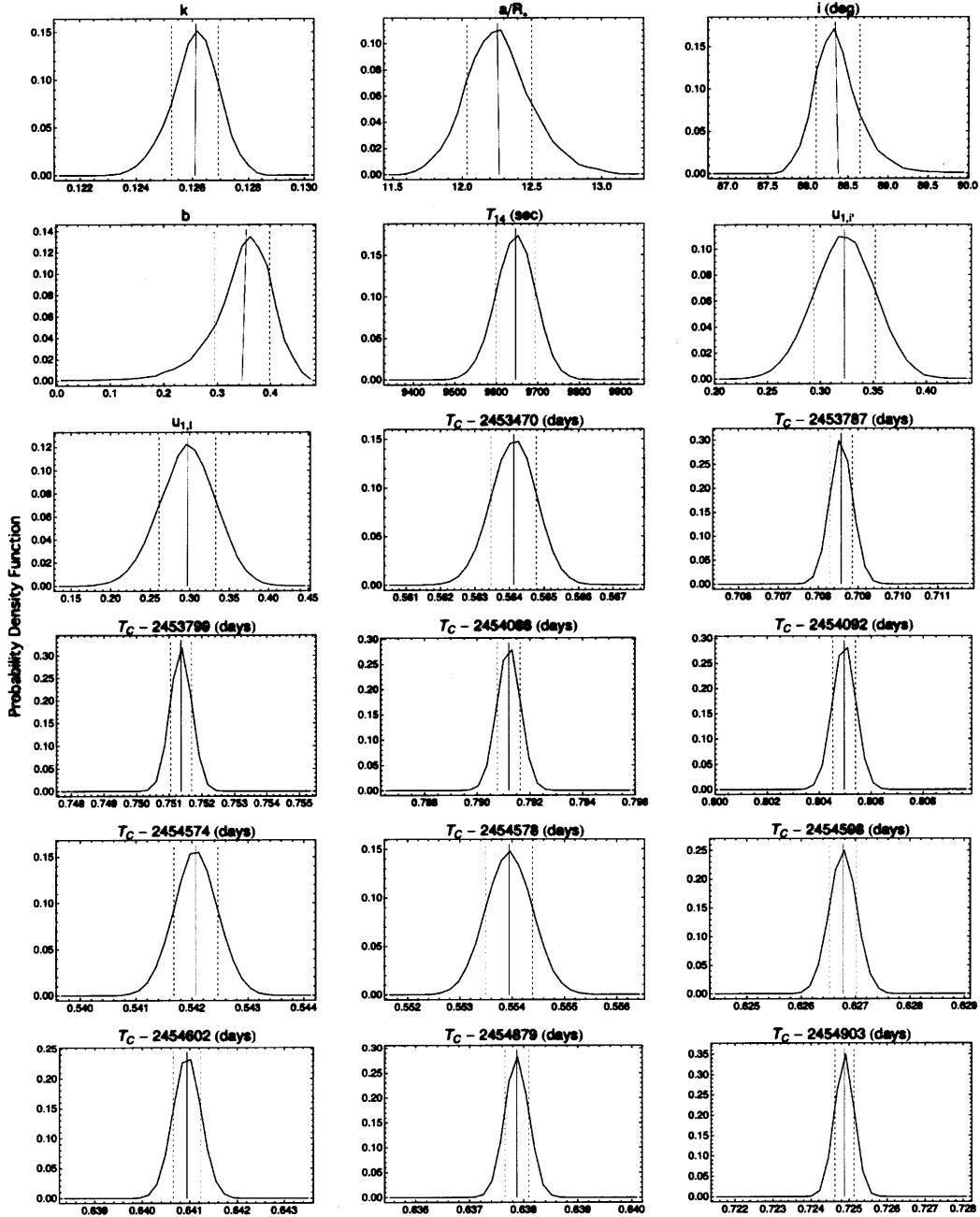


Figure 2-2 Parameter distributions for joint fit to eleven transits of OGLE-TR-111b. Smoothed histogram of normalized parameter distributions, from which the parameters in Table 2.5 are derived. The solid line is the median value (which is very close to the mean value in all cases). Note that several of the distributions, particularly a/R_* , i , and b , are not strictly Gaussian. The dashed lines show the 68.3% credible interval. These values were calculated for 2,850,000 links.

from multiple sources. Both image subtraction and aperture photometry require fine-tuning a number of parameters, and there is no single prescription for how to get the absolute best light curve: the same method applied to the same transit could produce similar quality light curves, as measured by the scatter of residuals or out-of-transit flux, which nonetheless differ in depth by more than the formal fitted errors. It has been noted by Winn et al. (2007) that with image subtraction, slight changes in both the difference flux and the reference flux can cause the measured radius ratio to vary by a few percent of its value, although their estimate of that effect on their own data, $\delta k = 0.0002$, is much less than our formal fit error of 0.0008. This effect was also alluded to by Díaz et al. (2008) as an explanation for their shallow depths compared to previous results, although they did not provide a numerical estimate of the magnitude of this effect. An analysis by Gillon et al. (2007) of a different transiting planet, OGLE-TR-132b, found that image subtraction is particularly prone to misestimating the transit depth, compared to the alternative methods of aperture and deconvolution photometry. This effect for OGLE-TR-132b in their data causes the radius ratio to differ by 1-2% depending on the choice of parameters. If similar levels of error were present for OGLE-TR-111b, particularly in the Díaz et al. (2008) curves which were acknowledged to not be optimized toward finding the correct depths, the systematic error on the radius ratio would be 0.0013 – 0.0025, comparable to the formal fit error of 0.002 on the individual curves. Assuming a median value of 0.002 for the systematic error and adding it in quadrature with the formal fit error, a better error estimate on the radius ratio would be 0.003.

We attempted to quantify the systematic error for aperture light curve generation as follows. For each of our light curves, we used 4-5 sets of apertures, sky radii and widths, and different comparison stars, with a goal toward minimizing the scatter in the out-of-transit baseline. The choice of comparison stars in particular depends on the aperture and sky choices, because certain stars are usable under some choices but not others, especially stars of very different brightnesses. Additionally, we examined the effect of detrending light curves, which must be done carefully because systematic trends in the data can distort the measured radius, but so can an incorrectly-removed

slope. We only detrended transits which had strong slopes in the out of transit baseline or otherwise had distorted shapes, and then only for the parameters which best corrected the shape defects. It is possible that residual trends against parameters we did not consider, or slightly nonlinear trends, could remain in the data and distort our estimate of the radius; we chose to stick with linear trends against a few meaningful physical parameters to avoid introducing unnecessary complexity. To test whether any important slopes remained, we ran a joint MCMC fit which includes a differential extinction term (a trend with airmass), but found that the fitted airmass slopes were slight and the difference in resulting parameters were in all cases less than the formal 1σ errors. The results of our explorations of both the aperture and sky choices and the detrending parameters are that we can produce light curves with similar shapes and scatter, and that the radius ratios vary by 0.001-0.004 for an individual transit. (Some transits are much more resilient to parameter choices than others.) Thus, for aperture photometry also the systematic error on the radius ratio based solely on the parameter choice is of order the formal fit errors.

To estimate the amount of correlated noise in the light curves, we used two methods. The first is residual permutation, which shifts the residuals for each transit through every point in time and adds it to the best model fit; we also assumed time invariance and reversed the residuals, then permuted again, for a total of 214-1600 curves for each transit. We fit a least-squares transit model to each permuted curve for all eleven transits. For the radius ratio and the transit midtime, the errors from the residual permutation method for both values were greater by a factor of 1-3, depending on the light curve (note that this factor is not the same for each parameter; see Table 2.7). We got similar results when we ran a joint fit of all 11 transits with 10,000 curve ensembles, randomly selecting for each transit one of its individually permuted light curves.

An alternative way to estimate the error contributed by correlated noise is to calculate how the noise scales with time averaging (Pont et al., 2006). We calculate the standard deviation on the residuals in bin sizes from 10-30 minutes and compare that value to what we would expect if the noise behaved like Poisson noise (i.e., a

decrease in the noise with \sqrt{N} points). We calculate the amount by which the real noise is greater than the estimated noise, and find that it is greater by a factor of 1.5-3 times the purely Poisson noise level, depending on the transit. The increased noise factors agree with the values found by residual permutation, and for simplicity we use the scaled errors from the residual permutation throughout.

For all of these reasons, the formal fit errors reported in Table 2.5 are underestimated due to both systematic errors and correlated noise. The errors we adopted have been inflated based on the residual permutation method. This means that, once systematics are included, neither the observed timing variations for 20050409 and 20080418 nor the duration variation are statistically significant (see § 2.5.1 and § 2.5.2).

2.5 Results

2.5.1 Timing

The central midtimes for all 11 transits that we fit are summarized in Table 2.5 and illustrated in Figure 2-3. Recently Pietrukowicz et al. (2010) have reanalyzed the photometry for 30 transits of OGLE planets and planet candidates, among them OGLE-TR-111b, and they have found a different midtime than originally reported in Minniti et al. (2007): $T_{C,new} = 2453470.5676 \pm 0.0005$, compared to the original published value of $T_{C,orig} = 2453470.56413 \pm 0.00067$, a difference of 300 seconds. (It is not clear what is the source of such a large shift, but one possibility is a mistake in the UTC-BJD correction.) Significantly, the new time is much closer to the expected time of transit.

Another potential pitfall when comparing times from multiple groups has recently noted by Eastman and Agol (in prep). Most researchers, and indeed most common conversion tools (e.g., *barycen.pro* in IDL and *setjd* in IRAF) by default omit the correction from UTC to TT, which in 2009 was 66.184 seconds. We have confirmed that the times published by Pietrukowicz et al. (2010) and Winn et al. (2007) do not

account for the UTC-TT correction (personal communications), and we assume that the times in Minniti et al. (2007) and Díaz et al. (2008) likely did not either. We have therefore added the appropriate correction to the reported BJD times for these light curves. (Note that the smaller order deviations introduced by using UTC rather than TT times in calculating the BJD correction terms are at most a few seconds, and for this work those deviations fall well within the timing errors; however, with higher precision data on other systems it would be very important to consistently calculate the BJD times.) All of the transit midtimes in Table 2.5 have been corrected to the BJD-TT system; additionally, we have added 64.184 seconds to the Pietrukowicz et al. (2010) midtime to get $T_C = 245470.56834$ (BJD), the value used in all subsequent calculation.

The top panel of Figure 2-3 shows the ephemeris from Díaz et al. (2008), derived from the first five transits, along with the timing residuals for all eleven transit based on our joint-fit values (Table 2.5). To correct for the linear drift in the residuals, we calculate a new constant-period transit ephemeris, omitting the half-transit (20080418), which has very large errors, and using the new Pietrukowicz et al. (2010) time for 20050409, and find:

$$T_C(N) = 2454092.80717(16)[BJD] + 4.0144463(10)N. \quad (2.2)$$

where T_C is the predicted central time of a transit, and N is the number of periods since the reference midtime, and the values in parentheses are errors on the last digits. We find almost identical ephemeris values if we use all transits and if we use the original time for 20050409, although the errors are several times greater in both cases. Our adopted fit has a reduced $\chi^2 = 0.5$.

The lower panel in Figure 2-3 shows the new ephemeris and the timing residuals. (Note that the same times are used in both panels, and only the ephemeris has changed.) With 1σ errors ranging from 36 s to 114 s, only the original 20050409 time is more than 2σ from zero, and of the other transits only the half transit 20080418, which is inherently less trustworthy, is more than 1σ . Thus, we conclude that the

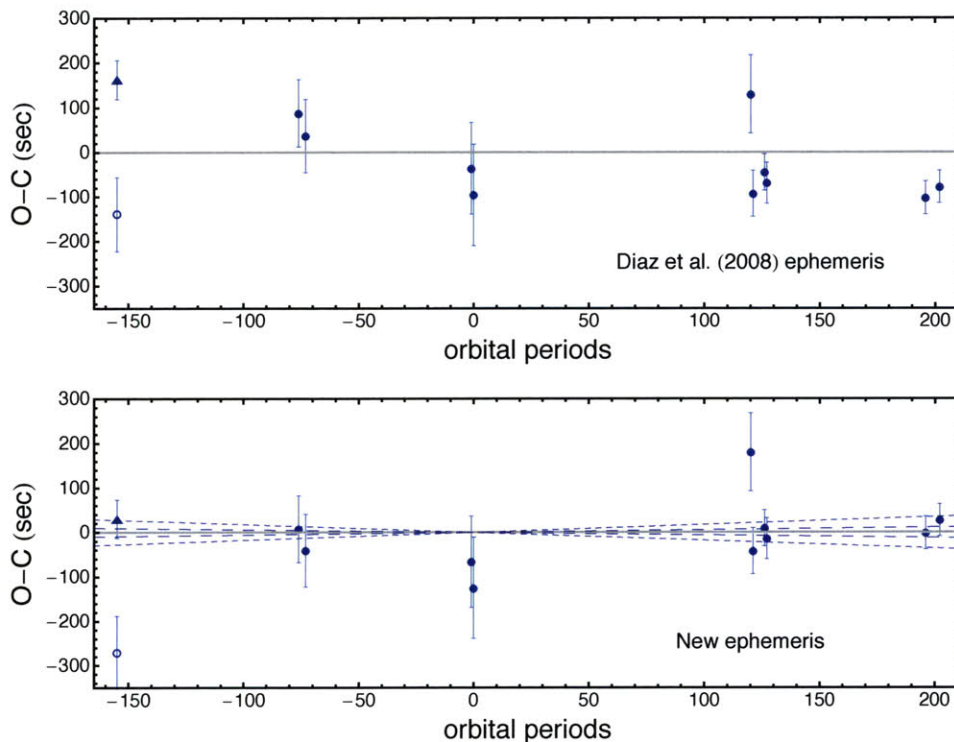


Figure 2-3 Observed minus calculated midtimes for OGLE-TR-111b. Top panel: timing residuals for eleven transits using the ephemeris from Díaz et al. (2008). Bottom panel: timing residuals using the new ephemeris (Equation 2.2). The O-C values and errors are shown in Table 2.6, and were calculated using the formal fit midtimes reported in Table 2.5 but rescaling the errors to more realistically account for systematic noise (see § 2.4.3). The solid line represents zero deviation from expected time of transit, while the dashed lines represent the 1σ and 3σ errors on the calculated orbital period, indicating the slopes that result for a mis-determined period. We plot our calculated midtime for 20050409, based on the photometry from Minniti et al. (2007), as an open circle, and the revised midtime and error reported by Pietrukowicz et al. (2010) as a solid triangle. The new ephemeris was calculated using only the solid symbols, i.e., using the Pietrukowicz et al. (2010) time.

Table 2.6. Timing residuals for OGLE-TR-111b

Transit	Number	O-C (s)	σ
20050409 ^a	-155	-271 ± 83	-3.3
20050409 ^b	-155	65 ± 43	1.5
20060221	-76	8 ± 75	0.1
20060305	-73	-41 ± 82	-0.5
20061219	-1	-66 ± 103	-0.6
20061223	0	-125 ± 114	-1.1
20080418	120	180 ± 87	2.1
20080422	121	-42 ± 52	-0.8
20080512	126	10 ± 41	0.3
20080516	127	-13 ± 46	-0.3
20090217	196	-1 ± 37	-0.02
20090313	202	28 ± 36	0.8

^aUsing our analysis of the original photometry from Minniti et al. (2007).

^bUsing the published time from reanalyzed photometry by Pietrukowicz et al. (2010).

timing deviations reported by Díaz et al. (2008), which depended heavily on the old time for 20050409, do not exist, and we see no evidence for timing variations in our data.

2.5.2 Parameter variation

Díaz et al. (2008) found that their value for the total duration was 4.4 minutes shorter than that found by Winn et al. (2007), a 1.6σ result given the respective quoted errors. If this decrease is real, it would be of great interest, since a likely explanation would be that the inclination of OGLE-TR-111b is precessing, possibly due to the presence of another planet. On the other hand, the variation could be due to errors in the photometry or undetected correlated noise. Our values for the best fit duration for each transit are plotted in Figure 2-4 and tabulated in Table 2.7, along with the parameters the duration was derived from: i , k , and a/R_* . Note that the errors in this table have been increased from the formal fit errors by a factor derived from the residual permutation method discussed in § 2.4.3.

At first glance there does appear to be a decrease in duration over time. To compare the durations of the 10 full transits (excluding 20080418) we fit the data

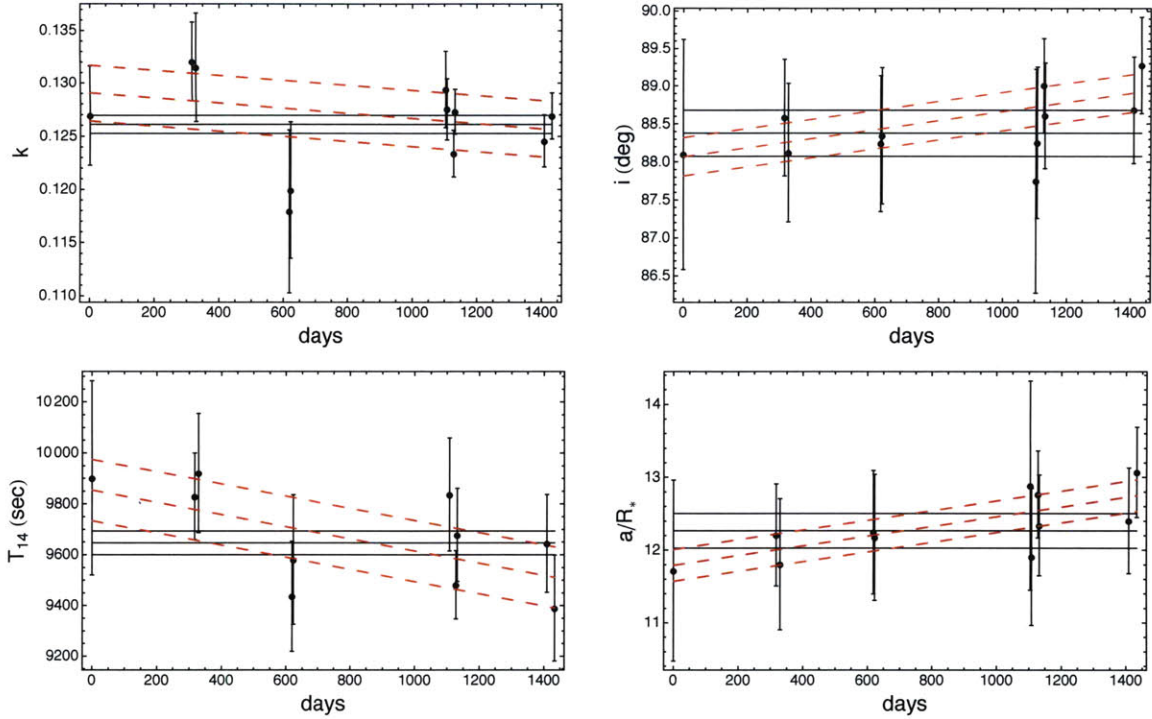


Figure 2-4 Parameter variation of individual transits of OGLE-TR-111b. Values are taken from individual MCMC fits (Table 2.7), for (clockwise, from top-left): k , i , a/R_* , and T_{14} . The errors have been scaled upward based on the factor calculated from residual permutation. The values derived from the joint MCMC fit to all transits (Table 2.5) are plotted as solid black lines with $\pm 1\sigma$ errors. The dashed red lines indicate the best sloped fit with $\pm 1\sigma$ errors, although all fits are only marginally significant (within 1σ of a constant value for the radius ratio and within 2σ for the other parameters).

using two models: (1) a flat line, corresponding to a constant duration, with reduced $\chi^2 = 0.9$, and a value of 9636 ± 58 s, very similar to the joint-transit fit value, and (2) a sloped line, with reduced $\chi^2 = 0.6$, and a slope of -0.24 ± 0.12 seconds per day. This is a much shallower slope than the hint of a trend reported by Díaz et al. (2008), and is not significant given the good fit achieved with the flat line.

Because the duration is a derived quantity, we must examine the parameters on which it depends (i , a/R_* , and k). Both the inclination and the semi-major axis exhibit slight slopes, but with low significance given the errors (i changes by 0.22 ± 0.09 degrees per year with reduced $\chi^2 = 0.2$, and a/R_* by 0.0007 ± 0.0002 stellar radii per year with reduced $\chi^2 = 0.2$). If the duration were really decreasing because the

Table 2.7. Individual transit parameters for OGLE-TR-111b (independently fit)

Transit	k^a	f^b	T_{14}^a	f^b	a/R_\star^a	f^b	i^a	f^b
20050409	0.127 ± 0.0047	1.0	9901 ± 381	...	11.7 ± 1.2	1.1	88.1 ± 1.5	1.3
20060221	0.132 ± 0.0038	2.0	9829 ± 170	1.2	12.2 ± 0.7	1.4	88.6 ± 0.8	1.1
20060305	0.132 ± 0.0051	3.2	9920 ± 234	1.6	11.8 ± 0.9	1.6	88.1 ± 0.9	1.4
20061219	0.118 ± 0.0076	3.1	9436 ± 217	1.0	12.2 ± 0.8	...	88.2 ± 0.9	...
20061223	0.120 ± 0.0064	1.8	9580 ± 255	1.2	12.2 ± 0.9	1.1	88.3 ± 0.9	...
20080418	0.129 ± 0.0036	1.2	8646 ± 1413^c	3.2	12.9 ± 1.4	1.8	87.7 ± 1.5	2.5
20080422	0.128 ± 0.0029	1.2	9837 ± 222	...	12.9 ± 0.9	1.2	88.3 ± 1.0	1.1
20080512	0.123 ± 0.0022	1.9	9482 ± 134	1.5	12.8 ± 0.6	1.5	89.0 ± 0.6	1.0
20080516	0.127 ± 0.0021	1.5	9677 ± 183	1.4	12.3 ± 0.7	1.3	88.6 ± 0.7	...
20090217	0.125 ± 0.0025	2.2	9644 ± 193	1.9	12.4 ± 0.7	1.6	88.7 ± 0.7	1.1
20090313	0.127 ± 0.0022	1.9	9390 ± 209	2.7	13.0 ± 0.6	2.2	89.2 ± 0.6	1.3

^aFormal individual MCMC fit value and error (scaled upward by factor f in adjacent column).

^bAmount by which the error in the previous column has been increased due to excess error from the residual permutation method over the MCMC fits. No value is given if the formal fit error was larger and was used instead. See § 2.4.3.

^cThe ill-constrained duration of the half-transit 20080418 was not used in any fits.

planet is precessing, this would be due to the planet moving away from the center of the stellar disk and hence the inclination would decrease; instead, the best-fit slope for the inclination is slightly positive, another indication that we are not picking up on a real effect.

On the other hand, the radius ratio does have real variations between transits, given the current photometry. We find variation from a low of $k = 0.118 \pm 0.002$ (transit 20061219, from Díaz et al., 2008) to a high of $k = 0.132 \pm 0.002$ (20060221 and 20060305, both from Winn et al., 2007), with the rest of the transits in between (see Table 2.7). (Note that our individual fits for the radius and error of the two transits from Winn et al. (2007) agree with those cited in that paper, indicating that our fitting methods are comparable.) The best fit line with a slope is not statistically significant (within 1σ of 0), and the most likely explanation of the variation in radius depths is due to systematic effects in how the photometry was reduced (see § 2.4.3).

If the star were active, the presence of stellar spots or active regions can affect the observed radius depths (see e.g.. Pont et al. (2008) for HD189733, Rabus et al. (2009) for TrES-1, and Czesla et al. (2009); Huber et al. (2009); Silva-Valio et al. (2010) for CoRoT-2, all of which are known or theorized to be spotty stars). There is no record

of variability for this star in the current literature. We examined two published data sets with observations over multiple non-transit nights: 4 nights of VIMOS data (Pietrukowicz et al., 2010; Minniti et al., 2007) and data spanning 115 nights from the OGLE survey Udalski et al. (2002b). We found that the long-term flux was stable to within a few mmag in both datasets (3 mmag and 5 mmag respectively).

Since the trends in the parameters i , a/R_* , and k are slight and unlikely to be physical, we cannot conclude based on the available data that the observed duration variation is a real effect.

2.5.3 Limits on perturber mass

Although there is no clear evidence of TTVs beyond the 2σ level in the current dataset, we can use the TTVs reported in Table 2.6 and shown in Figure 2-3 to place upper limits on the mass and orbital separation of a hypothetical perturbing planet in the system. For that purpose we use an implementation of the algorithm presented in Steffen & Agol (2005), kindly provided by D. Fabrycky.

We explored the full perturber’s mass parameter space for interior orbits and exterior exterior orbits for orbital periods from 0.9-17.5 days (0.2-4.4 times the orbital period of OGLE-TR-111b), and small initial eccentricity $e_c = 0.05$ (we also examined $e_c = 0$ and $e_c = 0.3$). All the orbits were assumed coplanar and the orbital instability regions in each case were determined following Barnes & Greenberg (2006). The orbital period of the perturber was increased by a factor of 1.1 for each step. For each period, the mass of the perturber also increased from an initial value of $0.0001 M_\oplus$ until reaching a mass that would produce a TTV equivalent to the 3σ confidence level of our results (i.e. $\Delta\chi^2 = 9$). We used the time reported by Pietrukowicz et al. (2010) for the transit 20050409 instead of the value we fit from the original photometry from Minniti et al. (2007), since the revised value is more in line with expectations; simulations run omitting that transit yield similar results. The mass limits placed by these tests are illustrated in Figure 2-3.

The constraints placed on the perturber’s mass are strongest near the low-order mean motion resonances, particularly in the interior and exterior 2:1 resonances,

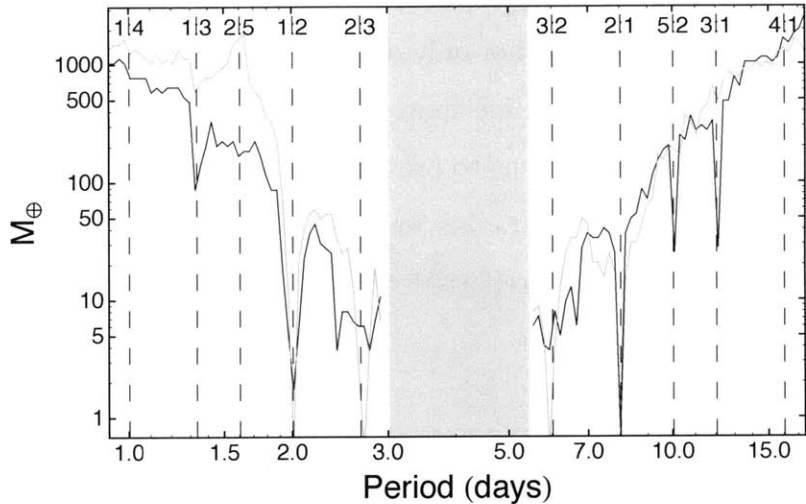


Figure 2-5 Upper mass limit on companions to OGLE-TR-111b. We examined companions with initial $e_c = 0.05$ (black) and $e_c = 0.0$ (gray). The constraints are strongest near the 2:1 mean-motion resonance, where objects as small as $1 M_\oplus$ would have been detectable; other interior and exterior resonances are also labeled. The shaded grey region shows the instability region for a $1 M_\oplus$, following Barnes & Greenberg (2006).

where we are sensitive to objects as small as $1 M_\oplus$ and $0.6 M_\oplus$, respectively if $e_c = 0.05$ ($e_c = 0$ yields even smaller constraints, but we choose to cite the more conservative value). No meaningful constraint can be placed on the region of the 4:1 external resonance, which was identified by Díaz et al. (2008) as a possible location for a $1 M_\oplus$ perturber that could explain their TTV, but since we do not reproduce their TTV such a perturber is no longer necessary.

Finally, our O-C data, with a 1σ precision of 36-114 seconds (after accounting for systematic errors), cannot constrain the presence of moons around OGLE-TR-111b, which would introduce a TTV signal of 4.6 seconds for a $1 M_\oplus$ moon (Kipping et al., 2009).

2.6 Conclusions

We have tested the previously claimed presence of TTVs and TDVs in the OGLE-TR-111 system by adding six new transit epochs, observed between 2008 and 2009, to

the five previously published results by Winn et al. (2007); Minniti et al. (2007); Díaz et al. (2008). This new analysis not only doubles the number of available data points, but also extends the TTV baseline from two to four years. In addition, combining the six new transits data allows us to provide a new, more precise value of the radius of this planet. We find a new radius for the planet of $1.019 \pm 0.026 R_J$, which is intermediate to the previously reported radii by Winn et al. (2007) and Díaz et al. (2008), and is more precise.

We find a slight variation over time of the duration of the transits of OGLE-TR-111b, as well as variations of other parameters, such as the inclination and semimajor axis of the orbit. Those variations could, in principle, be attributed to perturbations of the orbit of OGLE-TR-111b produced through interaction with additional planet(s) in the system, but we demonstrate that the variations can be instead explained by systematic errors in the data, and therefore should not be attributed to other planets.

We have also computed the transit midtimes of our new transits with formal precisions of 20-40 seconds, and more accurate precisions of 35-50 seconds for the full transits (and almost 2 minutes for the half-transit) once systematic errors are considered. The errors on the literature transits similarly increased when the photometry is refit using the same method to account for systematics, to 60-110 seconds depending on the light curve.

A longer time baseline and more precise timing data is still necessary to test further for the presence of other planets in the OGLE-TR-111 system, especially in potentially stable non-resonant orbits, but with the present results we conclude that OGLE-TR-111 belongs in the category of systems summarized in Table 2.1 for which there is no sign of additional planets more massive than a few M_\oplus in low-order resonant orbits, including a limit of 1 M_\oplus near the 2:1 resonances. The presence of massive (Earth-like) moons around OGLE-TR-111b is still possible, but to detect those we would require timing precision of a few seconds or better, beyond the current capability of ground-based instrumentation for this system.

2.7 Acknowledgements

E.R.A. received support from NASA Origins grant NNX07AN63G. M.L.M. acknowledges support from NASA through Hubble Fellowship grant HF-01210.01-A/HF-51233.01 awarded by the STScI, which is operated by the AURA, Inc. for NASA, under contract NAS5-26555. We would like to thank Brian Taylor and Paul Schechter for their tireless instrument support. We thank the Magellan staff, in particular telescope operators Jorge Araya, Mauricio Martinez, Hernàn Nuñez, Hugo Rivera, Geraldo Valladares, and Sergio Vera, for making these observations possible. We also thank Josh Carter and Dan Fabrycky for providing software, and Josh Winn for some helpful discussions.

Chapter 3

Eleven New Transits of OGLE-TR-56b

A version of this chapter will be submitted to ApJ as "Eleven New Transits of OGLE-TR-56b", Adams, E. R., Lopez-Morales, M., Elliot, J. L., Seager, S., & Osip, D. J., 2010.

3.1 Abstract

We present eleven new transits of the exoplanet OGLE-TR-56b observed with the Magellan Telescopes in Chile between 2006 June and 2009 July; previously, only a single high quality light curve, from 2006 July, was available (Pont et al., 2007). We derive a new planetary radius value of $1.33 \pm 0.06 R_J$, which is almost identical to the previously reported radius, and the error is mostly due to error on the stellar radius. Although the radius values agree well, the shapes of the new light curves (observed in Sloan i' or similar) are significantly different from the shape of the Pont et al. (2007) light curve (observed in R and V bands), and the differences in shape are not attributable solely to different limb darkening. We present new system parameters for the semi-major axis, $a = 0.0191 \pm 0.0009$ AU, the inclination, $i = 74.0 \pm 0.4^\circ$, and the transit's total duration, $T_{14} = 7823 \pm 88$ s. The midtimes of the new eleven transits have errors between 28-147 seconds, and show no clear indications of timing variations

relative to each other, although their predicted midtimes are about five minutes later than the times predicted by previous transit ephemerides. We recalculate a new ephemeris using only our transits, and find that only one (20090612) deviates by more than 3σ from expected, with a residual of -97 ± 28 s. We can place an upper limit on companion masses of $10M_{\oplus}$ near the 2:1 and 3:2 interior and exterior mean motion resonances.

3.2 Introduction

OGLE-TR-56b was the second transiting exoplanet discovered after HD209458b (Charbonneau et al., 2000; Henry et al., 2000), and the first one found by a photometric wide-field survey (Udalski et al., 2002c). The planetary nature of this object was confirmed by Konacki et al. (2003a), who derived a mass of $1.3M_J$ from radial velocity measurements of the host star. In spite of being a relatively faint target ($V = 16.56$, $I = 15.3$), the physical parameters of the OGLE-TR-56 system have slowly improved in the past few years with follow-up radial velocity measurements by Torres et al. (2004) and Bouchy et al. (2005); the determination of the host star’s fundamental parameters and chemical composition by Santos et al. (2006); and more recently the detection of OGLE-TR-56b’s atmosphere by Sing & López-Morales (2009). The radius of the planet, however, is currently constrained by only two light curves: the composite discovery curve in I from OGLE (Udalski et al., 2002c), and a single light curve in 2006 observed alternately in Bessel R and V filters (Pont et al., 2007). OGLE-TR-56b has also been identified by Southworth (2008) as a system where the precision of the planetary parameters is limited by the available photometry, and new light curves are needed.

In addition to the transit timing variations (TTVs) and transit duration variations (TDVs) mentioned in Chapter 2, we can search for changes in the orbital period to test for orbital decay. Because OGLE-TR-56b, with a period of just 1.2 days, is so close to its star, it has been the subject of several analyses for the time scale over which orbital decay could be seen (Sasselov, 2003; Pätzold et al., 2004; Carone & Pätzold, 2007;

Levrard et al., 2009). The estimates vary greatly due to different model assumptions and uncertainties and poorly constrained physical parameters (e.g., estimates for stellar tidal Q span five orders of magnitude; Pätzold et al., 2004). Models that rely on dissipation by turbulent viscosity generally find lifetimes of a few billion years. Sasselov (2003) estimated the orbital period would change by $\dot{P} = 2 \text{ ms yr}^{-1}$ (with large errors spanning $0.1\text{--}5 \text{ ms yr}^{-1}$, depending on model choices; the observationally-derived model estimates the remaining lifetime at 0.77 Gyr). Pätzold et al. (2004) and Carone & Pätzold (2007) find a longer lifetime, and estimate that OGLE-TR-56b will spiral into the Roche limit of the star in 3-3.5 Gyr, but there are many uncertainties in their model. Recently, Levrard et al. (2009) has challenged the assumption that stable or unstable tidal equilibrium modes are applicable, and finds that almost all transiting planets are doomed to fall into their stars, and some relatively soon. OGLE-TR-56b will be one of the first to go, in 7 Myr assuming $Q_* = 10^6$. (This timescale could be between 0.7 Myr to 70 Gyr for Q between 10^5 and 10^{10} .) For comparison, the lifetimes of the other OGLE planets (again assuming $Q = 10^6$) are estimated at 52 Myr for OGLE-TR-132b, 98 Myr for OGLE-TR-113b, 2.2 Gyr for OGLE-TR-10b, and a relatively safe 23.5 Gyr for OGLE-TR-111b. Observationally, the estimates for the decrease in the period due to orbital decay range from 0.1 to 10 ms yr^{-1} . The upper limit is only a few times smaller than the error on the period (86 ms from Pont et al., 2007). Hence, with three years' worth of precisely timed transits we are building up the data needed to start testing for orbital decay.

Here we present eleven new transits of OGLE-TR-56b observed from 2006 to 2009, which we use to improve the radius determination of the planet and also to study for the first time potential timing anomalies in this system. In § 3.3 we describe the collection and analysis of the data. In § 3.4 we describe the transit model fitting, and discuss additional sources of error not included in the formal fit. In § 3.4.3 we discuss the shape differences between the new i' light curves and the previously published R , V light curves. Finally, in § 3.5 we discuss the implications of our results.

3.3 Observations and data analysis

All eleven new transits were observed between 2006 June and 2009 July. Three instruments were used: POETS (2 transits), IMACS (1 transit), and MagIC-e2v (8 transits).

POETS (Portable Occultation, Eclipse, and Transit System) was installed on Magellan as a visiting PI instrument during 2006 June-July. The camera is a frame-transfer CCD which can be GPS triggered; for more details on the system see Souza et al. (2006). On the Clay telescope, it has a field of view of $23''$ and a plate scale of $0.''046$ per pixel. For the two transits observed, POETS was operated full-frame (no binning) in conventional mode with a gain of $3.4 \text{ e-}/\text{ADU}$ and read noise of 6 e- . The POETS filter used was Schuler Astrodon Johnson-Cousins I_s^1 .

One transit was observed in 2007 with the Inamori Magellan Areal Camera and Spectrograph (IMACS) on the Baade telescope (Dressler et al., 2006). We used the $f/4$ imaging mode with a subraster on one of the eight CCDs (chip 2), reading out only 1200×1200 pixels centered around $x=1080$ and $y=3015$, in order to decrease the readout time to roughly 35 seconds per frame in FAST mode. This chip has a gain of $0.9 \text{ e-}/\text{ADU}$ and read noise of 4.6 e- . We used a wideband filter, WB6300-9500, which is approximately centered on the same waveband region as Sloan i' but twice as wide.

Between January 2008 and December 2009, the Magellan Instant Camera (MagIC) was been mounted on the Baade. The MagIC-e2v detector, which shares a dewar with the older SiTe CCD, is identical to the red CCD on HIPO, a fast read-out direct imaging camera and one of the first generation instruments to be flown on SOFIA; both cameras use the LOIS control software (Dunham et al., 2004; Taylor et al., 2004; Osip et al., 2008). All of the MagIC-e2v transits were taken in the Sloan i' filter. The MagIC-e2v camera has a field of view of $38'' \times 38''$ and a plate scale of $0.''037$ per pixel unbinned. The camera can be operated in two different modes: single exposure mode, with a readout time of about 5 seconds per exposure, and frame transfer

¹Transmission curve: http://occult.mit.edu/_graphics/POETS/filters/SchulerJCfilterchart.jpg

mode, with a readout time of only 3 milliseconds between frames in an image cube. Three transits were observed in single exposure mode. The frame transfer mode first became available after engineering in July 2008, and was used for the last five transits of OGLE-TR-56b. The gain and read noise of the first four transits were 2.4 e-/ADU and 5.5 e- per pixel, respectively, and two amplifiers were used during readout; after July 2008, these values were changed to the current values of 0.54 e-/ADU and 5 e- per pixel, using only a single amplifier.

For our first transits with POETS, a very rapid cadence (2-4 s per exposure) was used in an effort to well-sample the transit ingress and egress. However, the noise per frame was such that we chose to bin every 10 and 8 frames for 20060622 and 20060714, respectively. For the rest of the transits, the exposure times were adjusted to maintain roughly 10^6 integrated photons on both for the target and multiple nearby comparison stars. Exposure times for unbinned (1x1) data ranged from 17-60 sec, and for binned data from 10-60 sec. Details of the observing settings are noted in Table 3.1.

Accurate timing is of the utmost importance for this project, so special care was taken to ensure that the correct times were recorded in the image headers. For the transits observed with POETS in 2006, each image frame was triggered by a GPS, so the UTC start times are accurate to the microsecond level. For the IMACS 2007 and MagIC-e2v 2008 transits, the UTC start times for each image were recorded from a network time server, which was verified by eye to be synchronized with the observatory's GPS clocks at the beginning of each night. For the MagIC-e2v 2009 observations, the times came from a small embedded control computer (a PC104), which received unlabeled GPS pulses every second. As with the network time server, the PC104 was synchronized with the observatory's GPS before each transit observation. In both cases the UTC time signals written to the image headers agree within one second with the GPS time, as verified by examining the system control logs.

Table 3.1. Observational and photometry parameters for OGLE-TR-56b

Transit (UT)	N_{Frames} used (discarded)	Exp. time (sec)	Filter	Binning	Readout (sec)	N_C^a	Aperture ^b (pixels)	Sky radius, width (pixels)	Scatter ^c (mmag)
20060622	6642 (121) ^d	2	Is	1x1	5	5	12.5 ^e	– ^f	1.0
20060714	2200 (588) ^g	4	Is	1x1	5	2	8.2	30, 10	1.7
20070830	352 (1) ^h	15, 30	WB ⁱ	1x1	25	3	7.6	20, 20	1.1
20080514	187 (0)	60	<i>i</i> '	1x1	5	5	14.5 ^e	– ^j	0.6
20080612	604 (64) ^k	17, 20	<i>i</i> '	1x1	5	5	12.2	50, 10	0.9
20080727	672 (0) ^l	10,12	<i>i</i> '	2x2	5	3	9.0	25, 30	1.3
20090504	623 (2) ^l	23, 25	<i>i</i> '	2x2	0.003 ^m	2	8.2	20, 30	1.1
20090510	460 (2) ^h	20, 30	<i>i</i> '	2x2	0.003 ^m	3	7.8	40, 10	1.0
20090612	772 (3) ^h	17, 20	<i>i</i> '	2x2	0.003 ^m	5	8.2	30, 10	0.8
20090613	715 (0)	20	<i>i</i> '	2x2	0.003 ^m	3	10.2	25, 10	1.1
20090728	535 (5) ^h	30-60	<i>i</i> '	2x2	0.003 ^m	2	8.2	15, 20	1.2

^aNumber of comparison stars

^bRadius around star, except as noted.

^cStandard deviation of the residuals on data binned to 120 s.

^dDiscarded during meridian crossing (images elongated).

^eBox half-width.

^fSky is not measured from an annulus around each star but rather from a single 30 pixel box centered 2.1'' west and 0.1'' south of the transiting planet host star.

^gDiscarded baseline after transit at a different pointing, which did not return to the same ratio level as before.

^hAnomalous ratios, e.g. due to poor seeing on one or more frames

ⁱWB6300-9500, a wideband filter from 630-950 nm.

^jSky is not measured from an annulus around each star but rather from a single 20 pixel box centered 2.0'' east and 0.3'' south of the transiting planet host star.

^kLow initial counts on target (50 points) and seeing spike (14 points).

^lDiscarded all frames with large target diameters (poor seeing): >11.5 pixel (20080727) and >11.0 pixel (20090504)

^mFrame transfer mode used.

3.3.1 Data analysis

All data were calibrated using IRAF.² The zero level for POETS and IMACS transits were calculated from bias frames taken before or after the transits, while the MagIC-e2v transits were corrected using overscan regions on each image. The images were flat-fielded using either dome or twilight flats in the appropriate filter, as available. Most of the light curve photometry was generated using the IRAF routine *phot*, part of the *apphot* package, using the process described in Chapter 2, with the apertures explored and the comparison stars used varied depending on the nightly conditions (e.g., seeing) and specific field of view. For some transits, an alternative aperture photometry method was used. In this method, boxes were drawn around the target and comparison stars, and the sky was determined using a single box drawn around an empty region of sky (not easy to find in this crowded field). This method, as implemented in *Mathematica*, is both slower and not as robust as IRAF's *phot*, particularly for data sets in which the stars shifted by more than a few pixels; but for two transits (20060622 and 20080514) it produced lower out-of-target scatter and cleaner light curves. We additionally explored using image subtraction photometry for one transit, 20090504, and produced a light curve with slightly superior scatter compared to the aperture light curve (1.0 vs 1.1 mmag in 2 min), but the depth of the image-subtracted light curve is much shallower ($k = 0.092 \pm 0.002$) than the aperture light curve for either the individual fit for that light curve ($k = 0.102 \pm 0.002$) or the joint fit ($k = 0.104 \pm 0.002$). Problems with the depth have been noted previously with image subtracted light curves (see discussion in Adams et al., 2010). We used aperture photometry to make all of the light curves for OGLE-TR-56b.

We examined each of the final light curves for linear trends in the out-of-transit flux against several variables: airmass, seeing, telescope azimuth, (x, y) pixel location, and time since beginning of transit. These parameters were chosen because they are either directly correlated with photometric trends (e.g. seeing, airmass), or are proxies

²IRAF is distributed by the National Optical Astronomy Observatories, which are operated by the Association of Universities for Research in Astronomy, Inc., under cooperative agreement with the National Science Foundation.

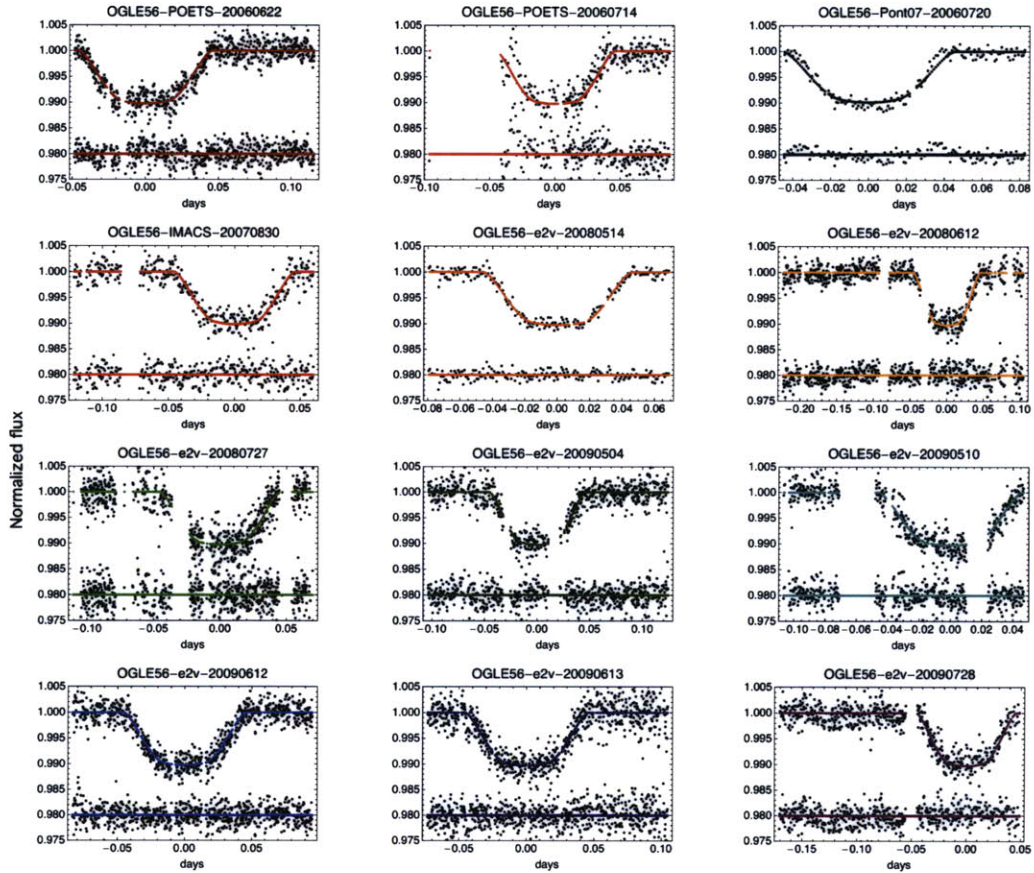


Figure 3-1 Twelve transits of OGLE-TR-56b (full data with residuals). The black curve (third from left) is from Pont et al. (2007); the rest are new transits. All available high-quality light curves are plotted unbinned (except for 20060622 and 20060714, which have been binned to 20 and 32 second bins, respectively), along with the joint model fit (solid lines). The residuals from the joint fit are plotted below; note the excellent agreement with the model in all cases except 20060720 (see § 3.4.3).

Table 3.2. Flux values for new transits of OGLE-TR-56b

Mid-exposure (UTC) ^a	Mid-exposure (BJD)	Flux	Error
2453908.670845	2453908.677416	1.002203	0.001641
2453908.670868	2453908.677439	1.007551	0.001641
2453908.670891	2453908.677462	0.9947374	0.001641
2453908.670914	2453908.677485	1.003771	0.001641
2453908.670937	2453908.677508	0.9926688	0.001641
...			

^aFull table available online.

for other effects that may be harder to measure (e.g. the telescope azimuth, which is a major component in the de-rotator rates, which were not recorded in the headers of all transit files). We fit for and removed linear trends from three transits: slight slopes in the flux over time for 20070830 and 20090504, and a slope with seeing for 20080727. See § 3.4 for a description of the fits we performed to search for additional trends in the system.

We now briefly describe the observations and the photometric reduction of each transit dataset. All transit fluxes and times are available on request; an excerpt is shown in Table 3.2. We also plot the full data for each transit in Figure 3-1 with the residuals from the best model plot; Figure 3-2 shows each transit binned to two minutes for comparison. See Appendix A for an image showing the regions used for aperture photometry on a sample night (20080516).

20060622

The first of two transits observed using POETS, transit 20060622 was observed with very short exposure times (2 s), although the curves were binned to 20 s before fitting. Conditions on 20060622 were excellent, with seeing between 0."25-0."5. The best photometry was found using a 20 pixel square box (using the alternative photometry method implemented in Mathematica), a 30 pixel square sky box, and 5 comparison stars.

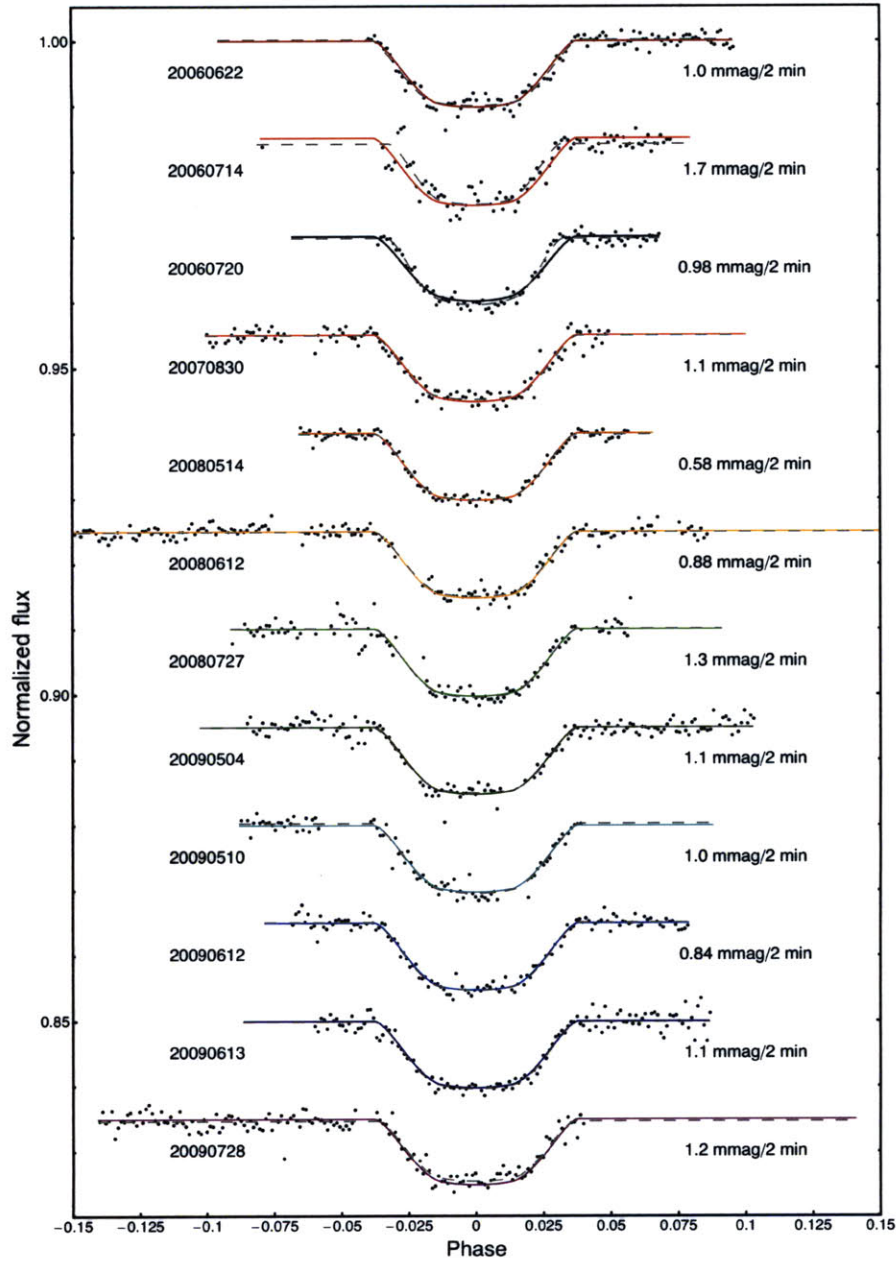


Figure 3-2 Twelve transits of OGLE-TR-56b. The black curve (third from top) is from Pont et al. (2007); the rest are new transits. All available high-quality light curves are plotted binned to 2 minutes to aid comparison. We show the joint model fit (solid lines), which was calculated using the parameter values in Table 3.3, and the individual transit model fit to each light curve separately (dashed lines), with parameters shown in Table 3.4; note that these models are almost indistinguishable except for transits 20060714 and 20060720 (see Section 3.4.3). We also report the standard deviation of the residuals from the joint model fit. Table 3.2 shows the unbinned data; a full table can be provided on request.

20060714

The second of two transits observed using POETS, transit 20060714 was also observed with short exposure times (4 s), although the curves were binned to 32 s before fitting. The seeing on 20060714 was again excellent, between 0."25-0."5, though the transparency was much more variable, and longer exposures were needed to reach the same counts as on 20060622. The best photometry was with an 8.2 pixel radius and a sky region of 30+10 pixel, with 2 comparison stars.

20070830

The only transit observed with IMACS, transit 20070830, had median seeing of 0."6 and stable conditions. The best photometry was with a 7.6 pixel radius and a sky region of 20+20 pixels, with 3 comparison stars. A trend against time was removed from the photometry before fitting.

20080514

The night of 20080514 was anomalously good, with very stable photometric conditions and 3 transits of different planets observable sequentially. (We will report on OGLE-TR-113b in Chapter 4 and OGLE-TR-10b in Chapter 5.) OGLE-TR-56b, the middle transit, had great seeing (never more than 0."4), and the best noise of any transit of OGLE-TR-56b available (0.6 mmag in 2 min). The best photometry was found using a 29 pixel box (using the alternative photometry method implemented in Mathematica), a 20 pixel sky box, and 5 comparison stars, though we note that the photometry derived using *phot* was also excellent.

20080612

Transit 20080612 was observed for almost nine hours under good seeing conditions (0."3-0."5). The best photometry was with a 12.2 pixel radius and a sky region of 50+10 pixel and 5 comparison stars. No trends were seen with airmass despite the long baseline.

20080727

Transit 20080727 was observed under under stable conditions, with seeing of 0."7 throughout and airmass ranging from 1-1.3. Much of ingress was lost due to an ill-timed crash of the LOIS instrument software, and a similar glitch occurred shortly after egress. The best photometry was with a 9.0 pixel radius and a sky region of 25+30 pixel and 3 comparison stars. A trend against seeing was removed from the photometry before fitting.

20090504

Transit 20090504 was observed with highly variable and often poor ($> 1''$) seeing during the first half of transit, although conditions later improved to 0."5. The airmass ranged from 1-1.2. The best photometry used two comparison stars and an 8.2 pixel radius and a sky region of 20+30 pixel and 2 comparison stars. A trend against time was removed from the photometry before fitting.

20090510

Transit 20090510 was observed under under stable conditions, with seeing of 0."7 throughout and airmass ranging from 1-1.3. Gaps in the data were due to accommodating other observing projects. The best photometry was with a 7.8 pixel radius and a sky region of 40+10 pixel and 3 comparison stars.

20090612

Transit 20090612 was observed under excellent conditions, with seeing of 0."4-0."7 throughout and airmass ranging from 1-1.3. The best photometry was with an 8.2 pixel radius and a sky region of 30+10 pixel, using 5 comparison stars.

20090613

Transit 20090613 was observed under good conditions, with somewhat variable seeing from 0."6-0."8 and airmass ranging from 1-2. The best photometry was with a 10.2

pixel radius and a sky region of 25+10 pixel, using 3 comparison stars.

20090728

Transit 20090728 was observed under highly variable conditions, with seeing ranging from 0."4-0."9 and airmass from 1-1.2. The best photometry was with an 8.2 pixel radius and a sky region of 15+20 pixel, using 2 comparison stars.

Literature light curves

The only published high-quality light curve for OGLE-TR-56b is from Pont et al. (2007), which was observed in both R and V , with alternating sequences of 7-8 exposures in each filter. As was done in the original analysis, we have combined both filters into a single light curve; experiments with fitting each filter individually yield similar light curve parameters for both, but with larger errors. We have used the original photometry and times, except for adding an extra UTC-TT factor of 65.184 seconds, which might have been missing in the original conversion, as noted by J. Eastman and E. Agol (2010, in preparation); however, since we do not end up using the transit time for this light curve the extra factor is irrelevant to our timing conclusions. We have also calculated the timing residuals for the original OGLE midtime (plus an additional 64.184 s), which is a composite light curve from 13 partial transits and data spanning several hundred nights (Torres et al., 2004; Udalski et al., 2002c); we have not refit the OGLE photometry and do not use it for our new ephemeris.

3.4 Transit fitting results

3.4.1 Model

Our transit model fits use the algorithm of Mandel & Agol (2002) and are described in more detail in Chapter 2. We assumed that OGLE-TR-56b has zero obliquity, oblateness and orbital eccentricity. The initial parameters for u_1 and u_2 were set to

the ATLAS values for the appropriate filter (Claret, 2000, 2004)³. In all transits we found it necessary to fix the quadratic term u_2 and only fit for the linear term, u_1 ; we additionally fixed the linear term for filters used by only a single transit (20060720 and 20070830). The values for u_1 and u_2 are calculated assuming $T = 6119$ K, $\log g = 4.2$, $[M/H] = 0$, and $V_{micro} = 2$ km/s. We used the Sloan i' filter for the MagIC-e2v data and the POETS data (actually taken with a Schuler Astrodon I_s filter, but the coefficients are very similar), a linear combination of the limb darkening coefficients for V and R for 20060720, and, for lack of a better alternative, the Sloan i' filter for 20070830, although the actual wide band filter used, WB6300-9500, is about twice as wide. We fixed the orbital period to $P = 1.211909$ days; later experiments with slightly different values had little effect. The other free parameters in the model are the radius ratio, k , inclination, i , semimajor axis in stellar radii, a/R_* , out-of-transit flux, F_{OOT} and transit midtime, T_C . We assume throughout the fits that $M_* = 1.17 \pm 0.04 M_\odot$, $R_* = 1.32 \pm 0.06 R_\odot$, and $M_p = 1.29 \pm 0.11 M_J$, based on Pont et al. (2007) and Torres et al. (2004).

3.4.2 Light curve fits

Each light curve was fit both independently and jointly with all other light curves using the Monte Carlo Markov Chain (MCMC) method described in Chapter 2. The distributions for each fitted parameter are shown in Figure 3-3. To estimate the errors that might be due to correlated noise, we used the residual permutation method on the individual light curves, and randomly selected a 10,000 subsets of permuted residuals for each curve to perform a joint light curve fit. We adopted the greater of either the residual permutation error or the formal MCMC error. The excess values from residual permutation roughly correspond to the values from examining the time-averaged residuals, which independently estimate that the light curves are above Poisson noise statistics by a factor of 1.1-2.8.

To account for errors introduced by removing slopes, we performed MCMC fits

³Initial values: $u_{1,I} = 0.1958$, $u_{2,I} = 0.3561$, $u_{1,i'} = u_{1,WB} = 0.2146$, $u_{2,i'} = u_{2,WB} = 0.3569$, $u_{1,VR} = 0.3157$, $u_{2,VR} = 0.35265$.

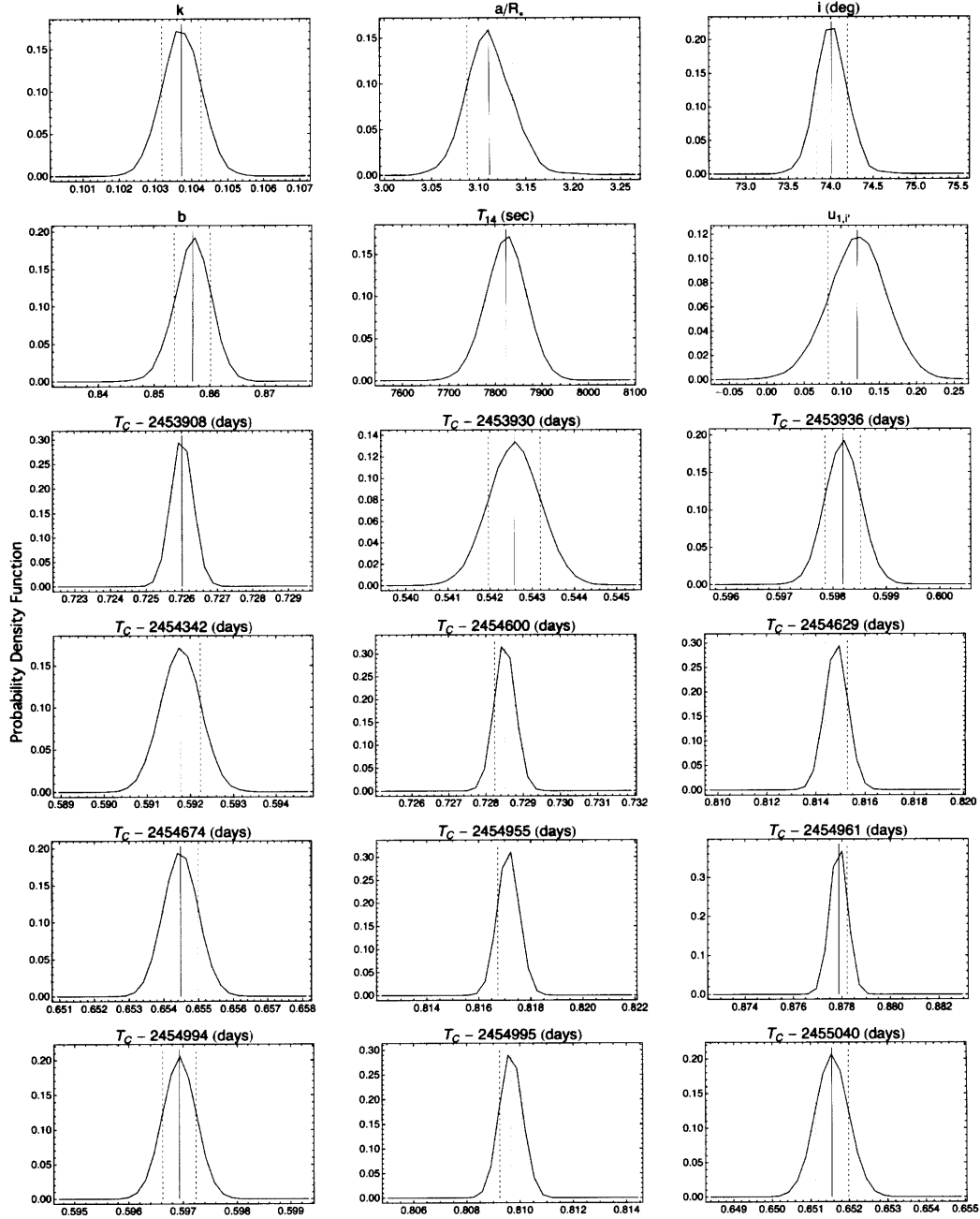


Figure 3-3 Parameter distributions for joint fit to twelve transits of OGLE-TR-56b. Smoothed histogram of parameter distributions, from which the parameters in Table 3.3 are derived. The solid line is the median value (which is very close to the mean value in all cases). The dashed lines show the 68.3% credible interval. These values were calculated for 2,850,000 links.

Table 3.3. Transit parameters for OGLE-TR-56b (jointly fit)

	Median value	Formal Error ^a	Adopted Error ^b
<i>Fitted Parameters</i>			
k	0.1037	0.0005	0.0009
a/R_*	3.11	0.02	0.05
i	74.0	0.2	0.4
$u_{1,i'}$	0.12	0.04	0.04
$u_{2,i'}$	0.36	(fixed)	...
$u_{1,V/R}$	0.32	(fixed)	...
$u_{2,V/R}$	0.35	(fixed)	...
$u_{1,WB}$	0.21	(fixed)	...
$u_{2,WB}$	0.36	(fixed)	...
$T_C - 2453908$	0.72601	0.00031	0.00044
$T_C - 2453930$	0.54258	0.00061	0.00220
$T_C - 2453936$	0.59819	0.00033	0.00109
$T_C - 2454342$	0.72851	0.00046	0.00055
$T_C - 2454600$	0.59178	0.00027	0.00039
$T_C - 2454629$	0.81483	0.00046	0.00063
$T_C - 2454674$	0.65449	0.00050	0.00063
$T_C - 2454955$	0.81714	0.00041	0.00079
$T_C - 2454961$	0.87787	0.00035	0.00081
$T_C - 2454994$	0.59693	0.00031	0.00032
$T_C - 2454995$	0.80966	0.00042	0.00049
$T_C - 2455040$	0.65155	0.00043	0.00114
<i>Derived Parameters</i>			
b	0.857	0.003	0.006
T_{14} (sec)	7823	44	88
R_p (R_J) ^c	1.332	0.061	0.063
a (AU) ^c	0.0191	0.0009	0.0009

^aFormal 68.3% credible interval from MCMC fit of all 12 light curves jointly.

^bAdopted error from residual permutation method, if greater than the formal error; see § 3.4.

^cAssuming $R_* = 1.32 \pm 0.06 R_\odot$ (Santos et al., 2006) and using $R_J = 71,492$ km.

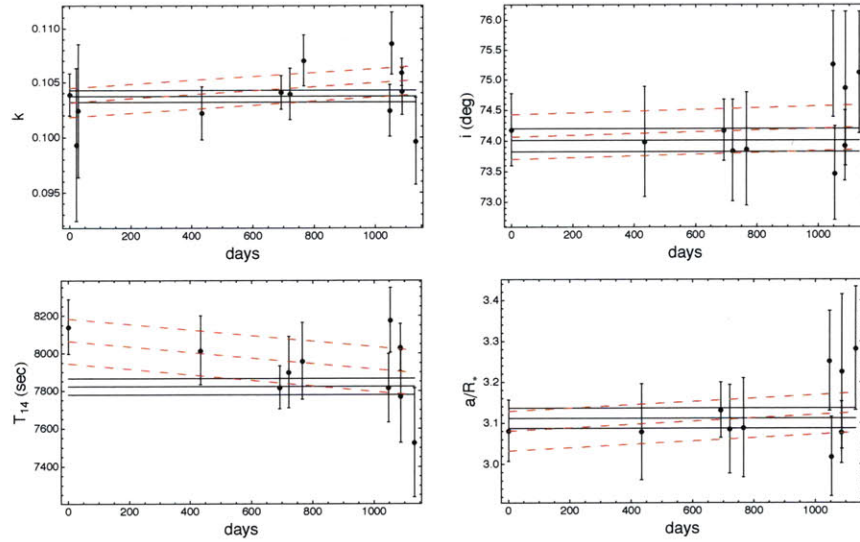


Figure 3-4 Parameter variation of individual transits of OGLE-TR-56b. Data is taken from individual MCMC fits (Table 3.4), for (clockwise, from top-left): k , i , a/R_* , and T_{14} . The errors have been scaled upward based on the factor calculated from residual permutation. The values derived from the joint MCMC fit to all transits (Table 3.3) are plotted as solid black lines with $\pm 1\sigma$ errors. The dashed red lines indicate the best sloped fit with $\pm 1\sigma$ errors, although all fits are only marginally significant (within 1σ of a constant value for the radius ratio and within 2σ for the other parameters). We do not plot the durations for 20060714 or 20060720, which are both much shorter than the scale of this plot (6722 ± 464 s and 6803 ± 671 s, respectively.)

with a free parameter for an airmass correction. Of the 12 light curves fit, only one (20060714) had a midtime shift greater than the MCMC fit error (80 seconds, or 1.3σ), but this is well within the error estimated by the residual permutation method (190 s). No other parameters shifted significantly, indicating that the light curve parameters are robust.

3.4.3 Discrepancy in shape of 20060720 transit

The individual and joint fit parameters generally agreed with each other, and we compare the parameters derived from each transit in Figure 3-4. Two light curves do not agree, however. The transit on 20060714 has high errors due to poor observing conditions, and is probably just poorly constrained in the individual fit. The literature light curve 20060720, however, has very low scatter, but the best individual fit

Table 3.4. Individual transit parameters for OGLE-TR-56b (independently fit)

Transit	k^a	f^b	T_{14}^a	f^b	a/R_\star^a	f^b	i^a	f^b
20060622	0.1039 ± 0.0020	1.7	8142 ± 145	1.3	3.08 ± 0.07	...	74.2 ± 0.6	...
20060714	0.0994 ± 0.0068	2.2	6722 ± 464	1.8	3.58 ± 0.23	1.0	76.2 ± 1.9	1.4
20060720	0.1025 ± 0.0061	3.4	6803 ± 671	5.0	3.79 ± 0.24	1.5	77.6 ± 1.9	2.2
20070830	0.1022 ± 0.0024	1.3	8017 ± 183	...	3.08 ± 0.12	...	74.0 ± 0.9	...
20080514	0.1041 ± 0.0016	1.4	7819 ± 115	1.1	3.13 ± 0.07	1.0	74.2 ± 0.5	1.0
20080612	0.1040 ± 0.0024	1.4	7901 ± 190	1.1	3.09 ± 0.11	...	73.8 ± 0.8	...
20080727	0.1070 ± 0.0024	...	7961 ± 204	...	3.09 ± 0.12	...	75.9 ± 0.9	...
20090504	0.1024 ± 0.0024	1.5	7817 ± 183	1.2	3.25 ± 0.12	...	75.3 ± 0.9	...
20090510	0.1086 ± 0.0029	1.6	8177 ± 172	...	3.02 ± 0.10	...	73.5 ± 0.8	...
20090612	0.1059 ± 0.0013	...	8032 ± 126	...	3.08 ± 0.08	...	73.9 ± 0.7	...
20090613	0.1042 ± 0.0022	...	7772 ± 245	...	3.23 ± 0.19	...	74.5 ± 1.3	...
20090728	0.0997 ± 0.0039	2.2	7527 ± 288	1.5	3.28 ± 0.15	...	75.1 ± 1.0	...

^aFormal individual MCMC fit value and error (scaled upward by factor f in adjacent column).

^bFactor by which the error in the previous column has been increased based on the residual permutation method; no value is given if the formal MCMC fit error was larger. See § 3.4.

(plotted in Figure 3-5 as a gray dashed line) is distinct from the joint fit to all transits (plotted as a solid black line); we note that two of the other transits were taken the month before the 20060720 transit, and the rest were taken 1-3 years later. The duration of transit 20060720 is over fifteen minutes shorter than the duration of the new transits, although the radius ratios for all transits are similar. Two highly correlated parameters can account for the difference in duration: the inclination ($i = 77.6 \pm 0.8^\circ$ for 20060720 individually vs. $i = 74.0 \pm 0.2^\circ$ for the joint fit) and the semimajor axis ($a/R_\star = 3.8 \pm 0.2^\circ$ for 20060720 individually vs. $a/R_\star = 3.1 \pm 0.2$ joint). We also combined the eight Sloan i' transits into a composite curve by phase shifting the times of transits. Fits to the composite curve yield almost identical values as the joint fit ($a/R_\star = 3.1 \pm 0.05$, $i = 74.1 \pm 0.5^\circ$).

Crucially, although the 20060720 transit was observed in shorter wavelength filters (V and R) than the rest of our transits, allowing the limb darkening coefficients to vary does not account for the difference in the light curve shapes. Because of the flat shape of the i' transits, we examined setting the limb darkening to zero for a representative transit, 20080514; we also allowed one or both limb darkening terms to vary while fixing the semimajor axis to agree with the value for the 20060720. Although we were able to produce several scenarios with reduced χ^2 values only 10-20% greater

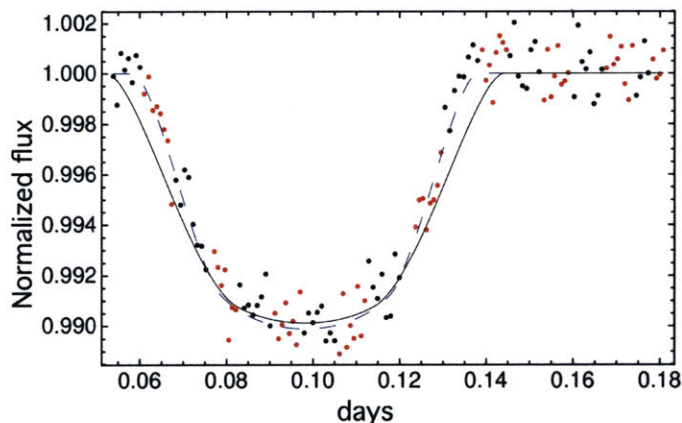


Figure 3-5 Transit of OGLE-TR-56b on 20060720. Data is from Pont et al. (2007). The portions observed in R are colored red while the V band data is black. The individual fit model (calculated only using this light curve) is shown as a dashed line while the best joint-fit model (calculated using all light curves) is a solid curve. Strong deviations near ingress and egress result in a measured transit duration that is over 15 minutes shorter for 20060720 compared to all other transits.

than the nominal case, none of these fits matched the observed shape of the the i' transit, particularly around ingress and egress, while still matching the values of the shape-determining parameters (radius ratio, semimajor axis, and inclination) found by the R/V transit.

What might account for the differences in shape between the 20060720 light curve on the one hand and our new transits on the other? It seems then that there are three broad explanations for the shape discrepancy between transits. The first is that the planet really did change values for a/R_* or i . This seems implausible, because the planet would have had to physically move from 3.1 to 3.8 stellar radii with a month (the values for a/R_* for transits on 20060622 and 20060720) and then back to 3.1 for the next three years, for which there is no realistic mechanism. Similarly, although it is theoretically possible that the planet could be experiencing rapid precession and hence real changes in observed inclination, it seems unlikely that we would not have observed any subsequent changes in inclination among later transits, particularly since three transits in 2008 and five transits in 2009 were taken only a few weeks or days apart.

A second possibility is that there is some real physical difference in the observed signature of the planet at shorter wavelengths; perhaps an optically thick exosphere or rings are present which are transparent at V and R and opaque at I band, leading to a transit that begins earlier and lasts longer. Any plausible scenario would have to be constructed so that it did not affect the overall depth of the transit (which agrees across all transits) while still affecting the duration (which does not).

A third possibility is that there is some unlucky correlated noise in the 20060720 light curve which somehow increased the flux both during ingress and during egress. Photometric error of this sort is particularly dastardly because it would be undetectable in a single light curve and would only become apparent when many high quality light curves could be observed and compared. Related to this is the possibility that switching between two filters somehow introduced errors in determining the beginning and end of transit, since both ingress and egress were only observed in a single filter (Figure 3-5). However, given the care with which the deconvolution photometry was applied to the 20060720 transit and the lack of any other reason to suspect the photometry, this claim is difficult to test without additional data in the R and V filters for comparison.

One unfortunate side effect of the possibility of subtle systematic errors in the photometry is that it also raises the possibility of timing errors. It is hard to quantify the possibility of such shifts in our data, so we will note that while the good agreement in shape between successive transits makes this less likely, it is still something to be concerned about.

3.4.4 Timing

The central midtimes for all 12 transits are summarized in Table 3.3 and illustrated in Figure 3-6. The most dramatic feature of Figure 3-6 is the roughly 5 minute shift between the ephemeris from Pont et al. (2007) and the original OGLE ephemeris from Torres et al. (2004) and almost all of the new transits. Because of the difficulties in comparing light curves produced using different photometric systems (both instruments and reduction methods), and because of the uncertainty about whether

consistent BJD corrections were applied (i.e., correcting for the UTC-TT shift; see Appendix C), we have only used our 11 transits in constructing the ephemeris below. We find the period to be almost unchanged from previous work:

$$T_C(N) = 2453936.6011(16)[BJD] + 1.2119094(24)N. \quad (3.1)$$

where T_C is the predicted central time of a transit, and N is the number of periods since the reference midtime and the values in parentheses are errors on the last digits. Our adopted fit has a reduced $\chi^2 = 4.6$, so we have scaled the errors on the parameters in Equation 3.1 by $\sqrt{4.6} = 2.1$. The poor fit indicates either genuine timing variations or underestimated errors; when we estimate the upper mass limits of companion planets we conservatively assume it is the latter and scale all of our midtime errors by 2.1.

The lower panel in Figure 3-6 shows the new ephemeris and the timing residuals. Note that there is an offset of about 5 minutes between most of our transit times and the literature times from the OGLE survey and from Pont et al. (2007). This appears to be a constant offset, since the period calculated using just our transits agrees quite closely with the published periods, and only the reference midtime is shifted. Possible explanations could include: correlated noise around ingress/egress that messes up the timing of the beginning or end of transit and hence the midtime, though this noise would have to be present in several light curves; an error in the recorded midtimes in the literature; an error in the conversion from the frame start time in UTC to the mid-exposure time in BJD; or some combination of the above. Given that our transits were recorded using three separate instruments and two completely independent timing systems, it is highly unlikely that there is a systematic problem in the recorded times, although it's always possible there is some undetected shift caused by a bug lurking in our analysis software. We can only speculate on timing problems in the literature data, which we have no reason to suspect except for this timing shift.

Examining only our eleven transits in Figure 3-6, we see that there is some scatter, with several points greater than 2σ from the nominal best fit line (see Table 3.5).

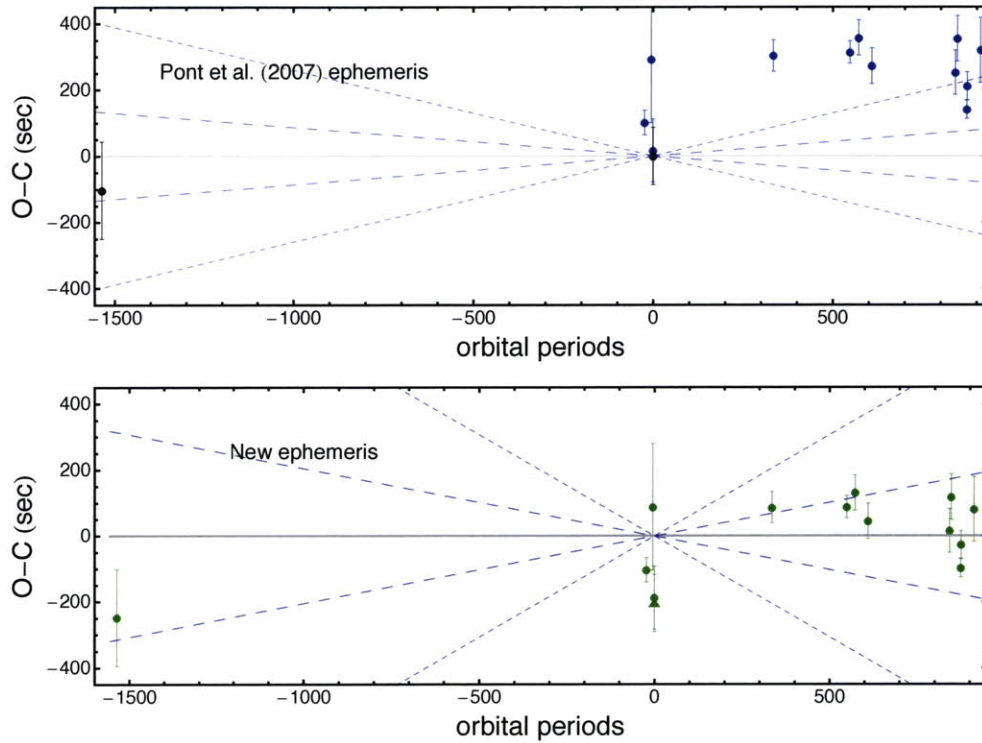


Figure 3-6 Observed minus calculated midtimes for OGLE-TR-56b. Top panel: timing residuals for eleven transits using the ephemeris from Pont et al. (2007). Bottom panel: timing residuals using the new ephemeris (Equation 3.1). The O-C values and errors are shown in Table 3.5, and were calculated using the formal fit midtimes reported in Table 3.3 but rescaling the errors using the residual permutation method to more realistically account for systematic noise (see § 3.4). The solid line represents zero deviation from expected time of transit, while the dashed lines represent the 1σ and 3σ errors on the calculated orbital period, indicating the slopes that result for a mis-determined period.

Table 3.5. Timing residuals for OGLE-TR-56b

Transit	Number	O-C (s)	σ
20010615 ^a	-1536	-247 ± 147	-1.7
20060622	-23	-102 ± 37	-2.8
20060714	-5	88 ± 191	0.5
20060720 ^a	0	-187 ± 95	-2.0
20070830	335	87 ± 47	1.8
20080514	548	88 ± 34	2.6
20080612	572	132 ± 54	2.5
20080727	609	45 ± 54	0.8
20090504	841	16 ± 67	0.2
20090510	846	118 ± 69	1.7
20090612	873	-97 ± 28	-3.5
20090613	874	-26 ± 42	-0.6
20090728	911	81 ± 99	0.8

^aAfter adding the UTC-TT conversion of 64.184 sec (20010615) and 65.184 sec (20060720) to the published times.

However, given the uncertainty about timing systematics and the relatively small number of points, it is hard to make any conclusive statement.

3.4.5 Limits on perturber mass

To avoid possible systematic differences between our data reduction and that of other groups, we used only our eleven transits to explore the limits that can be placed on the mass and orbital separation of a hypothetical perturbing planet in the system; we have additionally scaled the errors by a factor of 2.1 to account for their relatively poor fit to a flat line (note that increasing the errors mostly just increases the mass limits placed). We used an implementation of the algorithm presented in Steffen & Agol (2005), kindly provided by D. Fabrycky; see Chapter 2 for more details. We examined interior and exterior orbits for orbital periods from 0.9-17.5 days (0.2-4.4 times the orbital period of OGLE-TR-56b), and initial eccentricities of $e_c = 0.05$ and $e_c = 0$. The mass limits placed are illustrated in Figure 3-7.

The constraints placed on the perturber’s mass are strongest near the low-order mean motion resonances, particularly in the interior 1:2 and exterior 2:1 resonances, where we are sensitive to objects as small as $22 M_\oplus$ and $12 M_\oplus$, respectively. We note that for most of the periods surveyed, planets on circular orbits ($e_c = 0$) may have

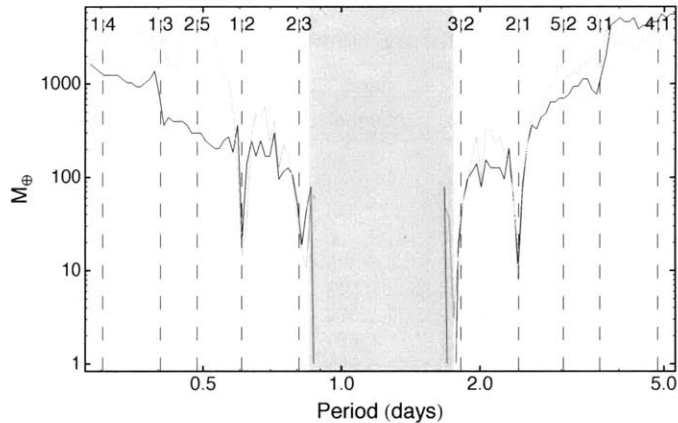


Figure 3-7 Upper mass limit on companions to OGLE-TR-56b. We examine companions with initial $e_c = 0.05$ (black) and $e_c = 0.0$ (gray). The constraints are strongest near the 2:1 and 3:2 mean-motion resonances, where objects as small as $10 M_{\oplus}$ would have been detectable; other interior and exterior resonances are also labeled. The shaded grey region shows the instability region for a $1 M_{\oplus}$ companion, following Barnes & Greenberg (2006).

larger masses than those with slight eccentricities ($e_c = 0.05$), particularly around the 2:5 interior resonance, where objects with zero eccentricity could be 10 times more massive than Jupiter and remain undetected. For non-resonant objects with orbital periods between the 1:2 and 2:1 resonances (0.6-2.4 days) we can place a rough upper limit of $1 M_J$.

3.5 Conclusions

We have observed eleven new transits of OGLE-TR-56b, vastly increasing the supply of high-quality data on the planet. Our observed radius value of $1.33 \pm 0.06 R_J$ is almost identical to the previously published value, and we note that the error is entirely supplied by error on the stellar radius; the formal fit uncertainty is ten times smaller.

We have observed that the shape of the transit differs between the longer-wavelength observations (mostly in Sloan i' but also I_s and a wideband filter from 630-950 nm) and the single light curve observed alternately in R and V on 20060720 by Pont et al.

(2007). Although it is possible the shape difference could be due to real physical changes in for instance the inclination, perhaps caused by rapid precession, such a scenario seems implausible given the timing of the discrepant transit (just a month after one of the new transits) and the complete lack of evidence for inclination changes in any of the other transits spanning 2007-2009. A more likely scenario is that the original photometry of 20060720 is somehow in error, since it disagrees with all of the new transits, which are however consistent with each other. Alternatively, the shape of the transit could be distorted by an exosphere or ring system that was transparent at shorter wavelengths but not at longer wavelengths, although such a scenario would have to account for the transit depths, which are consistent across all transits. New observations of a full transit in either R or V could determine whether the shape difference is wavelength-dependent.

Our new ephemeris for the predicted time of transit is five minutes later than that found by the OGLE survey and by Pont et al. (2007), for reasons which are not clear. However, our period (1.2119094 ± 0.0000024 days) agrees almost exactly with the previously published periods. With nine years of data (2001-2009), there are no signs of any period variation for OGLE-TR-56b. With respect to transit timing variations, although the residuals are somewhat scattered, no indication of TTVs are seen beyond one or two points at the $2-3 \sigma$ level, where $\sigma = 28 - 147$ seconds. We also see no sign of transit duration variations in any of the new eleven transits, although we note that the 20060720 transit has a somewhat shorter duration than any of the new transits.

We rule out objects larger than $22 M_{\oplus}$ and $12 M_{\oplus}$ in the interior 1:2 and exterior 2:1 resonances, respectively, and a non-resonant object between those resonances must be less massive than Jupiter.

3.6 Acknowledgements

We thank Paul Schechter for observing a transit of OGLE-TR-56b as part of MIT's Magellan queue. We thank Brian Taylor and Paul Schechter for their tireless instru-

ment support. We thank the Magellan staff, in particular telescope operators Jorge Araya, Mauricio Martinez, Hernàn Nuñez, Hugo Rivera, Geraldo Valladares, and Sergio Vera, for making these observations possible. We thank Georgi Mandushev for assistance with image subtraction. We thank Jenny Meyer for helpful discussions about orbital decay.

Chapter 4

Bright, Active Stars and High-Precision Transits: OGLE-TR-113b and CoRoT-2b

4.1 Introduction

The best timing precision we were able to achieve in this thesis was on OGLE-TR-113b and CoRoT-2b, with the midtimes for all nine transits determined to better than 40 s, after accounting for systematic error; the error on our best light curve, transit 20080514 of OGLE-TR-113b, was only 9 s. With I -band magnitudes of 14-16, the OGLE stars are photon-noise limited even on the 6.5m Magellan telescopes. As the brightest OGLE star ($I = 14.4$), OGLE-TR-113 is additionally favored for high-quality photometry because it is located $3''$ from a slightly brighter comparison star ($\Delta I = -0.5$). CoRoT-2b was added to our target list in 2008 because it was the only bright star ($I = 11.5$) visible in the southern hemisphere that also has a usable comparison star within the $38'' \times 38''$ field of view of our instrument. This comparison star is $4''$ from CoRoT-2 and may be gravitationally bound (Alonso et al., 2008). Because it is also much fainter, by 2.8 magnitudes, photon noise on the comparison star limits the precision of these observations, which partly explains why we achieved

similar precision with both CoRoT-2 and OGLE-TR-113 despite the former being 3 magnitudes brighter. (A comparison star that is 1.7 mag brighter than CoRoT-2b was used during observations taken with MORIS on the IRTF, which has a slightly larger field of view of about $60'' \times 60''$.) We note that our transits of CoRoT-2b, which were taken with 5 s exposures, occurred before the frame transfer mode was operational, so we lost roughly half of the photons we could have collected solely to readout time (5 s in single-frame mode). An additional factor in favor of these two systems is the transit depths: OGLE-TR-113b and CoRoT-2b are our deepest transits, at roughly 2.5% and 3%, respectively.

It is an interesting coincidence that our most precise light curves also happen to be of planets that orbit variable stars. The variability of CoRoT-2, a late G dwarf, is well-known (Alonso et al., 2008; Lanza et al., 2009; Wolter et al., 2009), with the stellar flux out of transit varying by up to 5%, both on time scales similar to the stellar rotation period (about 4.5 days) and a longer, approximately 55 day modulation associated with the lifetime of the largest active regions (Lanza et al., 2009). OGLE-TR-113, a K dwarf, is much less active, although it has been noted to be variable at the 1-2% level with a rough periodicity of 30 days by Snellen & Covino (2007), consistent with the stellar rotation period. We can see clear signs of variability during both transits of CoRoT-2b, especially 20080515, which had a slope in the out of transit flux that might have been due to real stellar variability, and which also has several bumps remaining in the photometry. During our highest quality transit of OGLE-TR-113b, on 20080514, we have also identified a bump during the transit which is 2σ greater than the residuals during the 5.5 hours of observations, and which we speculate might be a star spot; see discussion in Section 4.3.2).

4.2 OGLE-TR-113b

OGLE-TR-113b was first observed to transit by Udalski et al. (2002b) and was confirmed to be of planetary mass by Bouchy et al. (2004) and Konacki et al. (2004). Several high-quality follow-up light curves were subsequently obtained: two transits

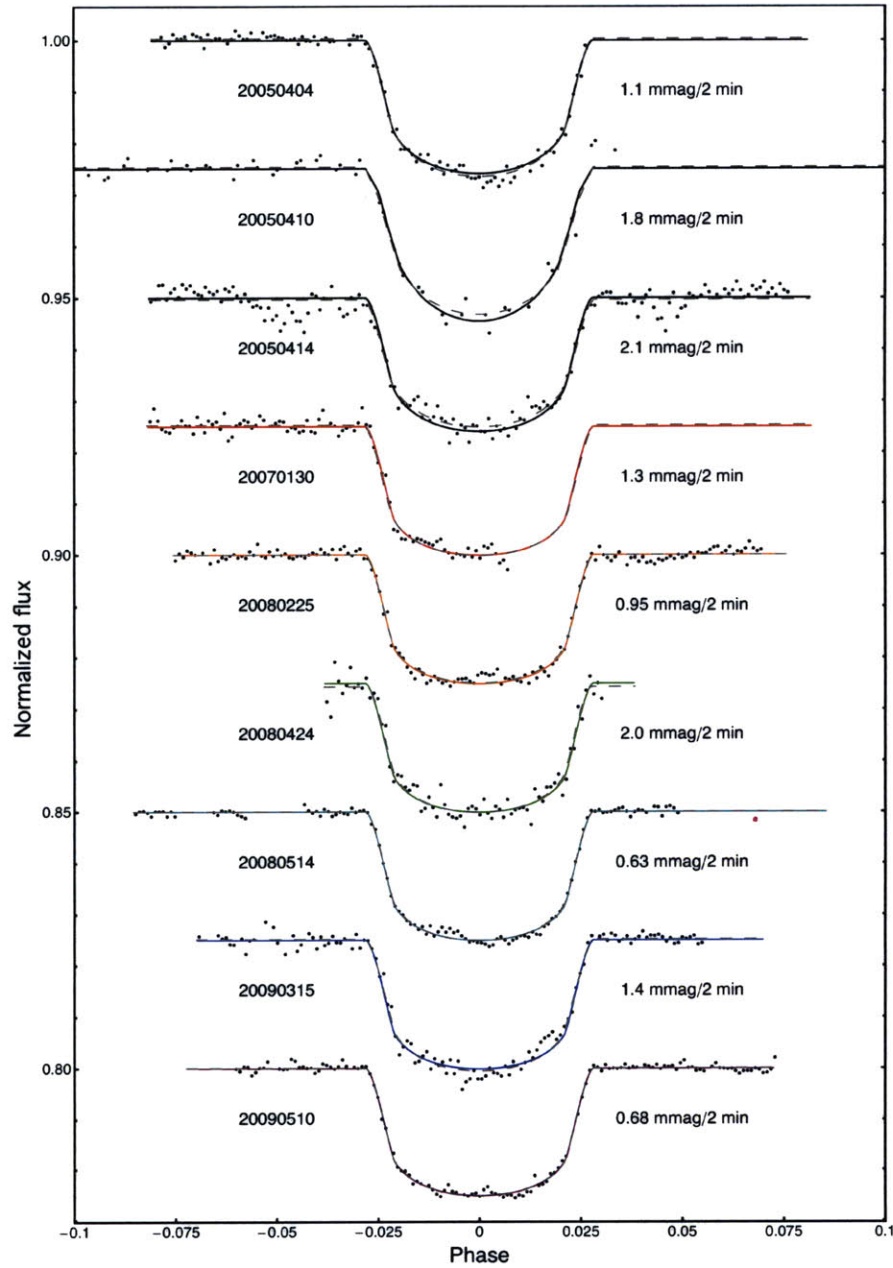


Figure 4-1 Nine transits of OGLE-TR-113b. All available high-quality light curves are plotted vs. orbital phase, with the data binned to 2 minutes to aid comparison. The flux of each light curve has been offset by 0.025 for display. The top three transits are taken from Gillon et al. (2006) and Pietrukowicz et al. (2010), while the rest of the transits are new. The joint model fit (solid lines) calculated using the parameter values in Table 4.3 is almost indistinguishable from the individual model fits for each transit independently (dashed lines). The stated standard deviations are the residuals from the joint model fit. Table 4.2 shows the unbinned data; a full table can be provided on request.

in R band by Gillon et al. (2006), one transit in K band by Snellen & Covino (2007), and one transit in V band by Díaz et al. (2007), later reanalyzed by Pietrukowicz et al. (2010). (An additional K band transit for OGLE-TR-113b was observed by Díaz et al. (2007) but no individual parameters or photometry were reported.) Figure 4-2 illustrates the variability of the star out-of-transit by plotting 115 nights of OGLE survey observations Udalski et al. (2002b) and 4 nights of data on the VLT with the VIMOS instrument (Díaz et al., 2007; Pietrukowicz et al., 2010).

4.2.1 Observations

We observed six transits of OGLE-TR-113b in the Sloan i' filter using the 6.5m Magellan telescopes at Las Campanas Observatory. Two transits were observed using the MagIC-SiT_e CCD, in 2007 January (when the instrument was mounted on the Clay telescope) and 2008 February (when it was mounted on the Baade). Four additional transits were observed between 2008 April and 2009 May using the new MagIC-e2v CCD. The SiT_e CCD has a field of view of $142'' \times 142''$, with an unbinned pixel scale of $0.''069$ per pixel, while the MagIC-e2v camera has a field of view of $38'' \times 38''$ and a pixel scale of $0.''037$ per pixel unbinned. The transit observed on 20090510 was binned 2×2 , while the rest were unbinned. All data were calibrated and photometry generated as described in Chapter 2.

20070130

Transit 20070130 was taken during a fortuitous gap in the clouds, during 3.5 hours of what was otherwise a completely cloudy night; unfortunately, egress was lost to clouds. The airmass during observations fell from 1.7 to 1.2, and the seeing was about $0.''6$. The best photometry was for a 13.6 pixel aperture with a sky radius of $30+10$ pixels, and 10 comparison stars. Detrending the transit for telescope azimuth changes the out of transit baseline slightly (it becomes a little flatter), but more important is that with detrending the depth of the transit agrees with the other five transits.

Table 4.1. Observational and photometry parameters for OGLE-TR-113b

Transit (UT)	N_{Frames} used (discarded)	Exp. Time (sec)	Binning	Readout (sec)	N_{Comp}	Aperture ^a (pixels)	Sky radius, width (pixels)	Scatter ^b (mmag)
20070130	137 (19) ^c	30, 60	1x1	24	10	13.6	30,10	1.3
20080225	371 (1) ^d	10-30	1x1	24	1	12.6	30, 10	1.0
20080424	130 (52) ^e	10, 60	1x1	5	1	4.0	40, 10	2.0
20080514	379 (0)	30	1x1	5	3	24.0	120, 10	0.6
20090315	215 (39) ^f	10-120	1x1	0.003 ^g	1	7.8	50, 10	1.4
20090510	1398 (104) ^h	17, 20	2x2	0.003 ^g	1	13.0	30, 10	0.7

^aRadius around star

^bStandard deviation of the residuals on data binned to 120 s.

^cDiscarded due to clouds.

^dAberrant ratio.

^eDiscarded after-transit baseline due to huge slope.

^fSeeing spike (14) plus clouds (25).

^gFrame transfer mode used.

^hOne or more stars used saturated.

20080225

Transit 20080225 was observed under stable conditions, with airmass increasing from 1.2 to 1.6 and the seeing between 0."5-0."7. The best aperture was 12.6 pixels, with a sky radius of 30+10 pixels, and using 1 comparison star (the close, bright companion star, which was also used in several other transits as the only companion).

20080424

Transit 20080424 was observed under stable conditions with airmass from 1.2-1.3 and seeing from 0."6-0."4. For most photometry settings we tried, there was a strong slope that was roughly correlated with the strongly variable seeing, but not closely enough that we could detrend for it. However, we found that by using a very small aperture (4 pixels) for this target, a sky radius of 40+10 pixels, and only the single closest companion star, we were able to get a flat light curve of the appropriate depth for all of the transit (although not during the after-transit baseline). It is not immediately clear why this transit had such a strong slope; it was not, for instance, a sky determination problem like 20090315 (detailed below).

Table 4.2. Flux values for new transits of OGLE-TR-113b

Mid-exposure (UTC) ^a	Mid-exposure (BJD)	Flux	Error
2454130.599893	2454130.601328	0.9989387	0.001434
2454130.60128	2454130.602715	1.002829	0.001434
2454130.602397	2454130.603832	1.003339	0.001434
2454130.603408	2454130.604843	1.00098	0.001434
2454130.603408	2454130.604843	1.00098	0.001434
...			

^aFull table available on request.

20080514

Transit 20080514 was observed under extremely stable conditions with airmass from 1.2-1.4 and seeing always 0."4 or better. The best photometry used a 24 pixel radius, a sky radius of 120+10 pixels, and 3 comparison stars. Two gaps in the photometry before transit indicate telescope software glitches, but otherwise this light curve is of exquisite quality. The small bump just before midtransit is discussed in § 4.3.2.

20090315

Transit 20090315 was taken under 0."7 seeing and variable transparency for the first half of the transit. For unclear reasons, perhaps due to the variable (by a factor of 3) counts on the star and relatively high seeing, we were unable to get a good measurement of the sky around the target and its nearby companion star. Instead, we used the sky measured by *phot* around a third, isolated star for each star; the sky radius used was 50+10 pixels. The best light curve came from a 20 pixel radius aperture and the single closest, brightest comparison star. A trend against seeing was removed from the photometry before fitting.

20090510

Transit 20090510 was observed with average 0."7 seeing, which frequently spiked to smaller values. 1398 frames were used out of 1502 taken; the rest were discarded due to saturation of the target. The best light curve was with an aperture of 13 pixels, a

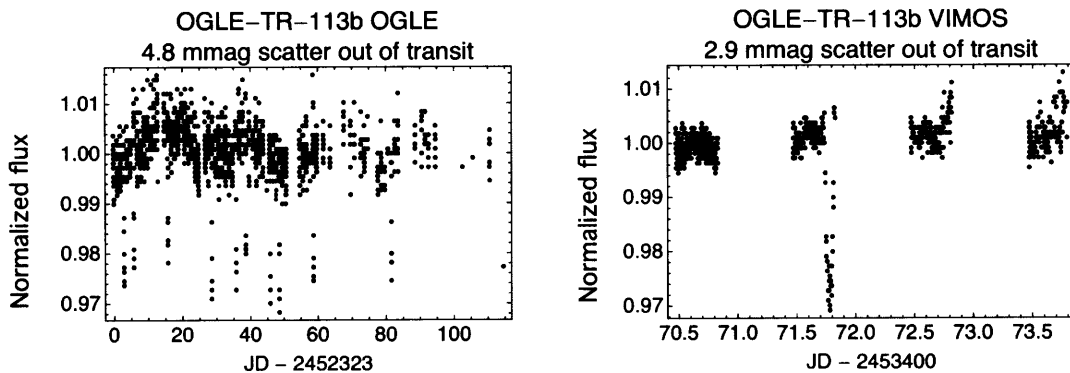


Figure 4-2 Long-term variability of OGLE-TR-113b. Literature data from the OGLE survey (left panel, Udalski et al., 2002b) and four nights of VIMOS data (right panel, Pietrukowicz et al., 2010).

sky radius of $30+10$ pixels, and a single comparison star.

Literature light curves

To ensure uniform parameters, we re-fit the original photometry of three light curves from the literature: the two R -band transits observed by Gillon et al. (2006) on 20050404 and 20050414 UT, and the V -band transit on 20050410 observed by Díaz et al. (2007), although we used the photometry that was re-analyzed by Pietrukowicz et al. (2010).

4.3 Transit fitting results

4.3.1 Model and light curve fits

Each light curve was fit as described in § 2.4. We assumed that OGLE-TR-113b has zero obliquity, oblateness and orbital eccentricity. We used a quadratic limb darkening law for the Sloan i' , R_C , and V_J filters (Claret, 2000, 2004)¹, assuming $T = 4804$ K, $\log g = 4.52$, $[M/H] = 0$, and $V_{micro} = 2$ km/s. We fixed the orbital period to $P = 1.43248$ days; experiments with slightly different values had little effect. The

¹Initial values: $u_{1,R} = 0.5398$, $u_{2,R} = 0.1885$, $u_{1,V} = 0.6905$, $u_{2,V} = 0.1029$, $u_{1,i'} = 0.4348$, $u_{2,i'} = 0.2261$.

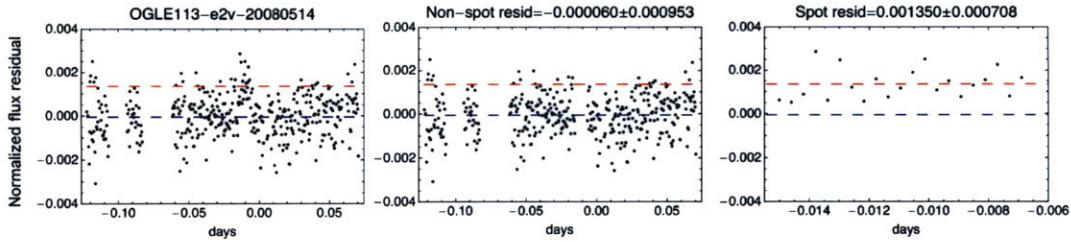


Figure 4-3 Potential starspot on transit of OGLE-TR-113b on 20080514. Left panel: residuals on all data from the best fit model vs. time in days. Notice the spike around frame 200. Middle panel: residuals on all data except for 20 high points identified as a potential spot. Right panel: residuals on the 20 high points. The lines are the same in all three panels, with the lower, black dashed line representing the mean value for all residuals and the upper, red dashed line showing the mean value for the 20 high points. The mean value of the 20 high points is about 2σ above the mean value of all residuals.

other free parameters in the model are the radius ratio, k , inclination, i , semimajor axis in stellar radii, a/R_* , out-of-transit flux, F_{OOT} and transit midtime, T_C . We assume throughout the fits that $M_* = 0.78 M_\odot$, $R_* = 0.77 R_\odot$, and $M_p = 1.32 M_J$, based on the spectroscopic work of Santos et al. (2006).

All transits were jointly fit to our Monte Carlo Markov Chain (MCMC) model, and each transit was also fit independently to check for variation in system parameters (the radius ratio, inclination, semimajor axis, and duration) between individual transits. We plot the best model fit with the data in Figure 4-1 and tabulate the fit results in Table 4.3, where we report for each parameter the median value and the 68.3% credible interval (the equivalent to a 1σ standard deviation if the distribution is Gaussian). The distributions for each parameter are shown in Figure 4-4.

The new radius ratio for OGLE-TR-113b based on an analysis of nine light curves yields a planetary radius $R_p = 1.084 \pm 0.004 R_J$, if we consider only the formal fit errors; accounting for the error on the stellar radius, which is now the dominant source of error, we find a more realistic error bar is $R_p = 1.084 \pm 0.029 R_J$.

As a test of the robustness of our parameter determination, we also ran additional MCMC fits for each transit independently, with results in Table 4.4 and Figure 4-5. We find no evidence of parameter variation over time.

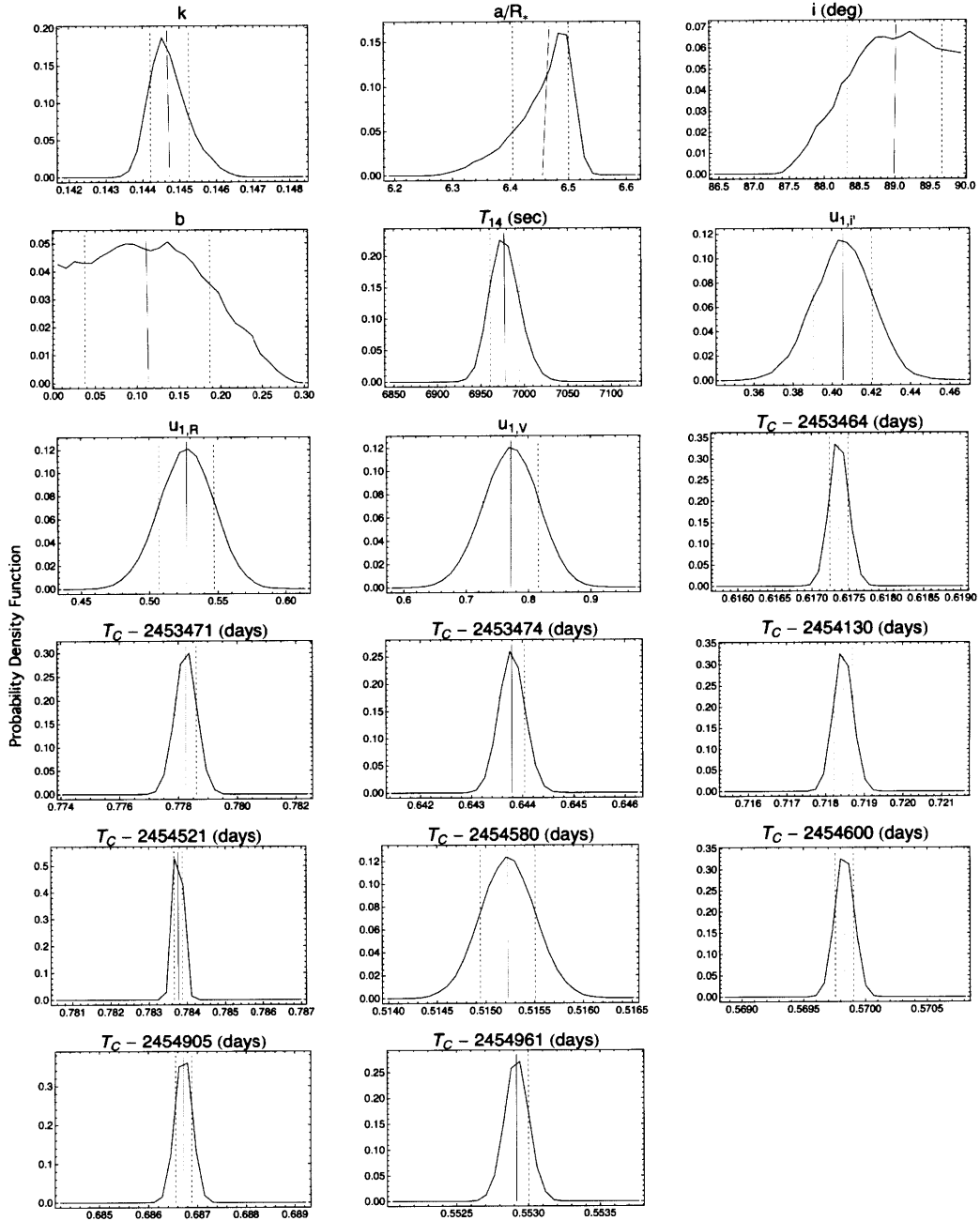


Figure 4-4 Parameter distributions for joint fit to twelve transits of OGLE-TR-113b. Smoothed histogram of normalized parameter distributions, from which the parameters in Table 4.3 are derived. The solid line is the median value (which is very close to the mean value in all cases). Note that several of the distributions, particularly a/R_* , i , and b , are not strictly Gaussian. The dashed lines show the 68.3% credible interval. These values were calculated for 2,850,000 links.

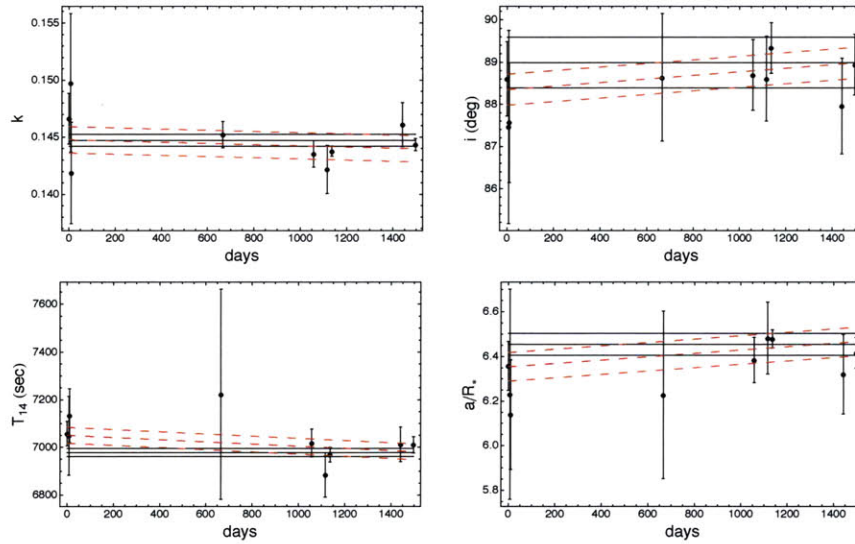


Figure 4-5 Individual transit parameter variation for OGLE-TR-113b. Values are taken from the individual MCMC fits (Table 4.4), for four parameters (clockwise, from top-left): radius ratio, k , inclination, i , semimajor axis, a/R_* , and duration, T_{14} . The errors have been scaled upward based on the factor calculated from residual permutation. The values derived from the joint MCMC fit to all transits (Table 4.3) are plotted as solid black lines with $\pm 1\sigma$ errors. The dashed red lines indicate the best sloped fit with $\pm 1\sigma$ errors. All fits are consistent with no transit parameter variation over the interval observed.

Table 4.3. Transit parameters for OGLE-TR-113b (jointly fit)

	Adopted value ^a	Formal Error ^b
<i>Fitted Parameters</i>		
k	0.1447 ± 0.0006	0.0005
a/R_*	6.47 ± 0.09	0.05
i	89.0 ± 1.0	0.7
$u_{1,i'}$	0.41 ± 0.02	0.02
$u_{2,i'}$	0.23 (fixed)	...
$u_{1,R}$	0.53 ± 0.02	0.02
$u_{2,R}$	0.19 (fixed)	...
$u_{1,V}$	0.77 ± 0.04	0.04
$u_{2,V}$	0.10 (fixed)	...
$T_C - 2453464$	0.61737 ± 0.00024	0.00012
$T_C - 2453471$	0.77825 ± 0.00053	0.00036
$T_C - 2453474$	0.64379 ± 0.00093	0.00025
$T_C - 2454130$	0.71846 ± 0.00028	0.00024
$T_C - 2454521$	0.78377 ± 0.00025	0.00011
$T_C - 2454580$	0.51523 ± 0.00027	0.00028
$T_C - 2454600$	0.56983 ± 0.00011	0.00007
$T_C - 2454905$	0.68672 ± 0.00033	0.00016
$T_C - 2454961$	0.55292 ± 0.00015	0.00008
<i>Derived Parameters</i>		
b	0.11 ± 0.09	0.08
T_{14} (sec)	9647 ± 31	18
$R_p (R_J)^c$	1.084 ± 0.029	0.004
a (AU) ^c	0.02315 ± 0.0014	0.0006

^aAdopted values are the median of the parameter distribution and the error from residual permutation method, if greater than the formal error; see § 2.4.3.

^bFormal errors are the limits of the 68.3% credible interval from MCMC fit of all 9 light curves jointly.

^cAssuming $R_* = 0.77 \pm 0.02 R_\odot$ (Santos et al., 2006) and using $R_J = 71,492$ km.

Table 4.4. Individual transit parameters for OGLE-TR-113b (independently fit)

Transit	k^a	f^b	T_{14}^a	f^b	a/R_*^a	f^b	i^a	f^b
20050404	0.14663 ± 0.0022	2.3	7057 ± 52	1.1	6.36 ± 0.11	...	88.6 ± 0.88	...
20050410	0.14977 ± 0.0061	1.8	7049 ± 165	1.4	6.23 ± 0.47	1.7	87.5 ± 2.3	1.5
20050414	0.14187 ± 0.0044	2.2	7134 ± 113	1.1	6.14 ± 0.25	...	87.6 ± 1.4	...
20070130	0.14523 ± 0.0012	1.0	7222 ± 440	...	6.23 ± 0.38	1.0	88.6 ± 1.5	1.6
20080225	0.14355 ± 0.0012	1.6	7018 ± 58	1.4	6.38 ± 0.10	...	88.7 ± 0.84	...
20080424	0.14218 ± 0.0021	...	6884 ± 93	1.0	6.48 ± 0.16	...	88.6 ± 1.0	...
20080514	0.14377 ± 0.00045	1.1	6969 ± 31	1.6	6.48 ± 0.041	1.1	89.3 ± 0.60	1.2
20090315	0.14611 ± 0.0019	1.4	7013 ± 73	1.1	6.32 ± 0.18	...	88.0 ± 1.1	...
20090510	0.14435 ± 0.00053	...	7011 ± 34	1.4	6.42 ± 0.069	...	88.9 ± 0.72	...

^aFormal individual MCMC fit value and error (scaled upward by factor f in adjacent column).

^bFactor by which the error in the previous column has been increased based on the residual permutation method; no value is given if the formal MCMC fit error was larger. See § 2.4.3.

4.3.2 Stellar variability

The variability of OGLE-TR-113b can be seen in observations of the star out of transit (see Figure 4-2). Several of the new light curves have features that might indicate intrinsic stellar noise rather than photometric defects, although the clearest case is for the transit on 20080514. During this, our highest-quality transit, there is one feature just before the midtime that is 2σ greater than the scatter of the residuals, which is quite low (0.6 mmag in 2 min). Figure 4-3 shows the residuals for the entire transit, with a group of 20 points around frame 200 that are clearly higher than the rest of the data. Generally, bumps of this size in other transits we have observed have been interpreted as glitches in the photometry. However, the lack of any other similar variation during 5.5 hours on this target, or during 3.5 hours spent that same night observing another high-quality, bump-free transit of OGLE-TR-56b immediately following the OGLE-TR-113b transit (see Chapter 3), lends support to this being a real feature, possibly a starspot. Other transits (e.g. 20080225) may also exhibit additional bumps, but the interpretation of these features is less clear.

4.3.3 Systematic errors and correlated noise

Since OGLE-TR-113 is known to be a variable star, some of the correlated features in the light curve are real variations in the stellar photometry. Nonetheless, an ill-placed star spot or stellar wiggle will affect the correct parameter determination of a planetary transit just as surely as any terrestrial source of correlated error, so it is important to estimate how much the formal parameter errors should be increased to allow for systematic errors. We estimated the correlated errors in two ways: the time-averaged residual method, and the residual permutation method (see Chapter 2 for more details). We found that the errors on the parameters in the formal MCMC fits were underestimated by a factor of up to 2 depending on the light curve and the method used to estimate the error. Note that for our most precisely timed transit, 20080514, this means the error increases from 6 s to 10 s, while the errors on the other new transits are 13-46 s.

4.3.4 Timing

The central midtimes for all nine transits that we fit are summarized in Table 4.3. The midtimes on the new transits are calculated using the UTC-TT conversion factor, which has not been used in some published HJD and BJD calculations, as recently noted by J. Eastman and E. Agol (2010, in prep). Two of the literature light curves were supplied with the original UTC times (Gillon et al., 2006), which we have converted using the same BJD calculations as our own transits. We have also added the appropriate UTC-TT conversion to the remaining two literature transits (64.184 s during the years 1999 to 2005). We note that it is not clear what method was used to calculate the BJD conversion, and it is possible this factor has been added incorrectly, in which case 64.184 seconds should be subtracted from the listed O-C values. However, given the agreement seen between the corrected times and our transit times in Figure 4-6 when all 10 timing epochs are jointly fit, the UTC-TT correction seems reasonable.

The top panel of Figure 4-6 shows the ephemeris from Gillon et al. (2006), derived from the two transits reported in that paper plus the original OGLE survey data, and reproduced here for comparison:

$$T_C(N) = 2453464.61665(10)[BJD] + 1.43247570(130)N, \quad (4.1)$$

where T_C is the predicted central time of a transit in Barycentric Julian Days (BJD), the first term is the reference midtime, and N is the number of periods since the reference midtime; the values in parentheses are errors on the last digits. The middle panel of Figure 4-6 shows our adopted fit, which includes all 10 transit epochs (the nine light curves fit here plus the OGLE time). We find that

$$T_C(N) = 2453464.61720(47)[BJD] + 1.43247477(62)N, \quad (4.2)$$

with reduced $\chi^2 = 3.3$; the errors reported in Equation 4.2 have been scaled upward by $\sqrt{3.3} = 1.8$ to account for this. Based on the relatively high reduced χ^2 and the

disagreement of some of our best-timed transits from the fit (e.g. our last transit, on 20090510, is early by 2.7σ), we have also calculated another ephemeris based solely on our new data, with

$$T_C(N) = 2453464.61873(8)[BJD] + 1.43247297(10)N. \quad (4.3)$$

The reduced $\chi^2 = 0.2$ for this fit, indicating excellent agreement of the data with the model, and perhaps over-estimated error bars. (To be conservative, we have not scaled the error bars in Equation 4.3 by $\sqrt{0.2} = 0.45$, or they would be smaller yet.) However, although Equation 4.3 fits the six transits from 2007-2009 quite well (the largest deviation is 17 ± 46 s), with errors on the midtime and period smaller by a factor of 6 compared to the fit to all data, it does *not* provide a good fit to the earlier data from the literature.

The difference in the periods determined by Equation 4.3 and Equation 4.1 is -0.24 ± 0.12 s, a 2σ result. Most of the error on this detection is due to the large error on the transit ephemeris from 2002-2005, which is both sparser and lower-precision than the Magellan data from 2007-2009. Three possible explanations for this discrepancy are: (1) we have underestimated the errors on one or more of the new transits, causing the fit to all transits (Equation 4.2) to have an acceptable reduced χ^2 , though we note that the reduced χ^2 of the fit to the new transits may indicate that the errors are actually overestimated; (2) there are unknown errors in the published midtimes of the transits in the literature, which if accounted for would cause them to agree with the ephemeris determined by the new transits; or (3) there are large-scale timing variations in the period of OGLE-TR-113b over many years, possibly due to orbital decay. The second possibility should be investigated, due to the known presence of timing discrepancies in the literature (e.g., the five minute shift in midtimes for the 20050409 transit of OGLE-TR-111b remarked on in Chapter 2, and a recent erratum shifting the midtime of a transit of WASP-10b by 550 s due to a misapplied HJD correction (Johnson et al., 2009, 2010)). A discrepancy in the BJD correction cannot account for all of the observed timing difference, however, since for

Table 4.5. Timing residuals for OGLE-TR-113b

Transit	Number	O-C (s) ^a	σ
20020219 ^b	-795	-68 ± 71	-0.95
20050404 ^b	0	14 ± 16	0.89
20050410 ^b	5	-114 ± 110	-1.0
20050414 ^b	7	-63 ± 21	-2.9
20070130	465	42 ± 46	0.93
20080225	738	16 ± 9	1.7
20080424	779	16 ± 35	0.45
20080514	793	12 ± 11	1.1
20090315	1006	-9 ± 28	-0.31
20090511	1045	-36 ± 13	-2.7

^aResidual from ephemeris calculated using all data.

^bAfter adding UTC-TT correction of 64.184 s.

two of the transits of OGLE-TR-113b we obtained the original UT times from M. Gillon (2010, personal communication) and converted them to BJD using the same method as our new data.

If real, the period change for OGLE-TR-113b would indicate quite rapid orbital decay. Our best estimate, comparing data taken from 2002-2005 with data from 2007-2009, is that the period decay is 240 ± 120 ms over 4.5 years, or 53 ± 27 ms/year. This is much faster than the estimated values of 0.1-10 ms/yr for OGLE-TR-56b even though the theoretical lifetime for OGLE-TR-113b has been estimated by Levrard et al. (2009) to be more than ten times longer than that of OGLE-TR-56b (98 Myr vs 7 Myr, respectively; see discussion of orbital decay in Chapter 3). However, while the value for the *amount* of orbital decay is still tentative, a firm detection of orbital decay of any magnitude would be important regardless of whether it conforms to present theoretical prediction, and could lead to better theoretical models, and perhaps a meaningful constraint on the Q value of a star.

4.3.5 Limits on perturber mass

We have estimated the limits placed on a companion object using the method described by Steffen & Agol (2005), as described in more detail in Chapter 2. Because

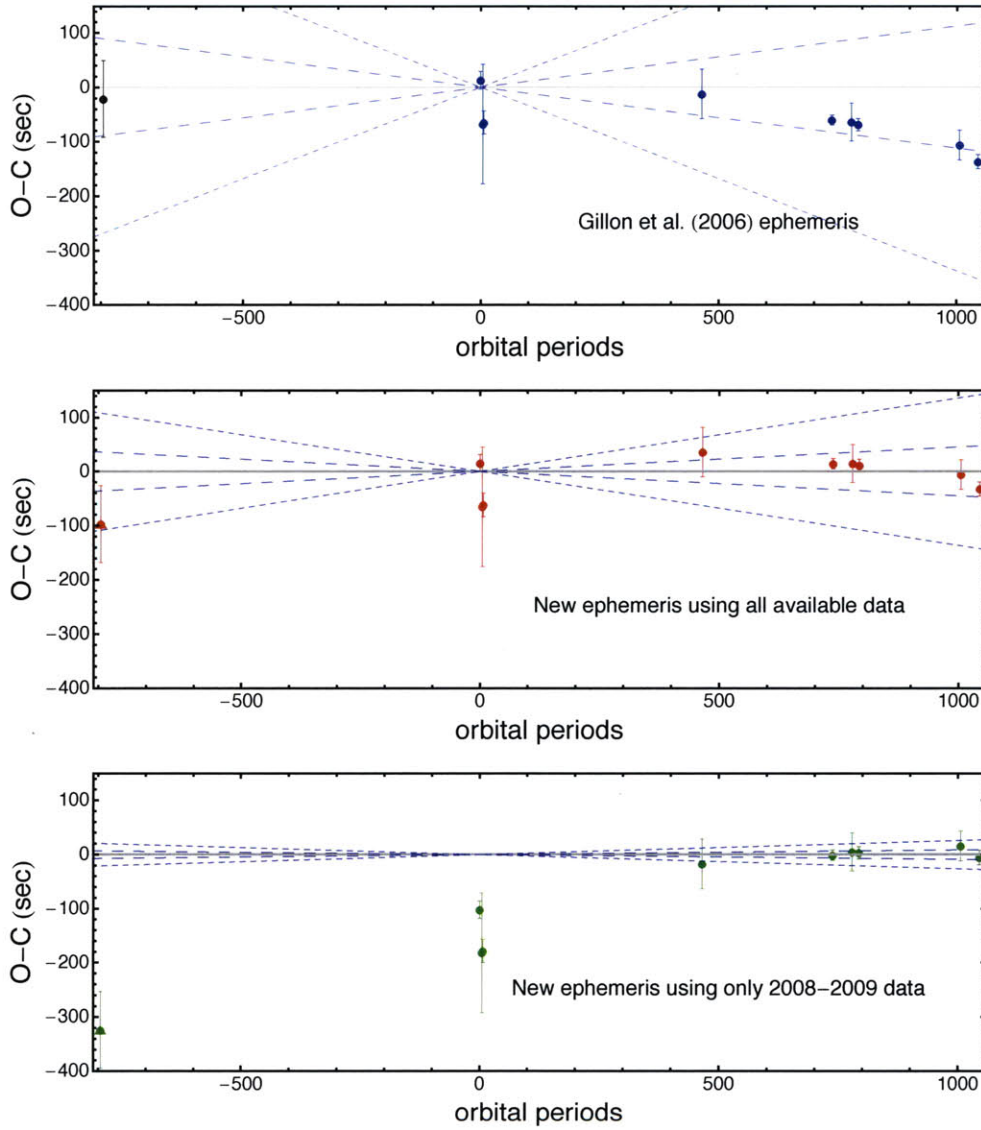


Figure 4-6 Observed minus calculated midtimes for OGLE-TR-113b. Top panel: timing residuals for eleven transits using the ephemeris from Gillon et al. (2006). Middle panel: timing residuals using the new ephemeris calculated from all 9 midtimes fit in this paper plus the original OGLE survey midtime. Bottom panel: timing residuals using a new ephemeris calculated using only our 6 new transits. The solid line represents zero deviation from expected time of transit, while the dashed lines represent the 1σ and 3σ errors on the calculated orbital period, indicating the slopes that result for a mis-determined period. Note that all points before orbital period 465 are taken from the literature (Udalski et al., 2002b; Gillon et al., 2006; Pietrukowicz et al., 2010).

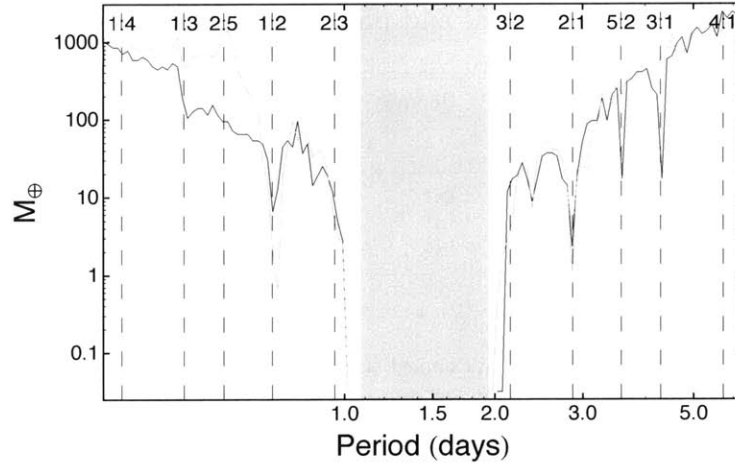


Figure 4-7 Upper mass limit on potential companion planets to OGLE-TR-113b. We examined companions with initial $e_c = 0.05$ (black) and $e_c = 0.0$ (gray). These constraints were placed considering only the six new transits. The constraints are strongest near the internal 1:2 mean-motion resonances, where objects as small as $1 M_\oplus$ on a circular orbit would have been detectable; other tight constraints (less than 2 to $20 M_\oplus$) are placed at the external 2:1, 5:2, and 3:1 resonances. The shaded grey region shows the instability region for a $1 M_\oplus$ companion, following Barnes & Greenberg (2006).

the full dataset of 10 transits do not have consistent midtimes, as noted in § 4.3.4, we have limited our stability analysis to the six new transits from 2007-2009. We examined perturbers both on initially circular ($e = 0$) and slightly eccentric orbits ($e = 0.05$), finding similar constraints for both cases, and plot the results in Figure 4-7. The constraints placed are strongest near the internal 1:2 mean-motion resonances, where objects as small as $1 M_\oplus$ on a circular orbit would have been detectable. Several external mean-motion resonances are also relatively tightly constrained (less than 2 to $20 M_\oplus$), including the 2:1, 5:2, and 3:1 resonances. These constraints are consistent with the lack of any short-term timing variations observed during two years of observations, and we find no evidence for companion planets in our data.

Table 4.6. Observational and photometry parameters for CoRoT-2

Transit (UT)	N_{Frames} used (discarded)	Exp. Time (sec)	Binning	Readout (sec)	N_{Comp}	Aperture ^a (pixels)	Sky radius, width (pixels)	Scatter ^b (mmag)
20080424	1156 (0)	5, 10	1x1	5	1	18	40, 20	0.8
20080515	1214 (2) ^c	4-10	1x1	5	1	16	50, 10	1.2
20080907	2715 (8) ^d	5	1x1	0.003 ^e	1	26	100, 10	1.4

^aRadius around star

^bStandard deviation of the residuals on data binned to 120 s.

^cAberrant ratio.

^dTelescope tracking glitch.

^eFrame transfer mode used.

4.4 CoRoT-2b

CoRoT-2 was the first bright ($V = 12.6$, $I = 11.5$) transiting-planet-hosting star discovered that is observable from the southern hemisphere ($\delta = +01$) and additionally has a comparison star, albeit 2.8 mag fainter, within the MagIC-e2v field of view. Its coordinates were released shortly before our first scheduled observations with the MagIC-ev, and serendipitously we found one partial and one full transit that fell during time already allocated to our transit program but not conflicting with a previously scheduled transit. Since CoRoT-2 is also observable from the northern hemisphere, we requested time for an additional two transits with the frame transfer camera, MORIS, which was newly installed on the IRTF.

4.4.1 Observations

Our transits with MagIC-e2v used the Sloan i' filter. Our transits with MORIS used a Thor long pass filter with lower cutoff at 700 nm², which is similar to the lower limit of Sloan i' , although it extends to longer wavelengths. With MORIS, we used the 1 MHz Conventional mode in 2.4x gain setting, which has a read noise of 6 e- per pixel and gain of 1.5e-/ADU.

²Transmission curve: <http://www.thorlabs.com/images/TabImages/FEL0700.jpg>

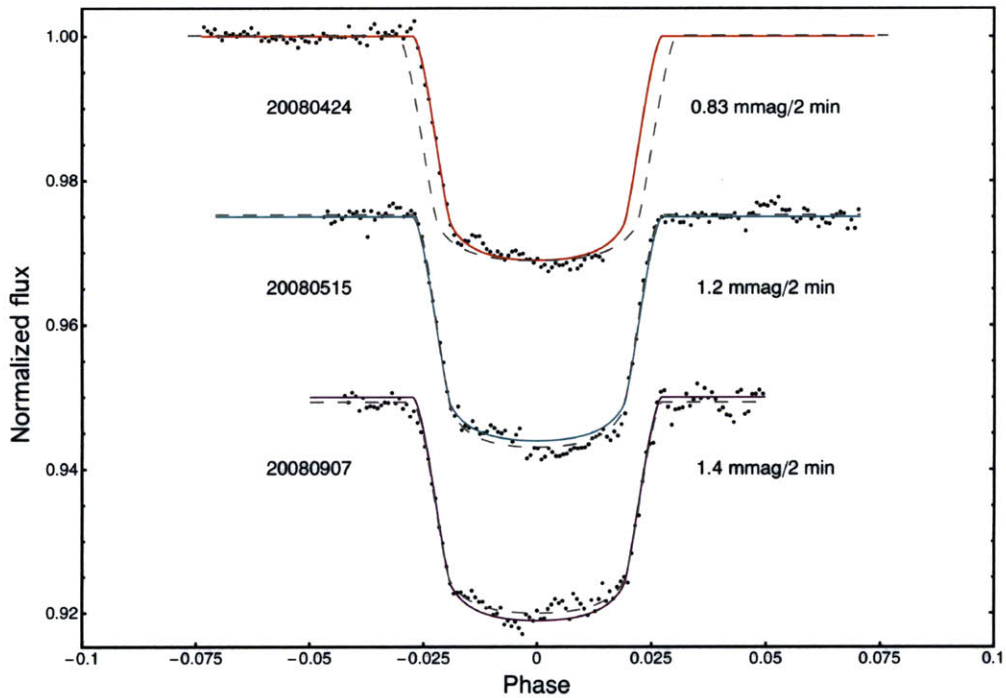


Figure 4-8 Three transits of CoRoT-2b. Three light curves are plotted vs. orbital phase, with the data binned to 2 minutes to aid comparison. The joint model fit (solid lines) were calculated using the parameter values in Table 4.8; the stated standard deviations are the residuals from the joint model fit. The individual model fits for each transit independently (dashed lines) are also plotted; note that the half-transit cannot constrain the total transit duration properly when fit on its own. The full data can be provided on request; an excerpt is shown in Table 4.7.

Table 4.7. Flux values for new transits of CoRoT-2b

Mid-exposure (UTC) ^a	Mid-exposure (BJD)	Flux	Error
2454601.736729	2454601.740217	1.003018	0.001918
2454601.737666	2454601.741154	0.9988006	0.001918
2454601.737846	2454601.741334	0.9986845	0.001918
2454601.73802	2454601.741507	0.9994551	0.001918
2454601.738193	2454601.741681	1.001149	0.001918
...			

^aFull table available on request.

20080424

At the end of the night of 20080424, after observing transits of OGLE-TR-132 (see § 5.2) and OGLE-TR-113 (see § 4.2), a half-transit of CoRoT-2 was fortuitously observable for the final two hours of the night. The best light curve was produced with an 18 pixel radius aperture, using a sky radius of 40+20 pixels and the close, faint comparison star

20080515

Transit 20080515 was observed on a night with good seeing (0."5) and somewhat variable transparency. The airmass ranged from 1.2 to 1.4. The best light curve was produced with a 16 pixel radius aperture, using a sky radius of 50+10 pixels and the close, faint comparison star.

20080907

Transit 20080907 was observed under stable conditions with about 1" seeing; the telescope was refocused twice to maintain good image diameters. The airmass ranged from 1.1 to 2.0. The best light curve was produced with a 26 pixel radius aperture, using a sky radius of 100+10 pixels and the more distant, brighter comparison star.

4.4.2 Model and light curve fits

We fit all three transits to a joint MCMC model, as described earlier. We assumed that CoRoT-2b has zero obliquity, oblateness and orbital eccentricity. We used a quadratic limb darkening law for the Sloan i' filters (Claret, 2000, 2004)³, assuming $T = 5625$ K, $\log g = 4.3$, $[M/H] = 0$, and $V_{micro} = 2$ km/s. We fixed the orbital period to $P = 1.7429964$ days, the value from Alonso et al. (2008). We assume throughout the fits that $M_* = 0.97 \pm 0.06 M_\odot$, $R_* = 0.902 \pm 0.018 R_\odot$, and $M_p = 3.31 \pm 0.16 M_J$, based on Alonso et al. (2008). Note that although the transit on 20080907 was observed with a long pass filter, we assumed the limb darkening parameters were similar enough to the Sloan i' filter, and fit all three light curves to common coefficients.

We plot the best model fit with the data in Figure 4-8 and tabulate the fit results in Table 4.8, where we report for each parameter the median value and the 68.3% credible interval (the equivalent to a 1σ standard deviation if the distribution is Gaussian). The distributions for each parameter are shown in Figure 4-9. The formal MCMC errors on our midtimes are quite low, 10 s for the half-transit and 7 s for each of the two full transits. As a conservative estimate of the systematic noise, which includes noise due to stellar variability, we used the time-averaged residuals method and calculated that the errors for each transit should be increased by factors of 3.9, 4.3, and 4.6 times, in chronological order, which means our adopted errors are 39 s, 30 s, and 32 s.

The new radius ratio for CoRoT-2b based on an analysis of nine light curves yields a planetary radius $R_p = 1.462 \pm 0.005 R_J$, if we consider only the formal fit errors; accounting for the error on the stellar radius, we find a more realistic error bar is $R_p = 1.462 \pm 0.030 R_J$.

³Initial values: $u_{1,i'} = 0.1448$, $u_{2,i'} = 0.3562$.

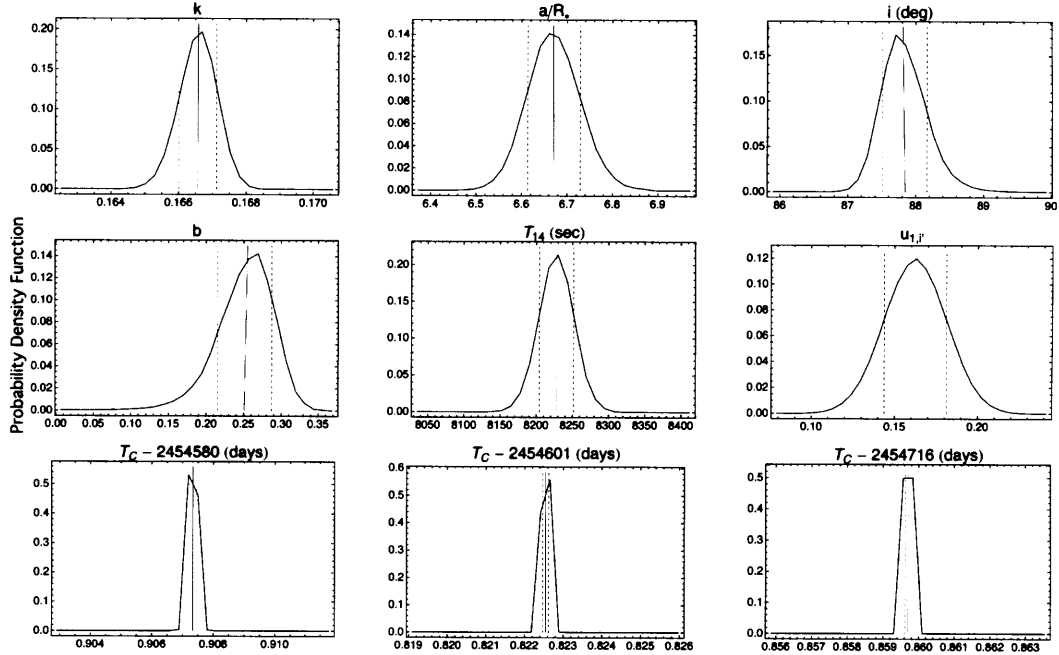


Figure 4-9 Parameter distributions for joint fit to twelve transits of CoRoT-2b. Smoothed histogram of normalized parameter distributions, from which the parameters in Table 4.8 are derived. The solid line is the median value (which is very close to the mean value in all cases). Note that several of the distributions, particularly a/R_* , i , and b , are not strictly Gaussian. The dashed lines show the 68.3% credible interval. These values were calculated for 2,850,000 links.

Table 4.8. Transit parameters for CoRoT-2b (jointly fit)

	Adopted value ^a
<i>Fitted Parameters</i>	
k	0.1666 ± 0.0006
a/R_*	6.67 ± 0.06
i	87.8 ± 0.4
$u_{1,i'}$	0.41 ± 0.02
$u_{2,i'}$	0.14 (fixed)
$T_C - 2453464$	0.90733 ± 0.00011
$T_C - 2453471$	0.82254 ± 0.00008
$T_C - 2453474$	0.85970 ± 0.00008
<i>Derived Parameters</i>	
b	0.26 ± 0.04
T_{14} (sec)	8228 ± 24
$R_p (R_J)^b$	1.462 ± 0.005
a (AU) ^b	0.02797 ± 0.00025

^aMedian value and 68.3% credible interval from MCMC fit of all 9 light curves jointly.

^bAssuming $R_* = 0.902 \pm 0.018 R_\odot$ (Alonso et al., 2008) and using $R_J = 71,492$ km.

4.4.3 Timing

We have compiled our results with fifteen available in the literature (Rauer et al., 2010; Vereš et al., 2009; Alonso et al., 2008); the last reference includes three pre-discovery light curves from BEST (Berlin Exoplanet Search Telescope) and ten light curves from the Amateur eXoplanets Archive, or AXA⁴. Many of the amateur and pre-discovery transits are not very precisely timed, so we limited our recalculation of the transit ephemeris to only those four with errors on the midtime less than 60 s (our three transits and the CoRoT time from Alonso et al., 2008). Note that although the CoRoT time was derived from several transit epochs, the individual midtimes of all but one transit have not been published.

The top panel of Figure 4-10 shows the ephemeris from Rauer et al. (2010), which was recalculated including pre-discovery images from a year before the CoRoT data were taken. The bottom panel shows our adopted fit, which includes the four most precisely timed transit epochs. We find

$$T_C(N) = 2454237.53565(51)[BJD] + 1.7429988(40)N, \quad (4.4)$$

where T_C is the predicted central time of a transit, the first term is the reference midtime, and N is the number of periods since the reference midtime. The values in parentheses are errors on the last digits. This fit had a reduced $\chi^2 = 3.6$, and we have scaled the errors in the equation upward by $\sqrt{3.6} = 1.9$ to account for the less-than-ideal fit. The residuals from the fit are shown in Table 4.9.

Our ephemeris equation in Equation 4.4 is almost identical to the one determined by Alonso et al. (2008), and does not agree with the slight adjustment proposed by Rauer et al. (2010), who found a period that was 0.9 ± 0.5 s shorter than the period found by the CoRoT survey, although they did not conclude that their finding was significant. Since both our ephemeris and that of Alonso et al. (2008) were calculated using transits with robustly measured midtimes (i.e., less than a minute), we attribute this slight difference in period to the effects of including less-precise transit times.

⁴<http://brucegary.net/AXA/x.htm>

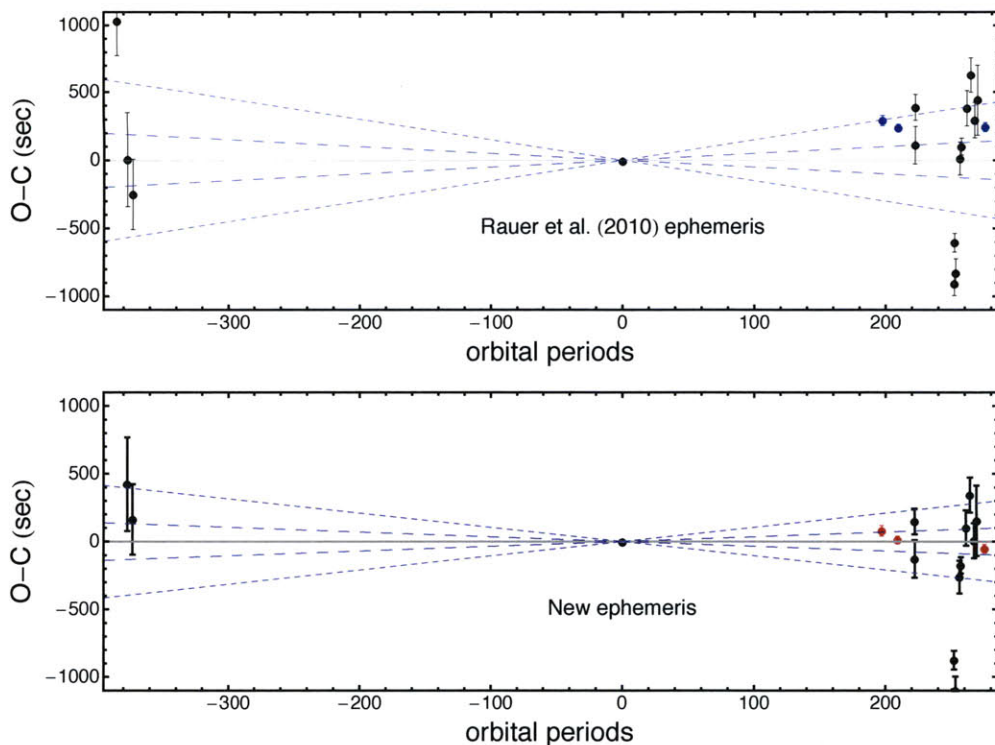


Figure 4-10 Observed minus calculated midtimes for CoRoT-2b. Top panel: timing residuals using the ephemeris from Rauer et al. (2010). The colored points represent the three new transits while the black points are taken from Rauer et al. (2010); Vereš et al. (2009); Alonso et al. (2008). Bottom panel: timing residuals using a new ephemeris calculated using only transits with errors less than 60 seconds (ours plus CoRoT). The solid line represents zero deviation from expected time of transit, while the dashed lines represent the 1σ and 3σ errors on the calculated orbital period, indicating the slopes that result for a mis-determined period.

Note that both published ephemerides and this new work indicate that several of the AXA curves and the first pre-discovery transit have strongly discrepant midtimes (up to 20 minutes), which could indicate strong timing variations. However, given the heterogeneity of sources of both photometry and timing information, particularly from the amateur light curves, further investigation is needed before making any definitive claims. We have not attempted to add any UTC-TT corrections to any of the literature data, which may introduce an additional error of about a minute, which is smaller than most of the errors on the midtimes and the largest timing residuals.

Table 4.9. Timing residuals for CoRoT-2b

Transit	Number	O-C (s)	σ
Rauer et al. (2010)	-385	1458 ± 259	5.6
Rauer et al. (2010)	-377	422 ± 346	1.2
Rauer et al. (2010)	-373	163 ± 259	0.6
Alonso et al. (2008)	0	-3 ± 12	-0.2
This work (20080424)	197	80 ± 38	2.1
This work (20080515)	209	13 ± 28	0.5
AXA	222	-128 ± 138	-0.9
AXA	222	149 ± 95	1.6
AXA	252	-1179 ± 86	-14
AXA	252	-876 ± 69	-13
AXA	253	-1101 ± 104	-11
AXA	256	-263 ± 121	-2.2
AXA	257	-176 ± 60	-2.9
AXA	261	101 ± 130	0.8
AXA	264	343 ± 130	2.6
AXA	267	6 ± 130	0.05
Vereš et al. (2009)	269	153 ± 259	0.6
This work (20080907)	275	-53 ± 32	-1.6

4.5 Conclusions

We have obtained some of the highest-quality ground based transits of OGLE-TR-113b, with timing precision of 9-46 s on all transits and photometric precision of 0.6-0.7 mmag in 2 minutes on our two best transits of OGLE-TR-113b (20080514 and 20090510). For CoRoT-2b we achieved 30-39 s timing precision and 0.8 mmag precision on our best light curve (20080424).

We have refined the system parameters for OGLE-TR-113b. The error on the planetary radius, $R_p = 1.084 \pm 0.029 R_J$, is now dominated by the error on the stellar radius, which is seven times greater than the formal fit error for the transit light curves. Improved stellar parameters are necessary to reduce errors on the planetary parameters.

We have examined the timing residuals of 10 transit epochs for OGLE-TR-113b and find no evidence of periodic timing variation that might indicate a companion planet. We do however find that the period measured from our new transits (observed from 2007-2009) is shorter than the period calculated for earlier transit epochs (data from 2002-2005) by 240 ± 120 ms, which if confirmed with future observations would be the first detection of orbital decay of an extrasolar planet. Due to the rapid rate

at which the period is currently estimated to be changing (about 50 ms per year), this would be an indication that OGLE-TR-113b may be falling in to its star on a quite rapid time scale.

Similarly, for CoRoT-2b we find no evidence of timing or period variations. If the midtimes for the individual transits observed by CoRoT are released, our three data points, which were observed a few months later, will help place tighter limits on any timing variations in the system.

4.6 Acknowledgements

Thanks to: Amanda Gulbis and Bobby Bus, in particular, for their work on MORIS; the IRTF telescope operators Bill Golisch, Dave Griep, Paul Sears, and Eric Volquardsen; Matt Lockhart, for observing two transits of CoRoT-2b with MORIS; Josh Winn and Adam Burgasser, for observing one transit each of OGLE-TR-113b as part of MIT's queue program; and the Magellan staff, in particular telescope operators Jorge Araya, Mauricio Martinez, Hernàn Nuñez, Hugo Rivera, Geraldo Valladares, and Sergio Vera, for making these observations possible.

Chapter 5

Other Planets: OGLE-TR-132b, OGLE-TR-10b, XO-2b

5.1 Additional planets

We observed transits of several additional planets which we will now discuss. OGLE-TR-132b, as the faintest OGLE planet, had somewhat poorer precision than the other targets, but due to its short period we were able to observe seven transits. Both the transit light curve parameters and the timing agree well with previously published values. We also observed OGLE-TR-10b and XO-2b, and present three and two transits, respectively, for those systems, and discuss some of the problems we experienced with each system that limit the precision of our data. We see no signs of transit timing deviations in OGLE-TR-10b in our own data, although we note two anomalous literature times; similarly, our data for XO-2b agrees very well with the published transit midtimes.

5.2 OGLE-TR-132b

OGLE-TR-132b was first announced as a planet candidate by Udalski et al. (2003) and confirmed to be of planetary mass by Bouchy et al. (2004). High quality photometry was provided with two *R*-band transit light curves by Moutou et al. (2004) and Gillon

Table 5.1. Observational and photometry parameters for OGLE-TR-132b

Transit (UT)	N_{Frames} used (discarded)	Exp. Time (sec)	Binning	Readout (sec)	N_{Comp}	Aperture ^a (pixels)	Sky radius, width (pixels)	Scatter ^b (mmag)
20080419	227 (0)	60	1x1	5	7	13	30, 20	1.0
20080424	160 (0)	60, 120	1x1	5	4	19	40, 30	1.7
20080511	136 (5) ^c	120	1x1	5	3	26	50, 20	1.0
20090207	1190 (10) ^d	10, 15	2x2	0.003 ^e	2	15	30, 10	1.2
20090311	2322 (0)	10, 15	2x2	0.003 ^e	2	12	30, 10	1.1
20090424	476 (0)	20-75	1x1	0.003 ^e	3	15	30, 10	1.3
20090511	440 (0)	35, 40	2x2	0.003 ^e	8	9	20, 10	1.0

^aRadius around star

^bStandard deviation of the residuals on data binned to 120 s.

^cDiscarded due to tracking problem.

^dDiscarded due to low counts.

^eFrame transfer mode used.

et al. (2007). The host star is somewhat larger than the sun, with $M_* = 1.26 \pm 0.03 M_\odot$ and $R_* = 1.34 \pm 0.08 R_\odot$ (Gillon et al., 2007). OGLE-TR-132 is the faintest star ($I = 15.7$) we observed, but the planet has a short period (1.69 days), so there are many transit opportunities. We attempted observations on 8 different nights.

5.2.1 Observations

20080203

The half-transit on 20080203 was intended as the first test of the new MagIC-e2v camera, but due to unresolved issues with excess instrument noise in that instrument we observed with MagIC-SiTe instead. 84 images, each 60 seconds, were observed of this target spanning 2 hours (only the second half of the transit was observable). Problems with the shutter not retracting during some images introduced noise into the light curve at about the percent level, obscuring any transit signal. The photometry for this transit is shown in Appendix A.

20080419

The first officially scheduled transit with MagIC-e2v, transit 20080419 was observed on a night with good seeing (0."5) and somewhat variable transparency. The airmass ranged from 1.2 to 1.4. The best light curve was produced with a 13 pixel radius aperture, using a sky radius of 30+20 pixels and 7 comparison stars. 227 exposures of 60 seconds each were taken.

20080424

Transit 20080424 had somewhat variable conditions for the second half of transit, and variable seeing of 0."6-0."7. The airmass ranged from 1.2 to 1.8. The best light curve was produced with a 19 pixel radius aperture, using a sky radius of 40+30 pixels and 4 comparison stars. 160 exposures of initially 60 seconds, and later 120 seconds, were taken. A trend against telescope azimuth was removed from the photometry before fitting.

20080511

Transit 20080511 was taken under stable photometric conditions with seeing of 0."5-0."7 and airmass ranging from 1.2 to 1.5. The best light curve was produced with a 26 pixel radius aperture, using a sky radius of 50+20 pixels and 3 comparison stars. 136 exposures of 120 seconds each were used. A trend against airmass was removed from the photometry before fitting.

20090207

Transit 20090207 was the first observed with the new frame transfer mode. Early in the transit there was some variable transparency (counts dropped by a factor of 2 at one point), although conditions improved later. The airmass ranged from 2.1 to 1.2, and the seeing from 0."5-0."7. The best light curve was produced with a 15 pixel radius aperture, using a sky radius of 30+10 pixels and 2 comparison stars. 1190 frames were used (out of 1200 taken; several images with low counts were discarded),

with exposure times of 10 or 15 seconds. A trend against airmass was removed from the photometry before fitting.

20090311

Transit 20090311 was observed under stable conditions, with the seeing around 0."6 for most of the transit and the airmass ranging from 1.2 to 1.6. The best light curve was produced with a 12 pixel radius aperture, using a sky radius of 30+10 pixels and 2 comparison stars. 2322 frames were used, with exposure times of 10-15 seconds. A trend against airmass was removed from the photometry before fitting.

20090424

Transit 20090424 was observed under variable sky conditions, with the seeing from 0."6-0."8 and the airmass ranging from 1.2 to 1.8. The best light curve was produced with a 15 pixel radius aperture, using a sky radius of 30+10 pixels and 3 comparison stars. 476 frames were used, with exposure times of 20-75 seconds. A trend against seeing was removed from the photometry before fitting.

20090511

Transit 20090511 was taken under stable photometric conditions with seeing of 0."5 and airmass ranging from 1.2-1.8. The best light curve was produced with a 9 pixel radius aperture, using a sky radius of 20+10 pixels and 8 comparison stars. 440 exposures of 35 or 40 seconds each were taken. A trend against airmass was removed from the photometry before fitting.

Literature light curves

In addition to the seven new light curves, we obtained the original photometry for the two *R* transits published by Gillon et al. (2007), which we have refitted jointly with our transits. The data tables were provided with the start time of each frame in UTC, to which we added 16 s (half the exposure time) and the converted into BJD times using the same method as with our transits (see Appendix C).

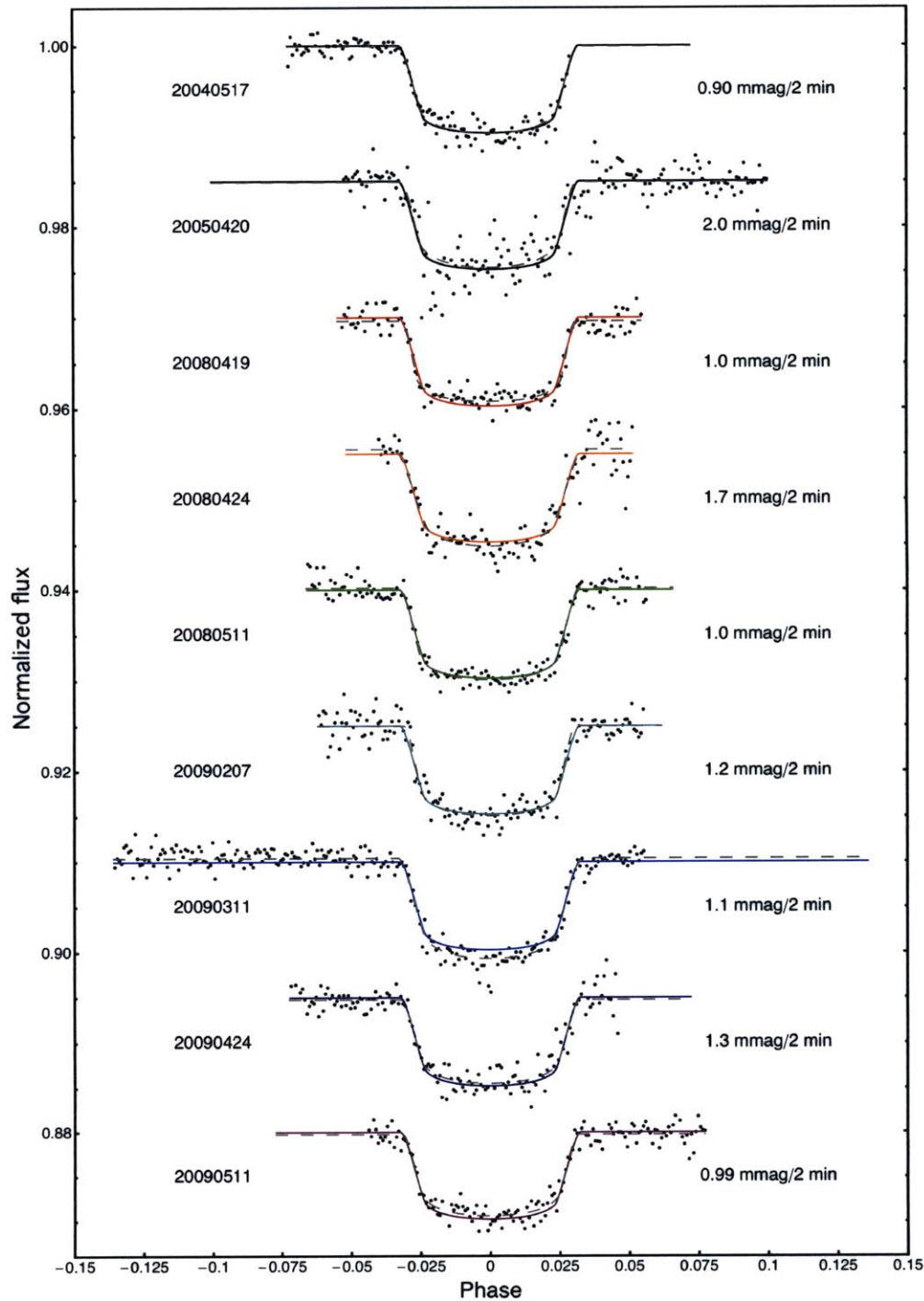


Figure 5-1 Nine transits of OGLE-TR-132b. All available high-quality light curves are plotted vs. orbital phase, with the data binned to 2 minutes to aid comparison; each transit has been shifted vertically by 0.015 for clarity. The top two transits are taken from Gillon et al. (2007), while the rest of the transits are new. The joint model fit (solid lines) were calculated using the parameter values in Table 5.3; the stated standard deviation is the residuals from the joint model fit. Table 5.2 shows the unbinned data; a full table can be provided on request.

Table 5.2. Flux values for new transits of OGLE-TR-132b

Mid-exposure (UTC) ^a	Mid-exposure (BJD)	Flux	Error
2454575.506679	2454575.510331	0.9996423	0.00122
2454575.507433	2454575.511084	1.001028	0.00122
2454575.508183	2454575.511834	0.9992174	0.00122
2454575.508936	2454575.512588	1.000828	0.00122
2454575.509689	2454575.513341	1.000836	0.00122
...			

^aFull table available on request.

5.2.2 Model and light curve fits

All nine light curves were fit using a Monte Carlo Markov Chain (MCMC) method, as described in Chapter 3. We used a quadratic limb darkening law for the Sloan i' filters (Claret, 2000, 2004)¹, assuming $T = 6411$ K, $\log g = 4.86$, $[M/H] = 0.0$, and $V_{micro} = 2$ km/s, based on Moutou et al. (2004). We fixed the orbital period to $P = 1.689868$ days and assume throughout the fits that $M_* = 1.26 \pm 0.03 M_\odot$, $R_* = 1.34 \pm 0.08 R_\odot$, and $M_p = 1.14 \pm 0.12 M_J$, based on Gillon et al. (2007). We combined 3 chains of 950,000 links each (the first 50,000 links were discarded) to produce the best joint fit to all light curves, with the resulting distributions shown in Figure 5-2. The adopted parameters, shown in Table 5.3, are the median and 68.3% credible intervals of the combined parameter distribution.

The revised planetary radius, $R_P = 1.23 \pm 0.07 R_J$, is slightly larger than, but consistent with, the value of $R_P = 1.18 \pm 0.07 R_J$ reported by Gillon et al. (2007). Note that the error on the stellar radius, $R_* = 1.34 \pm 0.08 R_J$ (Gillon et al., 2007), dominates the error on the planetary radius, which has a formal fit error of 0.01.

We also examined each light curve of OGLE-TR-132b independently to search for parameter variations, using individual MCMC fits as described in Chapter 3. We find no evidence of variation in any of the parameters examined (Figure 5-3).

¹Initial values: $u_{1,i'} = 0.1903$, $u_{2,i'} = 0.3644$, $u_{1,R} = 0.2379$, $u_{2,R} = 0.3760$.

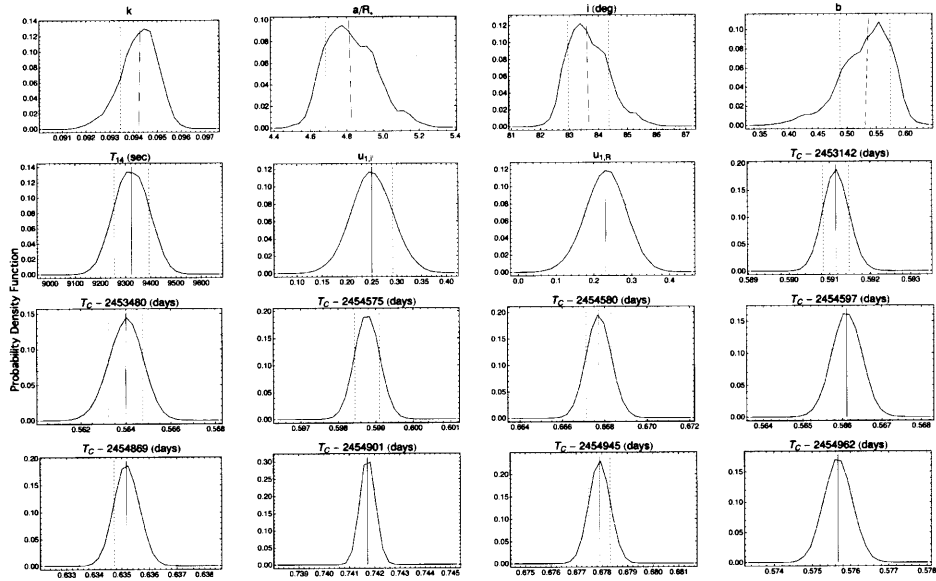


Figure 5-2 Parameter distributions for joint fit to nine transits of OGLE-TR-132b. Smoothed histogram of normalized parameter distributions, from which the parameters in Table 5.3 are derived. The solid line is the median value (which is very close to the mean value in all cases). Note that several of the distributions, particularly a/R_* , i , and b , are not strictly Gaussian. The dashed lines show the 68.3% credible interval. These values were calculated for 2,850,000 links.

Table 5.3. Transit parameters for OGLE-TR-132b (jointly fit)

	Median value	Formal Error ^a	Adopted Error ^b
<i>Fitted Parameters</i>			
k	0.0943	0.0008	0.0014
a/R_*	4.81	0.15	0.16
i	83.6	0.7	0.7
$u_{1,i'}$	0.25	0.04	0.04
$u_{2,i'}$	0.19	(fixed)	...
$u_{1,R}$	0.23	0.06	0.06
$u_{2,R}$	0.38	(fixed)	...
$T_C - 2453142$	0.59116	0.00032	0.00042
$T_C - 2453480$	0.56401	0.00078	0.00080
$T_C - 2454575$	0.59877	0.00033	0.00093
$T_C - 2454580$	0.66772	0.00059	0.00072
$T_C - 2454597$	0.56611	0.00038	0.00060
$T_C - 2454869$	0.63517	0.00047	0.00055
$T_C - 2454901$	0.74172	0.00030	0.00111
$T_C - 2454945$	0.67790	0.00041	0.00071
$T_C - 2454962$	0.57567	0.00037	0.00066
<i>Derived Parameters</i>			
b	0.54	0.05	0.05
T_{14} (sec)	9324	69	111
R_p (R_J) ^c	1.229	0.074	0.076
a (AU) ^c	0.030	0.0009	0.002

^aFormal 68.3% credible interval from MCMC fit of all 9 light curves jointly.

^bAdopted error from residual permutation method, if greater than the formal error.

^cAssuming $R_* = 1.34 \pm 0.08 R_\odot$ (Gillon et al., 2007) and using $R_J = 71,492$ km.

5.2.3 Timing

The top panel of Figure 5-4 shows the ephemeris from Gillon et al. (2007). The bottom panel shows our adopted fit, which includes all 9 transit epochs. We find a slightly revised period, with

$$T_C(N) = 2453142.59099(47)[BJD] + 1.68986531(67)N, \quad (5.1)$$

where T_C is the predicted central time of a transit, N is the number of periods since the reference midtime, and the values in parentheses are errors on the last digits. This fit had a reduced $\chi^2 = 1.4$, and we have scaled the errors in the equation upward by $\sqrt{1.4} = 1.2$ to account for this. OGLE-TR-132b has perhaps the simplest timing of any of the transits presented in this thesis, with no real evidence timing variations. We

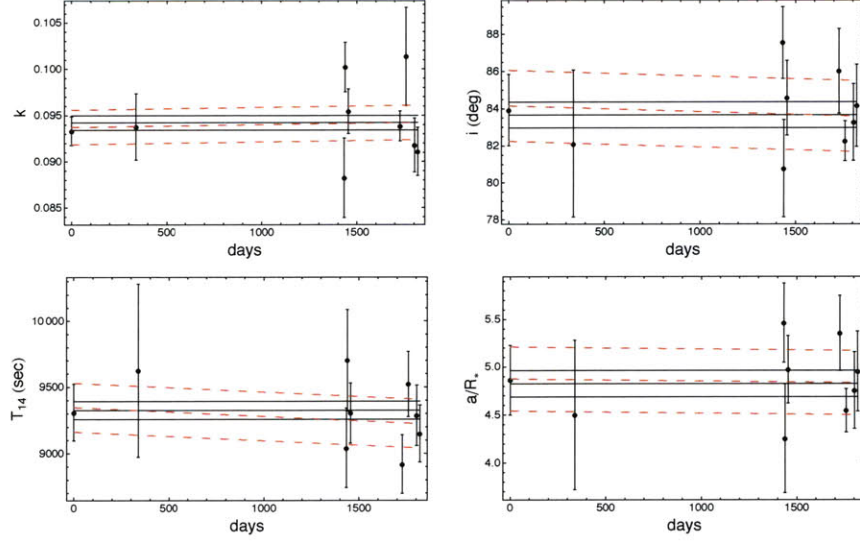


Figure 5-3 Parameter variation of individual transits of OGLE-TR-132b, based on individual MCMC fits (Table 5.4), for (clockwise, from top-left): k , i , a/R_* , and T_{14} . The errors have been scaled upward based on the factor calculated from residual permutation. The values derived from the joint MCMC fit to all transits (Table 5.3) are plotted as solid black lines with $\pm 1\sigma$ errors. The dashed red lines indicate the best sloped fit with $\pm 1\sigma$ errors. All fits are consistent with no parameter variation during the time period examined.

Table 5.4. Individual transit parameters for OGLE-TR-132b (independently fit)

Transit	k^a	f^b	T_{14}^a	f^b	a/R_*^a	f^b	i^a	f^b
20040517	0.0933 ± 0.0016	0.99	9310 ± 213	1.1	4.86 ± 0.36	...	83.9 ± 1.9	...
20050420	0.0938 ± 0.0036	...	9627 ± 654	...	4.50 ± 0.78	...	82.1 ± 4.0	...
20080419	0.0882 ± 0.0043	4.1	9041 ± 300	2.9	5.46 ± 0.42	1.9	87.6 ± 1.9	1.2
20080424	0.1002 ± 0.0027	...	9703 ± 384	1.1	4.25 ± 0.57	1.4	80.8 ± 2.6	1.4
20080511	0.0955 ± 0.0024	1.6	9305 ± 226	1.3	4.97 ± 0.35	...	84.6 ± 2.0	...
20090207	0.0939 ± 0.0016	...	8919 ± 223	1.3	5.35 ± 0.40	...	86.0 ± 2.3	...
20090311	0.1014 ± 0.0053	4.6	9523 ± 245	1.6	4.55 ± 0.23	...	82.3 ± 1.1	...
20090424	0.0918 ± 0.0029	1.7	9286 ± 228	1.1	4.76 ± 0.40	...	83.3 ± 2.1	...
20090511	0.0911 ± 0.0026	1.6	9150 ± 214	1.0	4.96 ± 0.42	...	84.2 ± 2.2	...

^aFormal individual MCMC fit value and error (scaled upward by factor f in adjacent column).

^bFactor by which the error in the previous column has been increased based on the residual permutation method; no value is given if the formal MCMC fit error was larger.

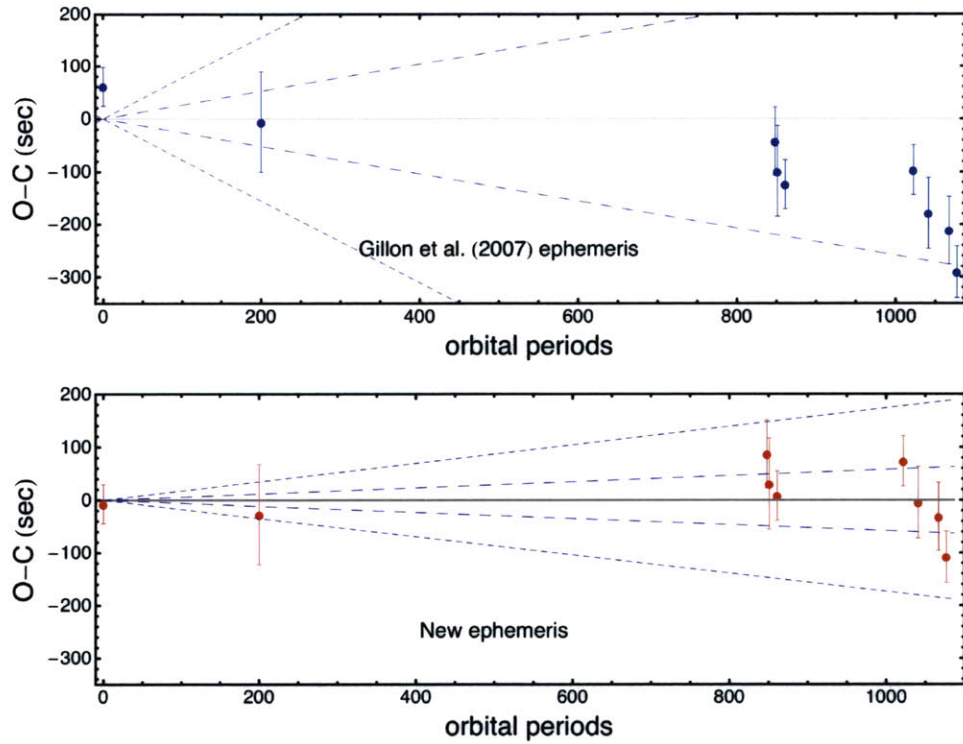


Figure 5-4 Observed minus calculated midtimes for OGLE-TR-132b. Top panel: timing residuals for eleven transits using the ephemeris from Gillon et al. (2007). Bottom panel: timing residuals using the new ephemeris (Equation 5.1), calculated using all nine transits. The solid line represents zero deviation from expected time of transit, while the dashed lines represent the 1σ and 3σ errors on the calculated orbital period, indicating the slopes that result for a mis-determined period.

will note that our period is five times more precise than the best period in literature, 1.689868 ± 0.000003 , thanks to the extra years of baseline, though it differs by less than 1σ , or 0.2 s, from that value (Gillon et al., 2007). There is no evidence of orbital decay within the current precision of the data.

Table 5.5. Timing residuals for OGLE-TR-132b

Transit	Number	O-C (s)	σ
20040517	0	-7 ± 37	-0.2
20050420	200	-27 ± 95	-0.3
20080419	848	87 ± 64	1.4
20080424	851	31 ± 86	0.4
20080511	861	8 ± 47	0.2
20090207	1022	73 ± 47	1.6
20090311	1041	-4 ± 68	-0.1
20090424	1067	-31 ± 65	-0.5
20090511	1077	-108 ± 49	-2.2

5.3 OGLE-TR-10b

OGLE-TR-10b was announced as a candidate by Udalski et al. (2002a) and eventually confirmed with additional radial velocity observations (Konacki et al., 2003b; Bouchy et al., 2005; Konacki et al., 2005). There has been some controversy over the parameters for this system, most notably the stellar temperature (and hence the stellar radius and mass derived from that value) and the depth of the transit (and hence the planetary radius ratio). Lower stellar temperatures have been found using spectra from Konacki et al. (2005, 5750 ± 100 K) and re-analyzed by Holman et al. (2007, 5800 ± 100 K), while other groups have found larger temperatures, including Bouchy et al. (2005, 6220 ± 140 K), Santos et al. (2006, 6075 ± 86 K) and Ammler-von Eiff & Santos (2008, 6020 ± 140 K). These temperatures translate to a range of stellar masses and radii, from a near-solar analogue with $1 M_{\odot}$ and $1 R_{\odot}$ (Konacki et al., 2005) to a much larger $1.22 \pm 0.05 M_{\odot}$ and $1.21 \pm 0.07 R_{\odot}$ (Bouchy et al., 2005), with other estimates in between.

Compounding the uncertainty over the stellar parameters is the independent problem of the wide range in reported transit depths, ranging from 2.2% for the original OGLE survey photometry (Udalski et al., 2002a) to 0.99% by Holman et al. (2007) to a recent low of 0.87% in the Sloan g' transit of Bentley et al. (2009). It was suggested by Pont et al. (2007) that the different transit depths might be due to different photometry methods; Holman et al. (2007) and Bentley et al. (2009) both used image subtraction, which can give incorrect radius values, as noted by Gillon et al. (2007) for the case of OGLE-TR-132b and mentioned in Chapter 2 as a possible reason for slightly discrepant values for OGLE-TR-111b. However, the original OGLE survey also used a photometry pipeline built around image subtraction (Udalski et al., 2002a). Holman et al. (2007) offered an alternate explanation, noting that only two of the seven OGLE-TR-10b transits obtained by the OGLE survey were full transits with baseline before and after, and both showed signs of being shallower than the reported depth. Full transits are much more reliable at estimating depths than half transits, particularly if there is a slope in the overall photometry. That said, Pont

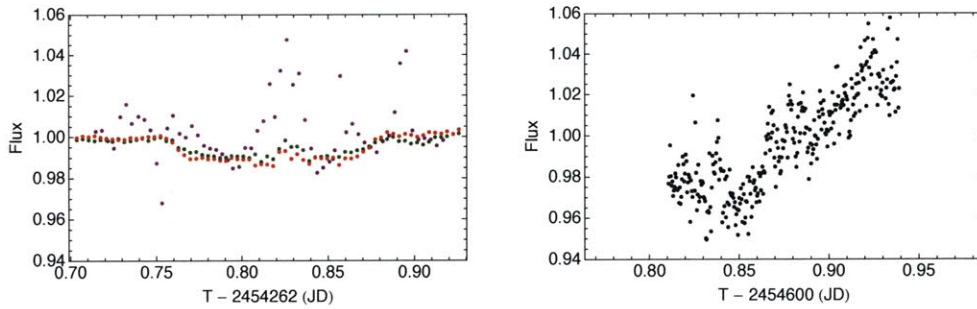


Figure 5-5 Variability of OGLE-TR-10b. Left: transit observed by Bentley et al. (2009) simultaneously in u' (purple), g' (green), and i' (red); the strong flare visible in the u' data makes the transit almost undetectable. Right: our transit attempt on 20080514, the same night excellent transits were observed of OGLE-TR-113b and OGLE-TR-56b. Although other stars on the same frame are flat at the 0.4% level, the flux from OGLE-TR-10 varies by 8%. Both axes have been adjusted so that the data are plotted on a common scale for comparison; the transit on 20080514 should have begun soon after the first data points were acquired.

et al. (2007) reanalyzed the original images of Holman et al. (2007) using aperture photometry and found a deeper depth, 1.2%, that was consistent with their own new half-transit, indicating that perhaps the values from Holman et al. (2007) were too low because of problems determining the correct reference level with image subtraction. Perhaps one of the largest problems to plague this planet has been incomplete time sampling; of the seven nights on which transits were observed since the original survey (Holman et al., 2007; Pont et al., 2007; Bentley et al., 2009), only two resulted in full light curves with baseline before and after transit: one transit each from Holman et al. (2007) and Bentley et al. (2009).

Combining the uncertain stellar radius values with the uncertain photometric depths has resulted in a range of radius values for the planet from about 1-1.5 R_J , a completely unacceptable situation for theorists concerned with whether or not the planetary radius is inflated.

A possible solution to the discrepant measurements may have been found by Bentley et al. (2009), who observed a stellar flare during a transit observed simultaneously in three wavelengths, Sloan u' , g' , and i' (see Figure 5-5). The flare was brightest in u' , with the flux varying by about 5% during the five hours of observations;

Table 5.6. Observational and photometry parameters for OGLE-TR-10b

Transit (UT)	N_{Frames} used (discarded)	Exp. Time (sec)	Binning	Readout (sec)	N_{Comp}	Aperture ^a (pixels)	Sky radius, width (pixels)	Scatter ^b (mmag)
20080511	246 (5) ^c	30, 60	1x1	5	4	16	60, 10	1.2
20080611	670 (0)	25-60	1x1	5	2	22	100, 10	0.9
20090810	532 (7) ^d	12-30	2x2	0.003 ^e	2	11	50, 10	1.4

^aRadius around star

^bStandard deviation of the residuals from the independent model fit on data binned to 120 s.

^cDiscarded due to trailing images (temporary tracking problem).

^dDiscarded due to high noise just before ingress.

Bentley et al. (2009) estimated that it would compare to a class X13 solar flare, the 7th largest recorded solar flare². OGLE-TR-10 was listed by Kashyap et al. (2008) as having one of the highest X-ray luminosities of any planet-hosting star, with $\log_{10}(L_X) = 30.34 \pm 0.25 \text{ erg s}^{-1}$, based on an exhaustive search of X-ray survey archives. If the star is truly active, especially on an intermittent timescale, this could potentially explain both the observed spectral and photometric differences, although more work would need to be done to identify the type of variability.

Here we present three transits that we successfully observed of OGLE-TR-10b with Magellan between 2008 May and 2009 August, including two full and one partial event. We also discuss a failure to detect a transit one another night due to high stellar noise, possibly from another flare, although more theoretical modeling would be needed to determine if the pattern of variability we saw could be accounted for by the same type of flare event as observed by Bentley et al. (2009).

5.3.1 Observations

Due to the relatively long period (3.10 days) and telescope scheduling constraints, we have observed fewer transits of this target than of the other four OGLE planets, with 3.5 transits attempted (another half transit on 20090808 was weathered out). All observations were with the MagIC-e2v instrument on the Baade telescope.

²<http://www.spaceweather.com/solarflares/topflares.html>

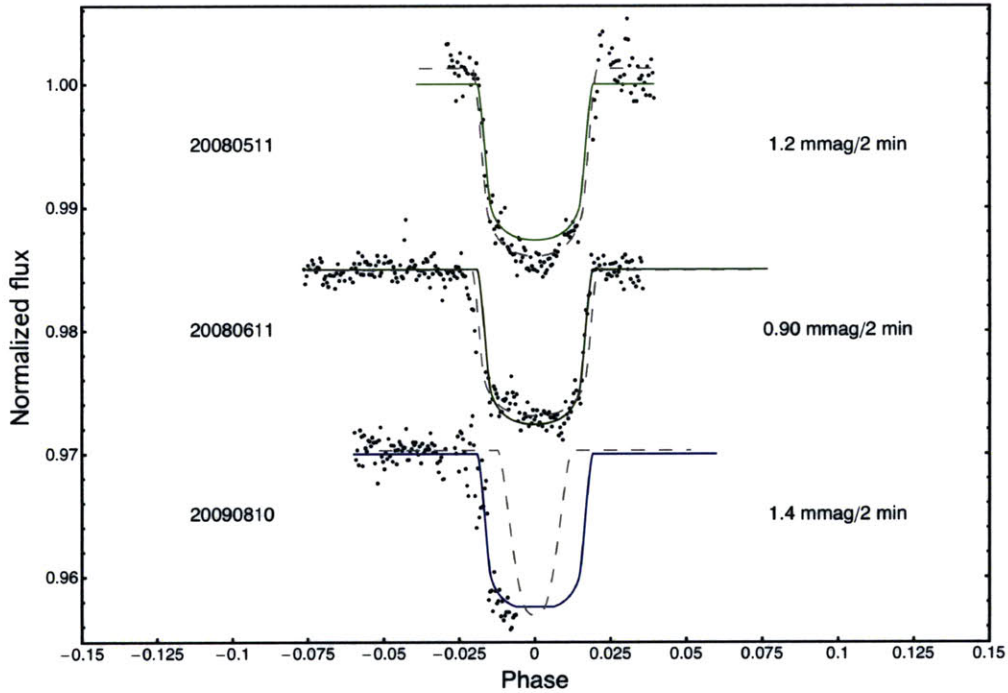


Figure 5-6 Three transits of OGLE-TR-10b. All new light curves are plotted vs. orbital phase, with the data binned to 2 minutes to aid comparison. The joint model fit (solid lines) to all three transits does not agree with the independent fits (dashed lines) to each transit individually, particularly on the depth, even when only the two full transits (20080511 and 20080611) are examined. Unlike in other similar plots in this thesis, here the stated standard deviation is the residuals from the individual model fits. (The residuals from the joint fits, in order 1.8, 1.1, and 1.5 mmag in 2 min, are much larger due to model discrepancies and are not good estimates of the intrinsic photometric variability).

20080511

Transit 20080511 was observed during stable photometric conditions and good (0."4) seeing. The best light curve was produced with a 16 pixel radius aperture, using a sky radius of 60+10 pixels and 4 comparison stars.

20080514

Transit 20080514 was also observed on a night with good seeing (0."4); it was the third transit observed on a night that produced spectacular light curves of OGLE-TR-113b (see Chapter 4) and OGLE-TR-56b (see Chapter 3). The airmass on the target was also low, from 1.0 to 1.4. However, despite the continuance of the good observing conditions during the observations, no transit could be detected because the noise on the target star was too great, with a roughly 8% increase in the relative stellar flux during 3 hours of observations. By comparison, the flux ratios of several bright comparison stars on the same fields reached millimagnitude precision, and a transit around those stars would have been obvious (see Figure A-10 in Appendix A for a comparison of the flux from our target and from another star). We conclude that we may have observed an episode of strong stellar variability, perhaps another flare, although with different characteristics from the one observed by Bentley et al. (2009). See discussion in § 5.3.2.

20080611

The best light curve of OGLE-TR-10b was observed on 20080611. The airmass ranged from 1.7 to 1.0 back to 1.7, and the seeing held constant around 0."4. The best light curve was produced with a 22 pixel radius and a sky radius of 100+10 pixels, using 2 comparison stars. A slight mismatch in the level of baseline before and after transit was removed by detrending against telescope azimuth.

20090810

Due to scheduling constraints, only the first half of transit 20090810 could be observed. The seeing was highly variable and poor, ranging from 0."6-1."2, though the airmass was low, ranging from 1-1.2. The best light curve was produced with an 11 pixel radius and a 50+10 pixel sky radius, using 2 comparison stars. Photometry was stable until shortly before ingress, when a noise bump can be seen (whether due to terrestrial or stellar variability is an open question).

5.3.2 Model and light curve fits

All three light curves were fit using a Monte Carlo Markov Chain (MCMC) method, as described in Chapter 3. We used a quadratic limb darkening law for the Sloan i' filters (Claret, 2000, 2004)³, assuming $T = 6220$ K, $\log g = 4.7$, $[M/H] = 0.5$, and $V_{micro} = 2$ km/s. We fixed the orbital period to $P = 3.10129$ days, the value from Pont et al. (2007). We assume throughout the fits that $M_* = 1.025 \pm 0.135 M_\odot$, $R_* = 1.095 \pm 0.055 R_\odot$, and $M_p = 0.57 \pm 0.12 M_J$, based on Holman et al. (2007). (Note that the precise values for all of these parameters do not have a strong effect on the fit results.)

We combined 3 chains of 950,000 links each (the first 50,000 links were discarded) to produce the best joint fit to all light curves, with the resulting distributions shown in Figure 5-7. The adopted parameters, shown in Table 5.7, are the median and 68.3% credible intervals of the combined parameter distribution.

When we fit each transit independently (see Table 5.8), we do not find that the measured radius ratios agree well. Ignoring the half-transit, which is too incomplete to have a well constrained shape, we find that transits 20080511 and 20080611 disagree on their independently derived radius ratios, 0.1168 ± 0.0018 and 0.1017 ± 0.0007 , respectively, by 6σ . The durations, semimajor axes, and inclinations, however, all agree within 1σ . We note that our radius ratios are intermediate to the high found by the OGLE survey, 0.148, and the low found by Bentley et al. (2009), 0.093. We

³Initial values: $u_{1,i'} = 0.2264$, $u_{2,i'} = 0.3689$.

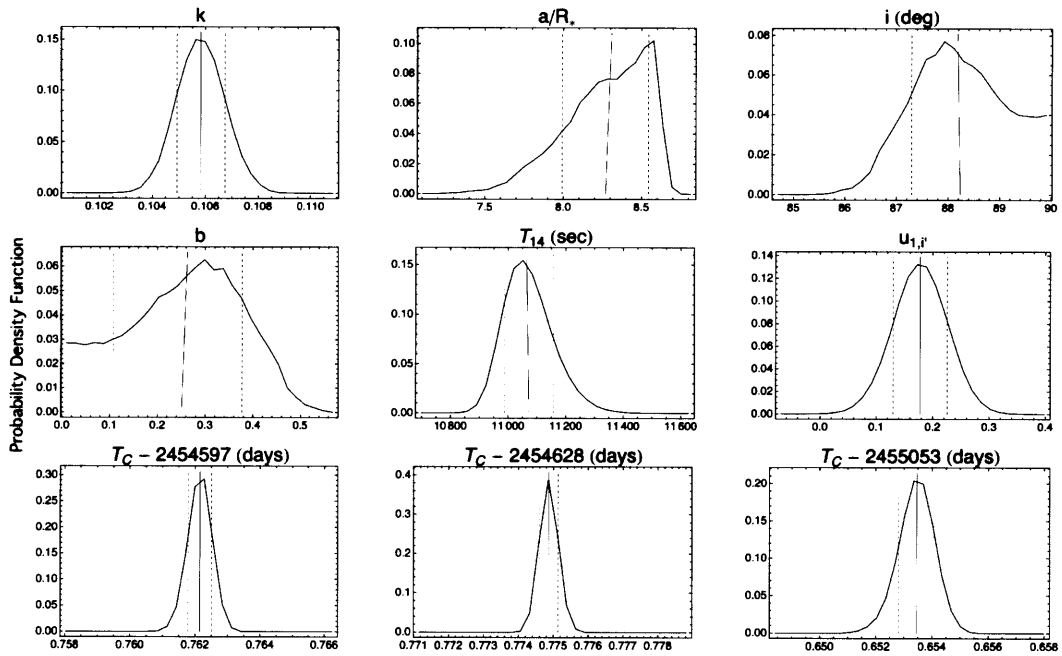


Figure 5-7 Parameter variation of individual transits of OGLE-TR-10b. Smoothed histogram of normalized parameter distributions, from which the parameters in Table 5.7 are derived. The solid line is the median value (which is very close to the mean value in all cases). Note that several of the distributions, particularly k , a/R_* , i , and b , are not strictly Gaussian. The dashed lines show the 68.3% credible interval. These values were calculated for 2,850,000 links.

examined our best seeing images on 20080611 ($<0.''4$) and found that there is a faint comparison star $1.''2$ away from OGLE-TR-10b. We used PSF fitting to remove this star and several other, more distant faint companions, and found a very clean residual pattern, with no evidence of other, undetected faint stars. Based on the seeing and aperture settings we used for that frame, the contribution of all faint stars to the flux of the star was estimated at 0.08% of the normalized stellar flux. This translates into a radius ratio error of 0.03, much greater than the formal error on our radius ratio. Depending on the precise aperture settings used and the variability of the seeing on a given night, these faint stars could explain the differences in our aperture photometry (and perhaps in other work as well).

Using our joint fit results, we calculate the planetary radius as $R_P = 1.127 \pm 0.06 R_J$, assuming $R_* = 1.095 \pm 0.055 R_\odot$ (Holman et al., 2007), and including the formal stellar radius error. We do not account for the spread in stellar radius values, as noted earlier, nor do we factor in the uncertain contribution of the faint nearby stars, both of which would make the real uncertainty larger.

Variability

Aperture photometry on OGLE-TR-10 is harder than on the other 4 OGLE stars examined in this thesis because the field is particularly crowded (more so than OGLE-TR-111, OGLE-TR-113, and OGLE-TR-132), and because despite the large number of nearby stars most of them are fainter than the target (unlike OGLE-TR-56, which is similarly crowded but has many bright stars). This means that depending on the field of view there are relatively few good comparison stars to use. Additionally, the presence of the faint comparison star $1.''2$ away discussed in the previous section means that on nights with variable seeing a large aperture might include variable amounts of contamination. These are two reasons why we might see variable photometry that are unrelated to physical changes.

However, the star itself may also be intermittently active, the strongest support for which is the simultaneous observations in three wavelengths by Bentley et al. (2009) and the detection in all three of them of a probable stellar flare. The flare

Table 5.7. Transit parameters for OGLE-TR-10b (jointly fit)

	Adopted value ^a
<i>Fitted Parameters</i>	
k	0.1058 ± 0.0009
a/R_*	8.31 ± 0.23
i	88.2 ± 1.1
$u_{1,i}$	0.18 ± 0.05
$u_{2,i}$	0.37 (fixed)
$T_C - 2454597$	0.76215 ± 0.00035
$T_C - 2454628$	0.77480 ± 0.00027
$T_C - 2455053$	0.65347 ± 0.00061
<i>Derived Parameters</i>	
b	0.262 ± 0.004
T_{14} (sec)	11064 ± 93
$R_p (R_J)^b$	1.127 ± 0.010
a (AU) ^b	0.042 ± 0.003

^aMedian value and formal 68.3% credible interval from MCMC fit of all 3 light curves jointly.

^bAssuming $R_* = 1.095 \pm 0.055 R_\odot$ (Holman et al., 2007) and using $R_J = 71,492$ km.

Table 5.8. Individual transit parameters for OGLE-TR-10b (independently fit)

Transit	k^a	T_{14}^a	a/R_*^a	i^a
20080511	0.1168 ± 0.0018	11123 ± 161	7.8 ± 0.5	86.6 ± 1.2
20080611	0.1017 ± 0.0007	11199 ± 101	8.2 ± 0.3	88.5 ± 1.0
20080611	0.1222 ± 0.0267	15209 ± 4389	6.0 ± 1.3	86.0 ± 2.1

^aFormal individual MCMC fit value and error.

event that group observed was strongest in u' (5%), visible in g' (3%) and weakest, though still clear, in i' (0.5%). In our observations, we may be detecting stellar variability in one of our light curves (20080514), and it is possibly present in all of them (the unexplained bumps in 20080511 and 20090810 and the baseline mismatch in 20080611), though more work needs to be done to rule out sources of variability resulting solely from the photometry. We note that the stellar activity, if it is to account for our data, must be itself variable, either varying in intensity or in the peak wavelengths: the strong variability we saw on 20080514 was visible in i' at the 8% level, while the flare observed by Bentley et al. (2009) was brightest in u' , and was only visible at the 0.5% level in i' . Further observations of this system are necessary to resolve the nature of the variability.

Timing

We plot the midtimes of the three new transits in Figure 5-8, using the ephemeris from Holman et al. (2007). Given the published data, there are strong timing variations in this system, but prior experience leads us to investigate a few things before concluding these are bona fide TTVs. First, the transits that are discrepant the most, the high point from Pont et al. (2007) and the low point from the g' and i' transits by Bentley et al. (2009), were both the only transits of this planet observed by those groups, and in neither work was the timing of the transit the main focus. The two groups that had multiple transits to compare, Holman et al. (2007) with five and this work with two full transits, achieve more consistent result both internally and with each other. Second, it is hard to get good baseline flux measurements for half-transits, and a mismatch in the flux before and after transit might be missed or improperly removed, which could lead to a wrong estimate for the beginning or end of transit. Without the symmetry of the other half of the transit, it is hard to identify small features of correlated noise that occur right at ingress or egress. At a minimum, the error bars on all the half transits must realistically account for systematic errors.

Third, it is important to confirm that each group has applied the same BJD offsets have been applied inconsistently; we note that the magnitudes of the observed

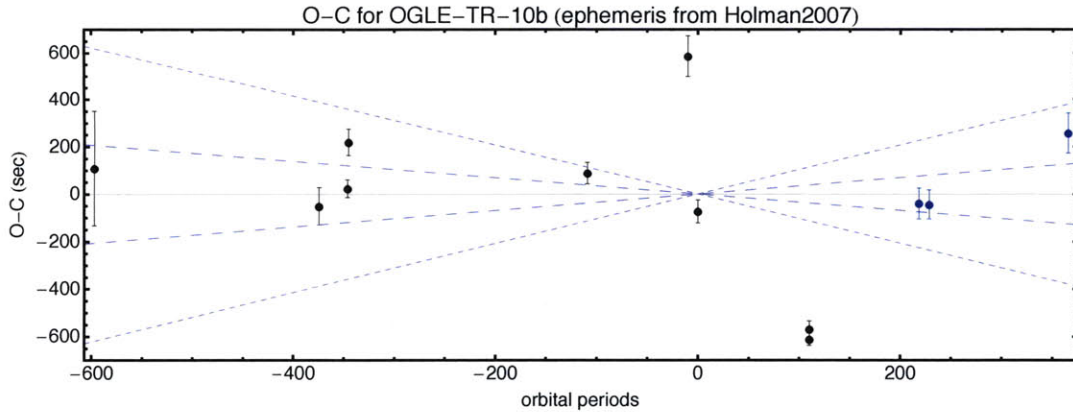


Figure 5-8 Observed minus calculated midtimes for OGLE-TR-10b. Timing residuals for twelve transits using the ephemeris from Holman et al. (2007). The solid line represents zero deviation from expected time of transit, while the dashed lines represent the 1σ and 3σ errors on the calculated orbital period, indicating the slopes that result for a mis-determined period. Our three transits (blue) are the most recent; the high point by Pont et al. (2007) is at orbital period number -10 and the low point by Bentley et al. (2009) is at orbital period number 110.

minus calculated (O-C) residual for the times from Pont et al. (2007) and Bentley et al. (2009) are similar to the UTC-BJD corrections for those days (550 s and 509 s, respectively). We note that published literature times have been off by a similar amount before due to just such an error (e.g., the 550 s shift for WASP-10b; Johnson et al., 2009, 2010). We have additionally made no attempt to correct for the TT-UTC error that might exist even between dates that had nominally been corrected to BJD (see Appendix C) in the literature curves, although the magnitude of that error is several times smaller than the two largest residuals.

A full reanalysis of all available transits, ideally starting from the raw data, might be necessary before any timing variation would be believed, but is beyond the scope of this thesis.

Table 5.9. Timing residuals for OGLE-TR-10b

Transit Number	O-C (s)	σ	Reference
597	109 ± 242	0.5	Konacki et al. (2005)
-374	-51 ± 79	-0.7	Holman et al. (2007)
-346	23 ± 37	0.6	Holman et al. (2007)
-345	219 ± 55	4.0	Holman et al. (2007)
-109	88 ± 46	1.9	Holman et al. (2007)
-10	586 ± 86	6.8	Pont et al. (2007)
0	-73 ± 48	-1.5	Holman et al. (2007)
110	-569 ± 35	-16.	Bentley et al. (2009)
110	-612 ± 26	-24.	Bentley et al. (2009)
218	-40 ± 65	-0.6	this work
228	-44 ± 61	-0.7	this work
365	257 ± 84	3.1	this work

5.4 XO-2b

XO-2b is our brightest target ($I = 10.5$), chosen particularly to see how well our new instrument MORIS would perform. XO-2b has only one other star nearby, a nearly-identical common proper-motion binary companion separated by $30''$, making it ideally suited for aperture photometry with MORIS. It was announced by Burke et al. (2007) with eleven light curves, and an additional six high quality light curves were provided by Fernandez et al. (2009), which is the most curves of any planet we have examined.

5.4.1 Observations

Because XO-2b was one of the first targets observed with MORIS, there were some technical difficulties associated with the observations. The most vexing was the problem of acquiring good flat fields, especially since the camera has a very steep illumination gradient, with the center about twice as bright as the edges. Eventually it was realized that the illumination pattern also changed depending on where the telescope was pointed, due to a faulty optical design; the illumination was observed to change from one pattern to another in less than a minute. Rather than introduce extra noise with faulty calibrations, the data we present here has not been flat-field corrected, only bias subtracted. On an unrelated note, we also experienced poor weather, which completely clouded out a transit attempt on 20090212 and decreased data quality on 20090220 and 20090326. We present our two best light curves, on 20081206 and 20081219.

All of our transits for XO-2b use a Thor long pass filter with lower cutoff at 700 nm^4 . With MORIS, we used the 1 MHz Conventional mode in 2.4x gain setting, which has a read noise of 6 e- per pixel and gain of 1.5 e-/ADU.

⁴Transmission curve: <http://www.thorlabs.com/images/TabImages/FEL0700.jpg>

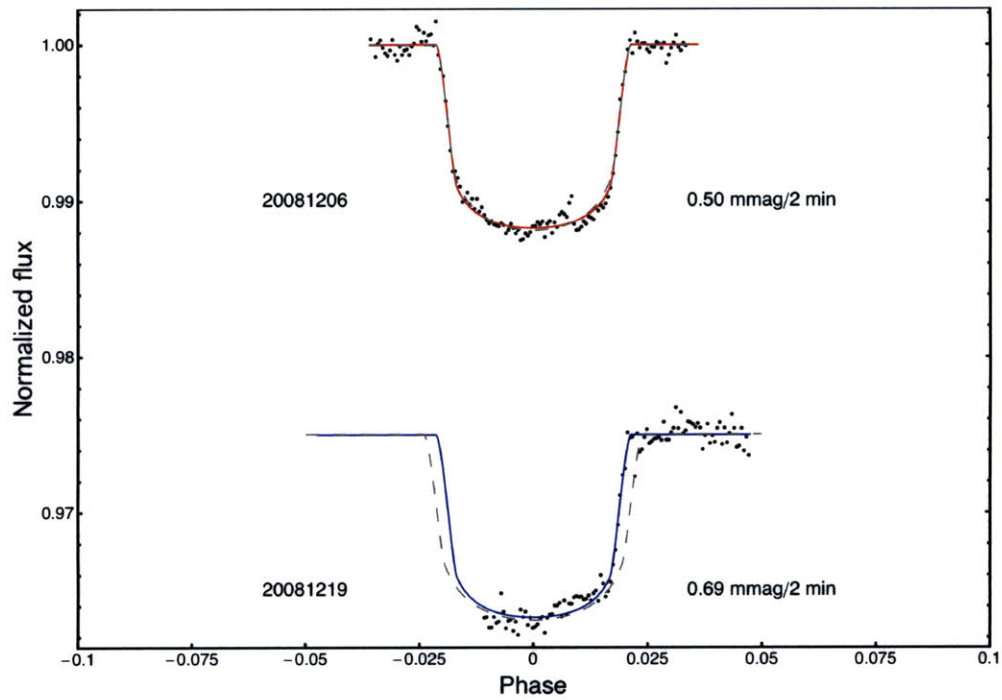


Figure 5-9 Two transits of XO-2b. All available high-quality light curves are plotted vs. orbital phase, with the data binned to 2 minutes to aid comparison. The joint model fit (solid lines) were calculated using the parameter values in Table 5.11; the stated standard deviation is the residuals from the joint model fit. A full light curve can be provided on request.

Table 5.10. Observational and photometry parameters for XO-2

Transit (UT)	N_{Frames} used (discarded)	Exp. Time (sec)	Binning	Readout (sec)	N_{Comp}	Aperture ^a (pixels)	Sky radius, width (pixels)	Scatter ^b (mmag)
20081206	7395 (3) ^c	2	1x1	0.003 ^e	1	30	60, 10	0.5
20081219	6280 (2378) ^d	2	1x1	0.003 ^e	1	20	60, 10	0.7

^aRadius around star.

^bStandard deviation of the residuals on data binned to 120 s.

^cDoubled image due to recentering.

^dLost to images tracking at non-sidereal rate over an unevenly illuminated chip.

^eFrame transfer mode used.

20081206

Our first transit of XO-2b was observed on 20081206. The airmass ranged from 2.2 to 1.2, and the seeing was around 1"; the instrument was refocused twice when the seeing began to worsen, and there are two features just before ingress and near the midtime associated with those refocusing events. The best light curve was produced with a 30 pixel radius and a sky radius of 60+10 pixels. A slight mismatch in the level of baseline before and after transit was removed with a slight trend against time.

20081219

The first hour of observations on 20081219 had to be discarded because of a steady drift in the telescope pointing that was discovered to be a mistakenly-applied non-sidereal tracking rate in the telescope control software (which was not accessible by the observer); combined with the non-uniform and variable illumination of the CCD, the ingress of the transit proved unsalvageable. After the problem was corrected, the images had stable pointing for the rest of the night. The seeing was 0."9, and the airmass ranging from 1.2-1.6. The best light curve was produced with an 20 pixel radius and a 40+10 pixel sky radius. No trends were removed.

Table 5.11. Transit parameters for XO-2b (jointly fit)

	Adopted values ^a
<i>Fitted Parameters</i>	
k	0.1006 ± 0.0004
a/R_*	8.25 ± 0.13
i	89.1 ± 0.7
u_1	0.28 ± 0.02
u_2	0.29 (fixed)
$T_C - 2454806$	0.94750 ± 0.00009
$T_C - 2454820$	0.02595 ± 0.00020
<i>Derived Parameters</i>	
b	0.13 ± 0.09
T_{14} (sec)	9560 ± 31
R_p (R_J) ^b	0.955 ± 0.024
a (AU) ^b	0.037 ± 0.001

^aMedian value and formal 68.3% credible interval from MCMC fit of all 3 light curves jointly.

^bAssuming $R_* = 1.095 \pm 0.055 R_\odot$ (Holman et al., 2007) and using $R_J = 71,492$ km.

5.4.2 Model and light curve fits

We fit both our transits using the method described earlier. We used a quadratic limb darkening law and assumed the Thor long pass 700 nm filter was similar to the Sloan i' filters (Claret, 2000, 2004)⁵, assuming $T = 5340$ K, $\log g = 4.48$, $[M/H] = 0.5$, and $V_{micro} = 2$ km/s. We fixed the orbital period to $P = 2.615864$ days, the value from Fernandez et al. (2009). We assume throughout the fits that $M_* = 0.971 \pm 0.034 M_\odot$, $R_* = 0.976 \pm 0.024 R_\odot$, and $M_p = 0.565 \pm 0.054 M_J$, based on Fernandez et al. (2009). Because we have only two transits, and one was missing ingress, we will only discuss parameters derived by fitting both transits jointly.

⁵Initial values: $u_1 = 0.3670$, $u_2 = 0.2850$.

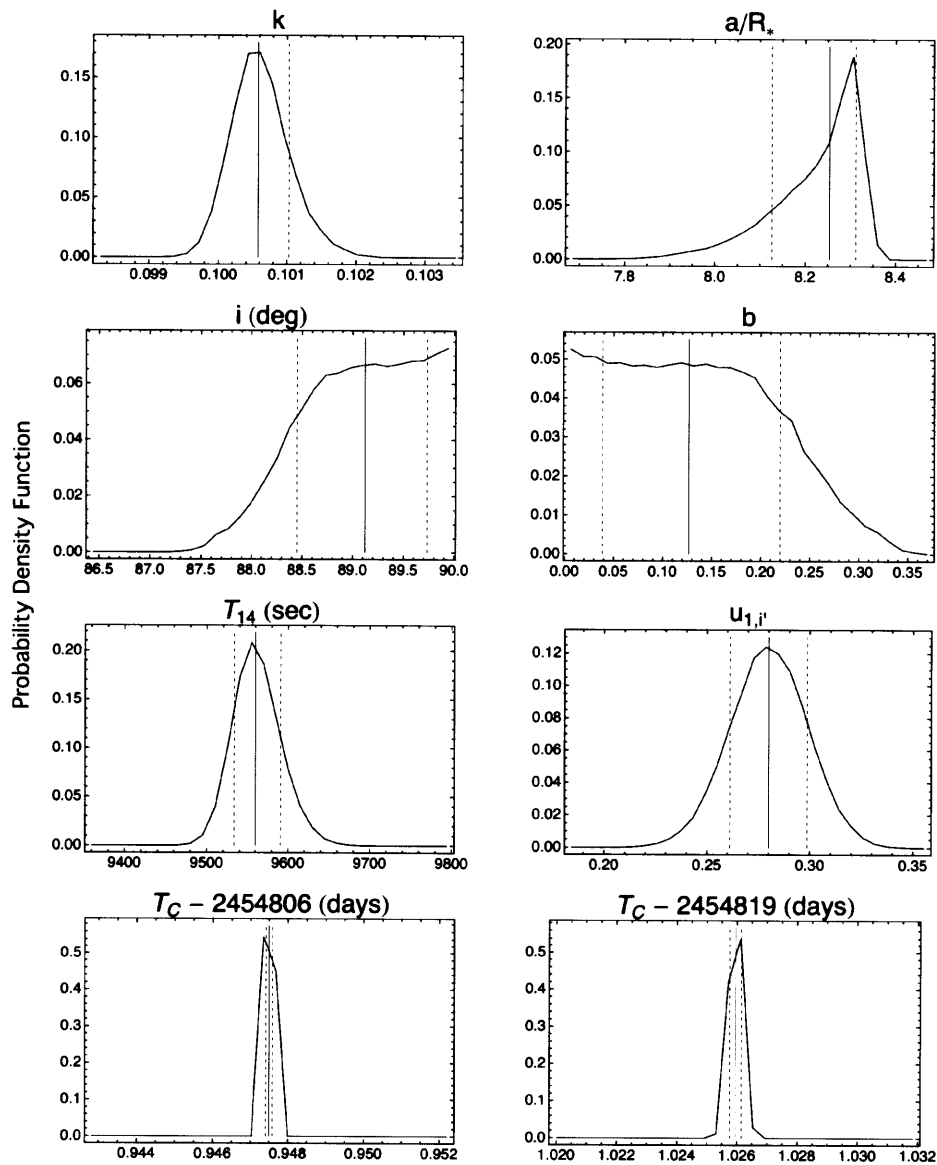


Figure 5-10 Parameter distributions for joint fit to nine transits of XO-2b. Smoothed histogram of normalized parameter distributions, from which the parameters in Table 5.11 are derived. The solid line is the median value (which is very close to the mean value in all cases). Note that several of the distributions, particularly a/R_* , i , and b , are not Gaussian. The dashed lines show the 68.3% credible interval. These values were calculated for 950,000 links.

The revised planetary radius, $R_P = 1.23 \pm 0.07R_J$, is slightly larger than, but consistent with, the value of $R_P = 1.18 \pm 0.07R_J$ reported by Gillon et al. (2007). Note that the error on the stellar radius, $R_* = 1.34 \pm 0.08R_\odot$ (Gillon et al., 2007), dominates the error on the planetary radius, which has a formal fit error of 0.01.

Our midtimes for the transits 20081206 and 20081219, which have formal fit precisions of 7 s and 17 s, have been inflated by a factor of 3.1, the value found through time averaged residuals analysis. (Evidence of correlated noise can clearly be seen in our two light curves and seems to be related to improperly removed effects of focus changes.)

5.4.3 Timing

XO-2b has 17 transit midtimes times in the literature, 11 from Burke et al. (2007) and 6 from Fernandez et al. (2009). Adding our two transits, we find that their observed minus calculated (O-C) values are 44 ± 23 s and -31 ± 53 s, using the ephemeris from Fernandez et al. (2009). (Note that we have made no attempt to correct the literature times for the UTC-TT factor.) We find that our midtimes agree with the Fernandez et al. (2009) ephemeris and find no need to recalculate a new ephemeris. Our timing residuals are plotted in Figure 5-11 and tabulated in Table 5.12.

Table 5.12. Timing residuals for XO-2b

Number	O-C (s)	σ	Reference
-425	-33 ± 180	-0.2	Burke et al. (2007)
-417	355 ± 180	2.0	Burke et al. (2007)
-130	77 ± 180	0.4	Burke et al. (2007)
-130	77 ± 180	0.4	Burke et al. (2007)
-127	-2 ± 180	-0.01	Burke et al. (2007)
-124	-81 ± 180	-0.5	Burke et al. (2007)
-122	106 ± 180	0.6	Burke et al. (2007)
-117	-40 ± 180	-0.2	Burke et al. (2007)
-114	219 ± 180	1.2	Burke et al. (2007)
-114	388 ± 180	2.2	Burke et al. (2007)
-114	-34 ± 180	-0.2	Burke et al. (2007)
0	39 ± 18	2.1	Fernandez et al. (2009)
5	-5 ± 34	-0.2	Fernandez et al. (2009)
16	13 ± 22	0.6	Fernandez et al. (2009)
21	-3 ± 62	-0.05	Fernandez et al. (2009)
24	-93 ± 37	-2.5	Fernandez et al. (2009)
25	-129 ± 64	-2.0	Fernandez et al. (2009)
130	44 ± 23	1.9	this work (20081206)
135	-31 ± 53	-0.56	this work (20081219)

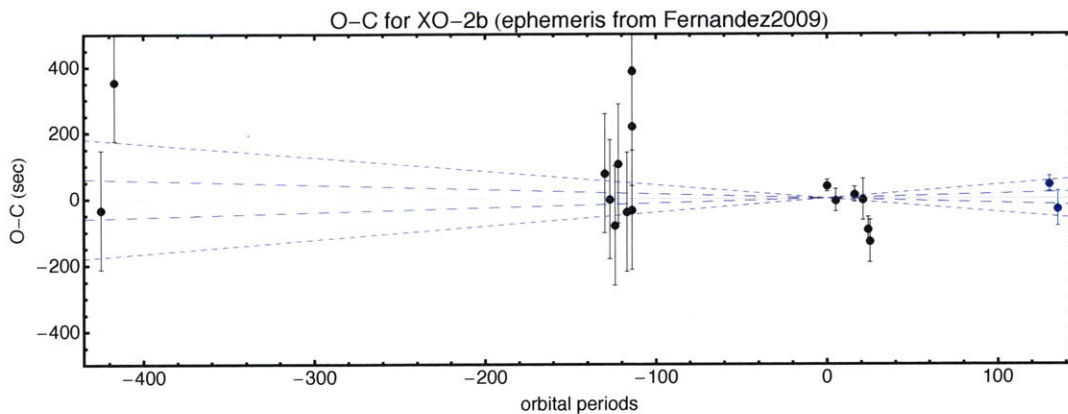


Figure 5-11 Observed minus calculated midtimes for XO-2b. Timing residuals for nineteen transits using the ephemeris from Fernandez et al. (2009). The solid line represents zero deviation from expected time of transit, while the dashed lines represent the 1σ and 3σ errors on the calculated orbital period, indicating the slopes that result for a mis-determined period.

5.5 Conclusions

We have provided seven new light curves for OGLE-TR-132, all comparable to the best light curve in the literature, and all in general agreement with the published transit parameters. We have adjusted the period to a slightly shorter value, but still within the errors of Gillon et al. (2007). With the new ephemeris, the timing residuals are very close to zero and there seem to be no systematic problems as we have seen with other systems.

To the confusion of radius ratio values for OGLE-TR-10b we can add our own observational difficulties. Independently-fit radius values for our two full transits, 20080511 and 20080611, disagree with each other by 6σ ; our half transit does not clearly reach minimum light and so cannot help with this problem. We have identified several faint stars, including one at $1.''2$, that might contribute to the flux at a few times greater than the formal radius error, indicating that care needs to be taken to get accurate baseline flux values. Although it is by no means conclusive, our complete failure to detect a transit on 20080514 may be indicative of the intermittently variable nature of OGLE-TR-10b and not of instrumental failures, since we produced excellent photometry that night on two different transiting planets. Furthermore, other stars

on the OGLE-TR-10 field have quite stable photometry. However, it is clear that this system would benefit from a systematic re-analysis of the existing photometry to better determine the nature of the stellar variability and to account for the wide variation in reported transit depths.

OGLE-TR-10b also has strong deviations in the timing residuals from the ephemeris of Holman et al. (2007), which could either indicate a real TTV caused by a perturber, or could indicate systematic offsets between different groups' analyses of this system. A careful reanalysis of all transits together is required before any TTV should be believed.

As we had hoped, we were able to produce excellent timing precision on our XO-2b transit, although instrument problems may have prevented us from achieving even greater accuracy. We find midtimes with errors of 7 s (on 20081206) and 17 s (on the partial transit on 20081219). We find that our two transits agree with ephemeris from Fernandez et al. (2009) and that XO-2 shows no signs of timing variability.

5.6 Acknowledgements

We thank Amanda Gulbis and Bobby Bus, in particular, for their work on MORIS, and also the IRTF telescope operators Bill Golisch, Dave Griep, Paul Sears, and Eric Volquardsen. We thank Adam Burgasser and Diane Wooden for kindly allowing us to get twilight flats during their scheduled IRTF time. We thank Paul Schechter for observing a transit of OGLE-TR-132b as part of MIT's Magellan queue. We thank Brian Taylor and Paul Schechter for their tireless instrument support. We also thank the Magellan staff, in particular telescope operators Jorge Araya, Mauricio Martinez, Hernàn Nuñez, Hugo Rivera, Geraldo Valladares, and Sergio Vera, for making these observations possible.

Chapter 6

Conclusions

We have presented 38 new, millimagnitude-precision light curves for seven transiting planetary systems: OGLE-TR-56b (11), OGLE-TR-132b (7), OGLE-TR-113b (6), OGLE-TR-111b (6), CoRoT-2b (3), OGLE-TR-10b (3), and XO-2b (2). These light curves were taken on three different telescopes (Baade 6.5m, Clay 6.5m and IRTF 3m) at two sites (Las Campanas Observatory, Chile, and Mauna Kea, Hawaii). For four of the OGLE systems (all except OGLE-TR-10b), we have provided more new light curves than previously existed in the literature for the planet, and also the highest-precision system parameters and midtimes available. We have achieved a precision of 9s on the midtime of our best transit of OGLE-TR-113b, among the best precision available for ground based light curves, and routinely achieved precisions of less than 30s for many full transits under good observing conditions.

Accurate transit timing with ground based photometry remains challenging. Our best light curves required good weather (outside of our control except for selecting good sites) and a stable telescope and instrument. Good comparison stars are also an absolute necessity; transits of the same planet (for example, OGLE-TR-10b) were better on some nights than others because the field of view had shifted slightly and contained more usable bright (but not too bright), isolated comparison stars.

One of the main challenges to comparing results between groups is the heterogeneity of both the data and the reduction methods. The stars in the crowded OGLE fields are spatially separated well enough in our data that aperture photometry has

proved to be an acceptable method, but on other instruments the same star fields have been too crowded and require more complicated methods like image subtraction (*e.g.*, Winn et al., 2007; Díaz et al., 2008) or deconvolution photometry (*e.g.*, Gillon et al., 2006; Pont et al., 2007). Each different photometry method carries its own biases and fine-tunings and judgement calls, and it is only when results are compared between two different groups using completely different instruments and methods that certain problems become apparent (*e.g.*, the different depths measured for different transits of OGLE-TR-111b, or the different times found in two analyses of the same photometry of OGLE-TR-111b on 20050409, or the different shapes of transits of OGLE-TR-56b that were also taken in different filters). To accurately determine planetary parameters from multiple transit light curves, we must account for different methods for fitting light curves and estimating errors and different models for the stellar mass and radius, ideally by refitting all data with a uniform model. For precise timing work, it is also necessary to consider the source of the recorded transit times, and possible differences in methods for calculating Heliocentric Julian Days (HJD) or Barycentric Julian Days (BJD). In the high-precision regime in which we must work to compare transits across many years we must keep vigilant watch for systematic errors and biases, which may not be discernible with only one or two light curves.

6.1 Improved system parameters

We compile our results on the system parameters for all seven planets analyzed in Table 6.1. Errors on the stellar radii are now the dominant source of error for all five OGLE planets, with fit errors on the radius ratios 5-10 times smaller than the error contributed by stellar uncertainty. Improving the determination of stellar radii is an important area for future work.

We find that generally our reported radius values and other system parameters are consistent with the values in the literature, with two exceptions that we note here. (1) For OGLE-TR-111b, we find a radius ratio intermediate to the values of

Table 6.1. New light curve parameters for seven transiting planets

Planet	Radius ratio	Radius (R_J)	Inclination	Semimajor Axis (a/R_*)
CoRoT-2b	0.1261 ± 0.0011	1.229 ± 0.076	88.3 ± 0.3	12.3 ± 0.2
OGLE-TR-10b	0.1058 ± 0.0009	1.127 ± 0.010	88.2 ± 1.1	8.31 ± 0.23
OGLE-TR-56b	0.1037 ± 0.0009	1.332 ± 0.063	74.0 ± 0.4	3.11 ± 0.05
OGLE-TR-111b	0.1261 ± 0.0011	1.019 ± 0.026	88.3 ± 0.3	12.3 ± 0.2
OGLE-TR-113b	0.1447 ± 0.0006	1.084 ± 0.029	89.0 ± 1.0	6.47 ± 0.09
OGLE-TR-132b	0.0943 ± 0.0014	1.229 ± 0.076	83.6 ± 0.7	4.81 ± 0.16
XO-2b	0.1006 ± 0.0004	0.955 ± 0.024	89.1 ± 0.7	8.25 ± 0.13

Winn et al. (2007) and Díaz et al. (2008), which is probably explained by differences in photometry methods between the three groups. (2) For OGLE-TR-56b, we find almost identical radius ratio values to Pont et al. (2007), but our semimajor axis and inclination values, and hence the total transit duration, all disagree at the $2-3\sigma$ level, an effect that is readily apparent by eye when the data and models are overplotted (Figure 3-5); the cause of this discrepancy is unknown.

6.2 Transit timing

We have presented new ephemerides for five planets in this thesis, which we summarize below in Table 6.2. The period errors on three planets, OGLE-TR-111b, OGLE-113b, and OGLE-TR-132b, are all less than 0.1 s; the precision for OGLE-TR-56 is somewhat worse, 0.2s, because of greater scatter among the individual transits, while the precision on the period of CoRoT-2b is higher still, 0.4 s, because it relies on only four transits spanning a little over a year.

6.2.1 Placing limits on perturbers

In no system do we see clear cut evidence for transit timing variations due to companion planets. We have found that transit times tend to be consistent when all photometry has been analyzed by the same group. Among our own data, this is the

case for all of the transits we observed, with the possible exception of OGLE-TR-56b, for which we have some scatter in the timing residuals of our eleven new transits, though not with high significance. Despite the relatively high level of errors compared to other systems and a slight shift in the reference midtime, the period we derive for OGLE-TR-56b (1.2119094 ± 0.0000024 days) agrees almost exactly with the previously published periods (e.g., 1.211909 ± 0.000001 days, Pont et al., 2007).

For three systems with the most and best data, OGLE-TR-111, OGLE-TR-113, and OGLE-TR-56, we have performed numerical integrations to place limits on the mass of potential companion planets. Due to the higher TTV signals expected by objects in resonance, we find that our data does not allow any objects greater than $1 M_{\oplus}$ in the 1:2 mean motion resonance of either OGLE-TR-111b or OGLE-TR-113b, and other limits of $2 - 20 M_{\oplus}$ can be placed on additional resonances and on OGLE-TR-56b. We show the limits in Table 6.3; for a comparison with the limits placed on other systems in the literature, see Table 2.1. We report the more conservative limit of either eccentricity we examined ($e = 0$ or $e = 0.05$).

6.2.2 Orbital decay

Although we see no evidence for short term variation, we may have detected the first observed period change of an inspiraling exoplanet. For OGLE-TR-113b, the internal consistency among our six transits is of exquisite quality, with a period error of only 9 ms if we use only the new data, from 2007-2009. Notably, this period is shorter than the period reported by Gillon et al. (2006), based on data from 2002-2005, by 0.24 ± 0.12 s. Provided there are no problems with the literature transit times from 2002-2005, reported by Konacki et al. (2004), Gillon et al. (2006), and Pietrukowicz et al. (2010), then we might actually be seeing the first evidence of orbital decay. This detection is still tentative, and needs to be followed up by additional high-precision transit observations of OGLE-TR-113b over the next several years.

Table 6.2. New transit ephemerides

Planet	Reference Midtime (BJD)	Period (d) ^a	Period error (s)
CoRoT-2b	2454237.53565(51)	1.7429988(40)	0.35
OGLE-TR-56b	2453936.6011(16)	1.2119094(24)	0.21
OGLE-TR-111b	2454092.80717(16)	4.0144463(10)	0.09
OGLE-TR-113b ^b	2453464.61720(47)	1.43247477(62)	0.05
OGLE-TR-113b ^c	2453464.61873(8)	1.43247297(10)	0.009
OGLE-TR-132b	2453142.59099(47)	1.68986531(67)	0.06

^aValues in parentheses are errors on the last digits.

^bEphemeris using all available transits.

^cEphemeris using just new six transits presented in Chapter 4.

Table 6.3. Constraints on maximum perturber mass (M_{\oplus}) from this work

System	Max O-C (sec)	1:2 ^a	2:3	1:3	3:2	2:1	5:2	3:1	Non-resonant ^b orbits	Figure
OGLE-TR-56	-97 ± 28	10	20	^{-c}	3	10	^{-c}	^{-c}	300	3-7
OGLE-TR-111	180 ± 87	1	1-4	100	1-4	1	30	30	50	2-5
OGLE-TR-113	-63 ± 21	10	NA ^d	^{-c}	NA ^d	2	20	20	100	4-7

^aPerturber in n:m resonance completes m orbits while known planet completes n .

^bUpper limit on companions with half to twice the known planet's period.

^cMass limit is $1000M_{\oplus}$ or higher, in other words, essentially unconstrained.

^dUnstable.

6.3 Anomalies and future work

Within our own data, we have found the following anomalies that deserve follow-up analysis.

The timing of OGLE-TR-113b indicates a potential period change over many years, and observing additional transits of this target is a high priority. Additionally, several features in our light curves might be star spots, and further investigation is needed into the general variability of this star, particularly if that variability might somehow impact the timing.

CoRoT-2b, which orbits a relatively active star, also would benefit from an analysis that incorporated models of stellar variability. A few times in the literature disagree by 10-20 minutes, and should be investigated if possible to see if these times could result from either instrumental or photometric error, or if they are potentially real.

For OGLE-TR-56b, all of our transits have a markedly different shape than the single literature light curve of Pont et al. (2007), even accounting for the different filters used. It is possible that the light curve observed by Pont et al. (2007) is in error, since it is the only one observed in that wavelength, so an obvious first step is to acquire another transit in either R or V or the equivalent. If the shape of the transit truly is different in different wavelengths, with the duration of the transit being different by about 15 minutes, then that could indicate something very interesting is happening on the planet, perhaps an exosphere that is only opaque at longer wavelengths. More work would be needed to construct a theoretically plausible scenario that would account for the different durations while not modifying the depths of the transits, which are consistent.

Additionally, the timing of OGLE-TR-56b needs to be investigated closely. The reference time from Pont et al. (2007) disagrees with most of our transits and needs to be confirmed. Within our own data, several of the transits for OGLE-TR-56b deviate by a few standard deviations from the expected time based on most of our transits, particularly those transits observed in 2009 May-June. We will need to investigate whether there are systematic problems in the photometry for those light

curves, which would mean the current errors are underestimated and the points are not that deviant, or if these deviations are real what could cause them.

For OGLE-TR-10b, it is clear that more work remains to synthesize all the disparate and contradictory data points. The photometry on our three transits should be examined to see if it can be improved to provide consistent light curve parameters, particularly for the transit depth. Ideally the raw data for each light curve (new and literature) would be re-analyzed with a consistent photometry method that would carefully avoid contributions from nearby faint stars. This system should be monitored closely for evidence of stellar flares and variability. Additionally, several literature light curves show strong timing variations, which if not due to errors in BJD calculations or other timing systematics could indicate strong variability.

For several of our systems, notably OGLE-TR-132b, OGLE-TR-111b and XO-2b, no sign of either transit timing variations or period changes have been found, but these objects should still be monitored once or twice a year to search for smaller and long-term changes.

More generally, this thesis highlights the importance of understanding and mitigating the systematic errors present in a transit timing project. One way to do this is to use the same instrument and telescope combination for a large number of transits of the same system, though the realities of time-allocation committees make this difficult. Another option is to build a dedicated transit follow-up instrument, preferably with a large mirror, few optics, and a top-notch detector, ideally a frame transfer camera with a field of view of a few arcminutes (to provide companion stars for most planetary systems while still minimizing blends and providing good image sampling). At the very least, both the reduced photometric data (the tabulated light curves) and the raw data frames, including calibration data and logs, should be made publicly available to the broader astronomical community so that they can be re-analyzed consistently with future data. The success of future transit timing variation discoveries will depend not only on better instruments and telescopes, but also on a long time baseline of well-archived historical data. This thesis contributes towards that goal.

Appendix A

Observation Details

A.1 Finder charts

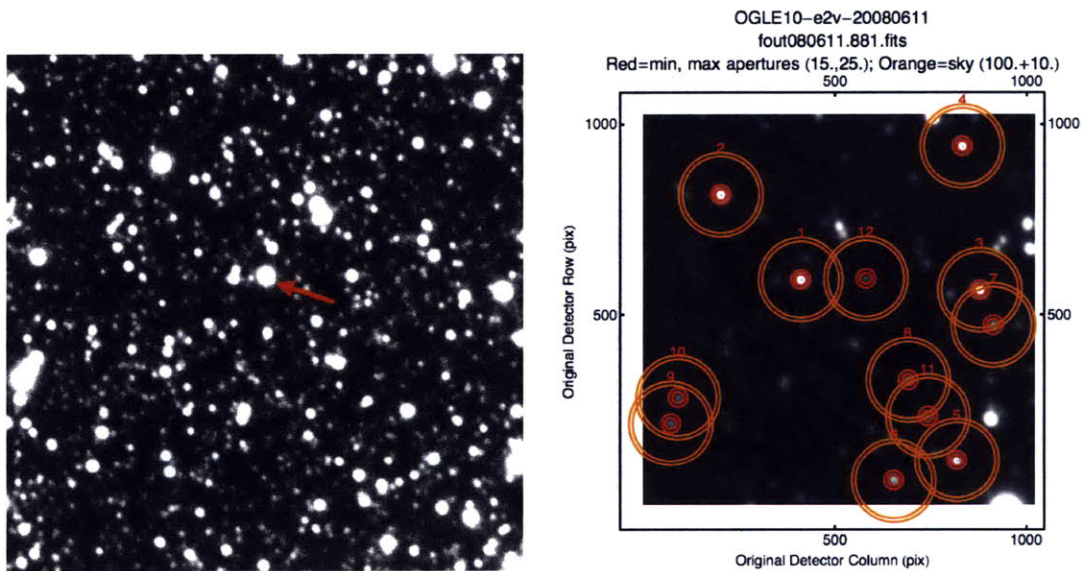


Figure A-1 Finder chart for OGLE-TR-10 on MagIC-e2v. Left: as observed on 2008 May 14 with MagIC-e2v on the 6.5 m Baade telescope. Field of view is $38'' \times 38''$, with north to the right and east down. Right: as observed on 2008 June 11. The target is numbered 1, and each potential companion star is circled with a range of circular apertures and the appropriate sky annulus, although only stars 2 and 3 were used.

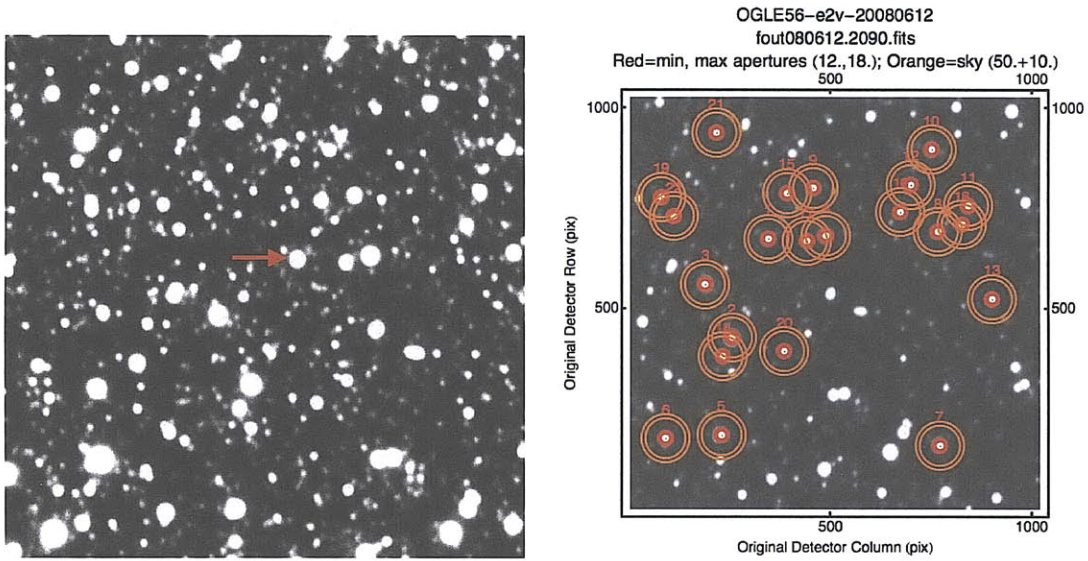


Figure A-2 Finder chart for OGLE-TR-56 on MagIC-e2v. Left: as observed on 2008 May 14 with MagIC-e2v on the 6.5 m Baade telescope. Field of view is $38'' \times 38''$, with north to the right and east down. Right: as observed on 2008 June 12. The target is numbered 1, and each potential companion star is circled with a range of circular apertures and the appropriate sky annulus, although only stars 4, 9, 12, 15, and 22 were used.

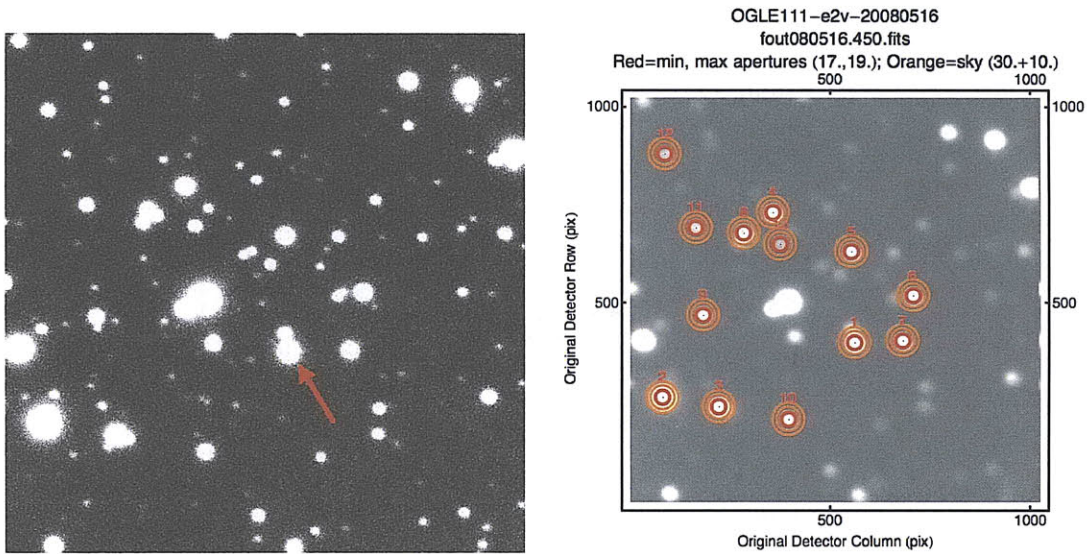


Figure A-3 Finder chart for OGLE-TR-111 on MagIC-e2v. Left: as observed on 2008 May 16 with MagIC-e2v on the 6.5 m Baade telescope. Field of view is $38'' \times 38''$, with north to the right and east down. Right: as observed on 2008 May 16. The target is numbered 1, and each potential companion star is circled with a range of circular apertures and the appropriate sky annulus, although only stars 2, 3, 5, 6, 9, 11, and 12 were used.

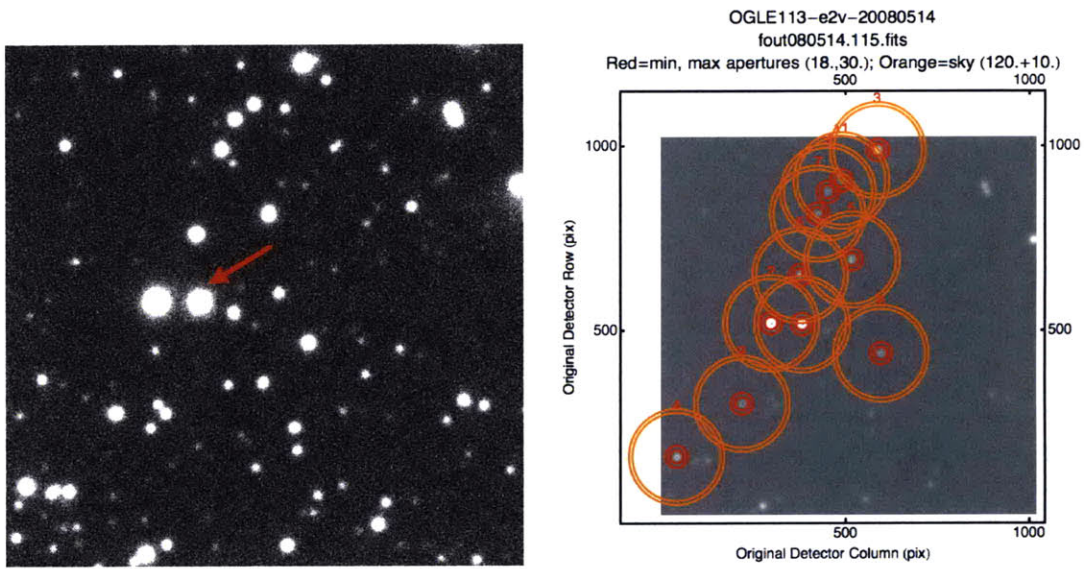


Figure A-4 Finder chart for OGLE-TR-113 on MagIC-e2v. Left: as observed on 2008 May 14 with MagIC-e2v on the 6.5 m Baade telescope. Field of view is $38'' \times 38''$, with north to the right and east down. Right: as observed on 2008 May 14. The target is numbered 1, and each potential companion star is circled with a range of circular apertures and the appropriate sky annulus, although only stars 2, 6 and 7 were used.

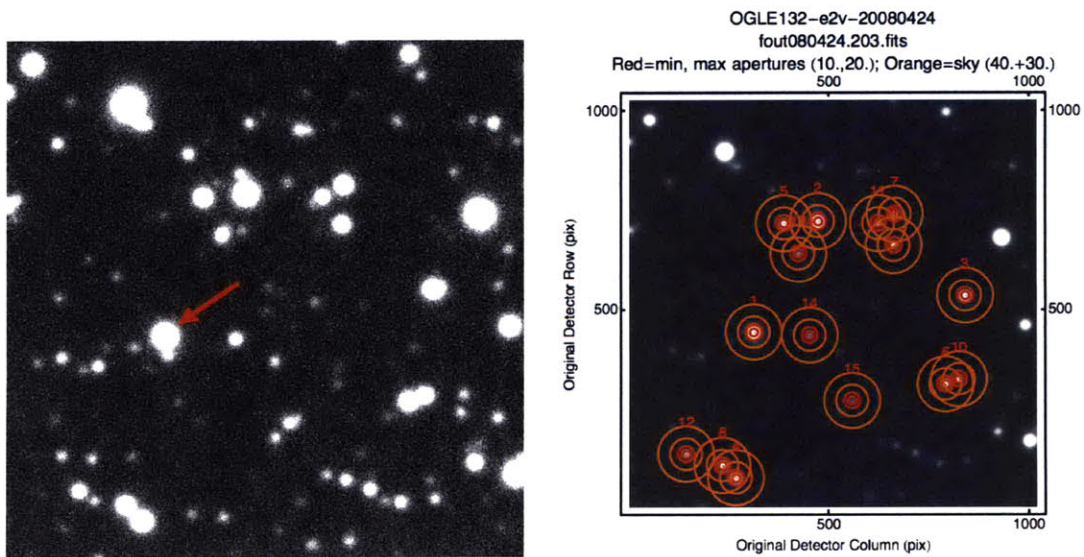


Figure A-5 Finder chart for OGLE-TR-132 on MagIC-e2v. Left: as observed on 2008 April 24 with MagIC-e2v on the 6.5 m Baade telescope. Field of view is $38'' \times 38''$, with north to the right and east down. Right: as observed on 2008 April 24. The target is numbered 1, and each potential companion star is circled with a range of circular apertures and the appropriate sky annulus, although only stars 3, 5, 7 and 9 were used.

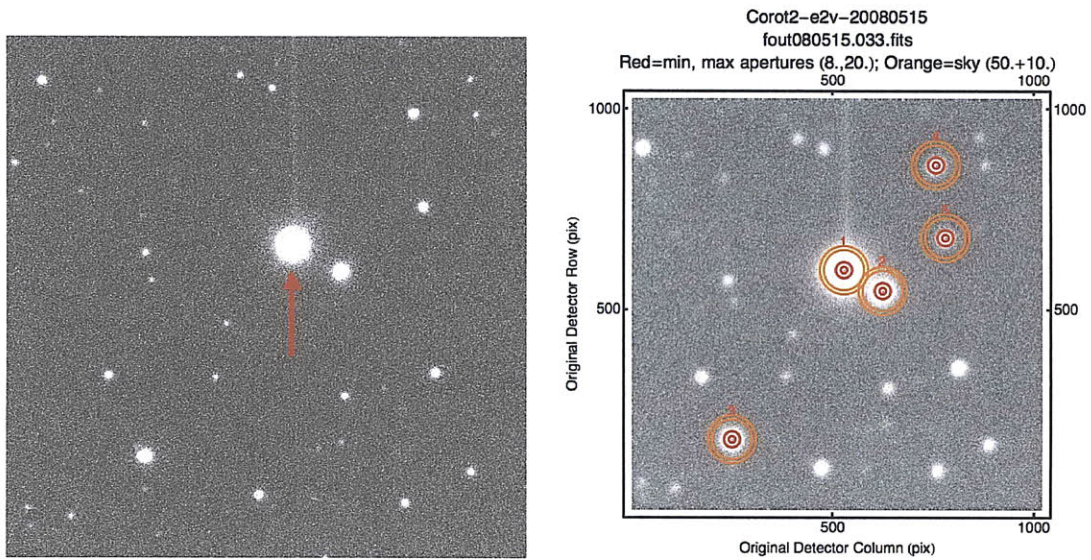


Figure A-6 Finder chart for CoRoT-2 on MagIC-e2v. Left: as observed on 2008 May 15 with MagIC-e2v on the 6.5 m Baade telescope. Field of view is $38'' \times 38''$, with north to the right and east down. Because the object is bright, a faint streak is visible above CoRoT-2, which is an artifact from the conventional read-out mode. Right: as observed on 2008 May 15. The target is numbered 1, and each potential companion star is circled with a range of circular apertures and the appropriate sky annulus, although only star 2 was used.

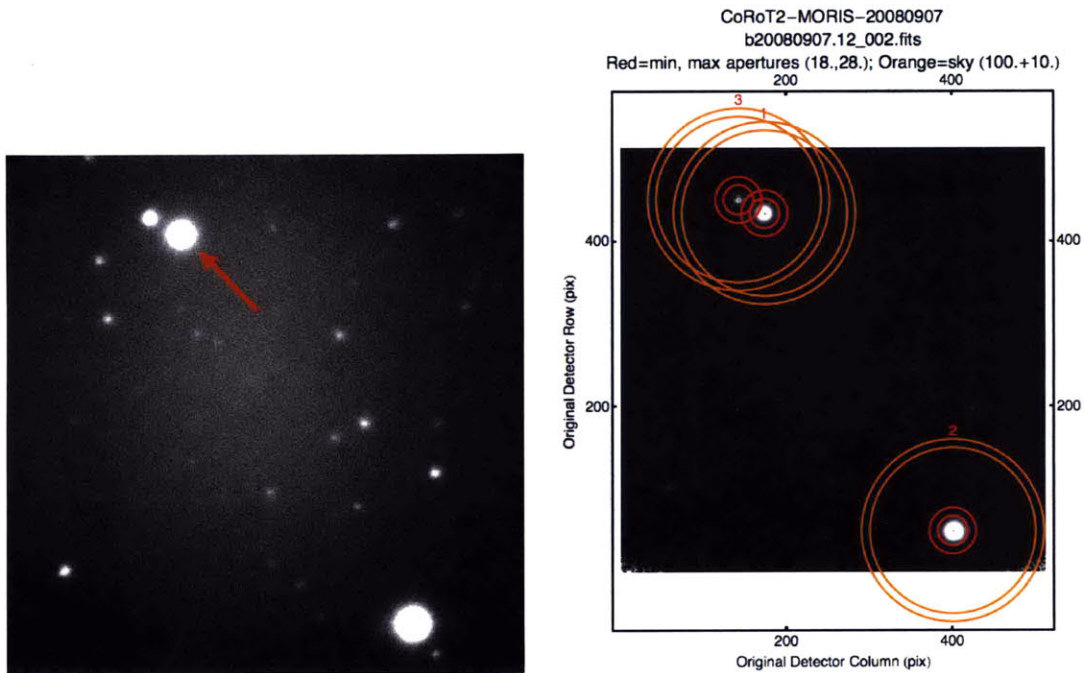


Figure A-7 Finder chart for CoRoT-2 on MORIS. Left: as observed on 2008 September 28 with MORIS on the 3 m IRTF. Field of view is $60'' \times 60''$, with north to the left and east up. Note the strong gradient in illumination, with the center about twice as bright as the edges. Right: as observed on 2008 September 28. The target is numbered 1, and each potential companion star is circled with a range of circular apertures and the appropriate sky annulus, although only star 2 was used.

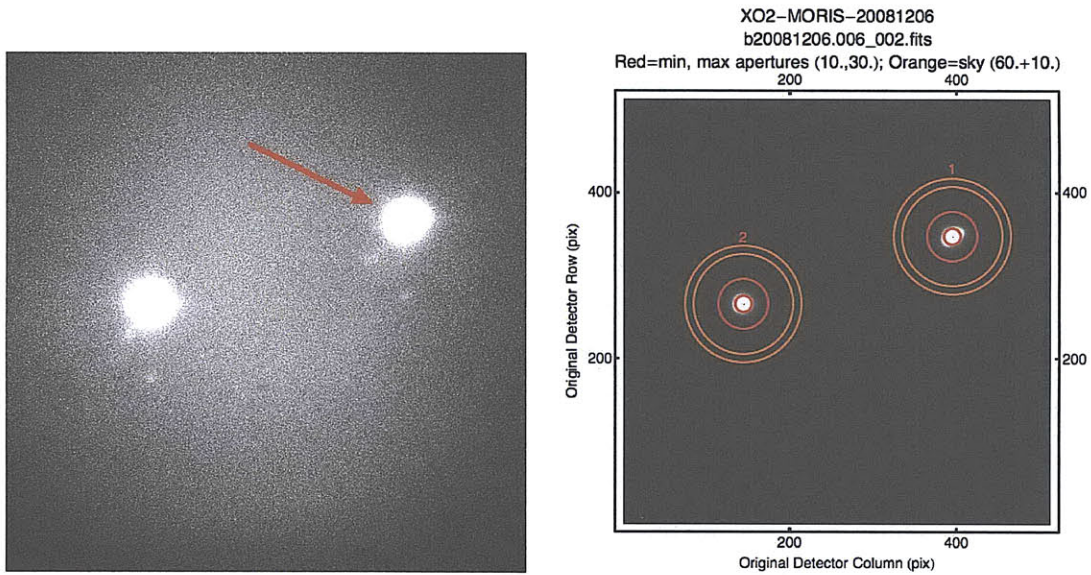


Figure A-8 Finder chart for XO-2 on MORIS. Left: as observed on 2008 December 6 with MORIS on the 3 m IRTF. Field of view is $60'' \times 60''$, with north to the left and east up. In addition to the illumination gradient also seen in Figure A-7, faint ghosts can be seen below and to the left of both stars. Right: as observed on 2008 December 6. Note that the target star (1) is more elongated than the comparison star (2) due to misaligned optics.

A.2 All full or partial transits observed

Every night on which transit observations were attempted for each of the seven planets analyzed in this thesis are shown in Table A.1, along with the telescope and instrument used, the filter, the total number of hours during which we took data on each planet, and the observer. For those transits which were not used in this thesis (all or in part), the reason is stated in the comments field. In addition, transit observations were scheduled on two nights that were lost to weather: 20080721 (OGLE-TR-56b) and 20090807 (OGLE-TR-10b). The observing time estimates do not include time for calibrations or time before or after the recorded data that was lost to telescope or instrument failure, although there were not an undue amount of the latter. A total of 185 hours of time on Magellan and 23 hours on the IRTF are represented below, with 26 hours of bad data discarded and an additional 15 scheduled hours never observed due to weather; this is the equivalent of 26 nights of successful observation and 5 lost nights.

Table A.1. All attempted transit observations for seven systems

UT Date	System	Telescope	Instrument	Filter	Hours	Observer ^a	Comments
20080511	OGLE-TR-10	Baade	MagIC-e2v	<i>i'</i>	5.0	ERA	
20080514	OGLE-TR-10	Baade	MagIC-e2v	<i>i'</i>	3.0	ERA	Unusable (unexplained noise)
20080611	OGLE-TR-10	Baade	MagIC-e2v	<i>i'</i>	8.0	MLM	
20090811	OGLE-TR-10	Baade	MagIC-e2v	<i>i'</i>	4.0	MLM	
20060622	OGLE-TR-56	Clay	POETS	<i>Is</i>	4.0	ERA	
20060714	OGLE-TR-56	Clay	POETS	<i>Is</i>	4.5	MLM	
20060720	OGLE-TR-56	Clay	POETS	None	5.5	MLM	Unusable (strong systematics)
20070830	OGLE-TR-56	Baade	IMACS	WB ^b	4.5	ERA	
20070915	OGLE-TR-56	Baade	IMACS	WB ^b	1	CAT	Unusable (clouds)
20080514	OGLE-TR-56	Baade	MagIC-e2v	<i>i'</i>	3.5	ERA	
20080612	OGLE-TR-56	Baade	MagIC-e2v	<i>i'</i>	8.0	MLM	
20080727	OGLE-TR-56	Baade	MagIC-e2v	<i>i'</i>	4.5	PLS	
20090504	OGLE-TR-56	Baade	MagIC-e2v	<i>i'</i>	5.5	MLM	
20090510	OGLE-TR-56	Baade	MagIC-e2v	<i>i'</i>	3.5	MLM	
20090521	OGLE-TR-56	Baade	MagIC-e2v	<i>i'</i>	4.0	MLM	Not used (data temporarily misplaced)
20090612	OGLE-TR-56	Baade	MagIC-e2v	<i>i'</i>	4.5	MLM	
20090613	OGLE-TR-56	Baade	MagIC-e2v	<i>i'</i>	4.5	MLM	
20090728	OGLE-TR-56	Baade	MagIC-e2v	<i>i'</i>	5.5	DJO	
20080418	OGLE-TR-111	Baade	MagIC-e2v	<i>i'</i>	3.5	ERA	
20080422	OGLE-TR-111	Baade	MagIC-e2v	<i>i'</i>	4.5	ERA	
20080512	OGLE-TR-111	Baade	MagIC-e2v	<i>i'</i>	4.5	ERA	
20080516	OGLE-TR-111	Baade	MagIC-e2v	<i>i'</i>	6.0	MLM	
20090217	OGLE-TR-111	Baade	MagIC-e2v	<i>i'</i>	7.0	DJO	
20090313	OGLE-TR-111	Baade	MagIC-e2v	<i>i'</i>	4.0	ERA	
20070130	OGLE-TR-113	Clay	MagIC-SiTe	<i>i'</i>	4.0	JNW	Lost egress to weather
20080225	OGLE-TR-113	Baade	MagIC-SiTe	<i>i'</i>	5.0	AJB	
20080424	OGLE-TR-113	Baade	MagIC-e2v	<i>i'</i>	3.5	ERA	
20080514	OGLE-TR-113	Baade	MagIC-e2v	<i>i'</i>	4.5	ERA	
20090315	OGLE-TR-113	Baade	MagIC-e2v	<i>i'</i>	4.5	ERA	
20090510	OGLE-TR-113	Baade	MagIC-e2v	<i>i'</i>	4.5	MLM	
20080203	OGLE-TR-132	Baade	MagIC-SiTe	<i>i'</i>	2.0	ERA	Unusable (shutter problem)
20080419	OGLE-TR-132	Baade	MagIC-e2v	<i>i'</i>	4.5	ERA	
20080424	OGLE-TR-132	Baade	MagIC-e2v	<i>i'</i>	3.5	ERA	
20080511	OGLE-TR-132	Baade	MagIC-e2v	<i>i'</i>	5.0	ERA	

Table A.1 (cont'd)

UT Date	System	Telescope	Instrument	Filter	Hours	Observer ^a	Comments
20090207	OGLE-TR-132	Baade	MagIC-e2v	<i>i'</i>	5.0	PLS	
20090311	OGLE-TR-132	Baade	MagIC-e2v	<i>i'</i>	8.0	ERA	
20090424	OGLE-TR-132	Baade	MagIC-e2v	<i>i'</i>	5.0	MLM	
20090511	OGLE-TR-132	Baade	MagIC-e2v	<i>i'</i>	5.0	MLM	
20080424	CoRoT-2	Baade	MagIC-e2v	<i>i'</i>	3.5	ERA	
20080515	CoRoT-2	Baade	MagIC-e2v	<i>i'</i>	5.0	MLM	
20080907	CoRoT-2	IRTF	MORIS	LP ^c	4.0	ML	
20080928	CoRoT-2	IRTF	MORIS	LP ^c	4.0	ML	Unusable (clouds)
20081206	XO-2	IRTF	MORIS	LP ^c	4.5	ERA	
20081219	XO-2	IRTF	MORIS	LP ^c	5.0	ERA	Ingress lost to bad guiding
20090220	XO-2	IRTF	MORIS	LP ^c	4.0	ERA	Not used (poor quality due to clouds)
20090326	XO-2	IRTF	MORIS	LP ^c	1.5	JLE	Not used (cut short by snow)

^aPrimary observer codes: ERA = Elisabeth R. Adams; MLM = Mercedes Lopez-Morales; CAT = Cristina A. Thomas; DJO = David J. Osip; ML = Matt Lockhart; JLE = James L. Elliot; PS = Paul L. Schechter; AJB = Adam J. Burgasser; JNW = Josh N. Winn

^bWB6300-9500, a wide band filter from 630-950 nm.

^cThor Labs 700 nm long pass.

A.3 Gallery of regrettable data

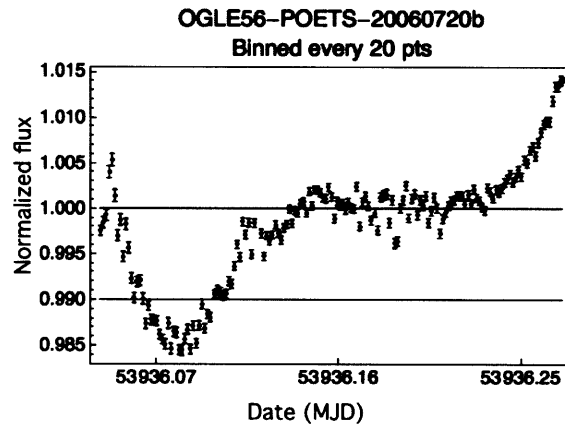


Figure A-9 Attempted transit of OGLE-TR-56b on 20060720 using POETS. (Note that this is the same day as the transit published by Pont et al. (2007) and would have been an excellent check on timing accuracy between two independent groups.) However, no filter was used for this transit. To attempt to correct for differential extinction, a light curve was constructed by detrending the comparison star and the target star separately for airmass before taking the ratio. Several different comparison stars were examined with no improvement. The best light curve, shown here, was constructed with a 10 pixel radius aperture and a 30+10 pixel sky region, but strong systematics remain and the transit does not match the shape of the other OGLE-TR-56b light curves.

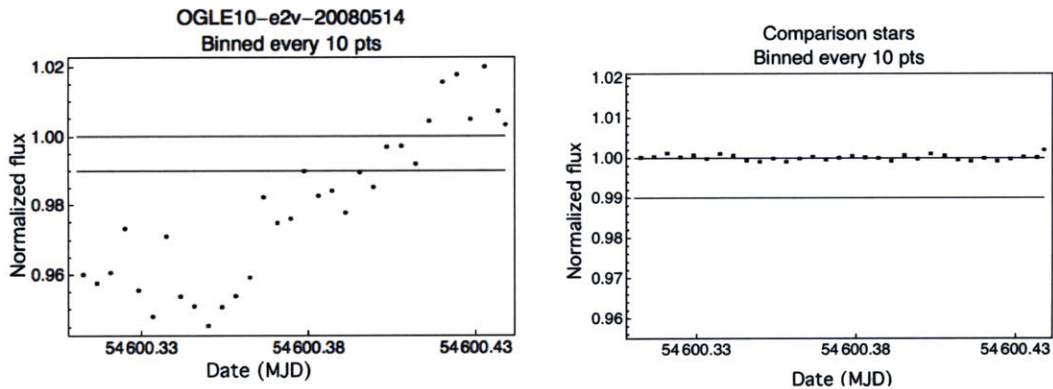


Figure A-10 Attempted transit of OGLE-TR-10b on 20080514 using MagIC-e2v. Left: Although observed under extremely good conditions (noise on two transits observed earlier that evening was 0.6 mmag in 2 minutes), the variation in stellar flux for the target was about 5%. Right: differential photometry of 2 other stars in the field, on approximately the same scale; the excess noise problem appears to rest with our target star. The two horizontal lines show the depth of the expected 1% transit and are the same in both panels. See discussion in Chapter 5.

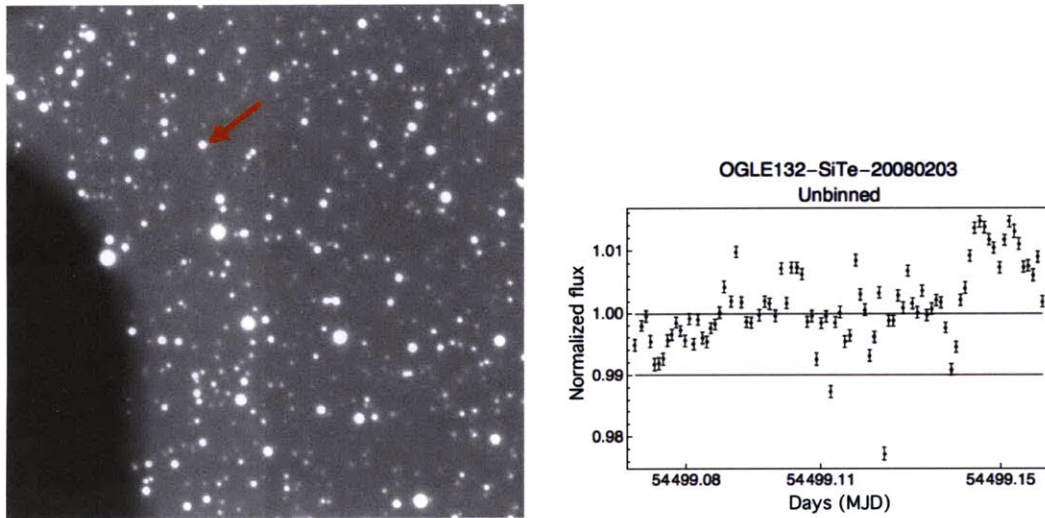


Figure A-11 The shutter monster. Left: sample image from 20080203 observations of OGLE-TR-132 using MagIC-SiTe on 20080203. The shutter was acting erratically and blocked part of the image on many frames. Although the target star was never fully obscured, differential shutter times across the field introduced too much noise for the the transit to be detected. The shutter mechanism was subsequently replaced. Right: resulting light curve from observations of OGLE-TR-132 using MagIC-SiTe on 20080203.

Appendix B

Actual vs. predicted precision

B.1 Predicted precision

B.1.1 Photometric error

When we first proposed this project in 2006, we estimated the precision we could reach for three of our targets on a 6.5m telescope, accounting only for photon and scintillation noise. The results of our simulations are shown in Table B.1. For comparison, we also determined the precision of several other telescopes that could potentially be used for transit observations, as shown in Figure B-1.

To estimate the theoretical photon noise, we assumed we were observing in I band with a flux density of $8.3 * 10^{-13} \text{ W cm}^{-2} \mu\text{m}^{-1}$, and a total quantum efficiency (accounting for losses from all sources) of 40%. We used the formulation of Dravins et al. (1998) for the scintillation noise:

$$\sigma_s = 0.09D^{-2.3}(\sec Z)^{1.75}e^{-h/h_0}/(2T)^{1/2}, \quad (\text{B.1})$$

where D is the telescope diameter in centimeters, Z is the airmass (fixed to 1.5 for simplicity), h is the telescope altitude, $h_0 = 8000 \text{ m}$ is the reference altitude, and T is the total integration time of the exposure. For most of the stars we imaged, which were $I = 14 - 15$ magnitude on a 6.5 m telescope, the scintillation noise is at most a few percent of the photon noise, though for XO-2 ($I = 10.5$ on a 3 m telescope) the

theoretical contribution of scintillation is about twice that of the photon noise. We included an estimate for the sky background noise, assuming an average lunar age of 7 days since full moon, although this term only contributed 1-2% of the total noise. Other noise sources, such as read noise, were assumed to be negligible.

B.1.2 Errors on transit parameters

Once we had estimates for the photometric error, we estimated the corresponding error on the most important transit light curve parameters, the depth (equal to the radius ratio squared) and the midtime. The errors on the radius ratio and transit midtime were estimated using a least-squares fit to a transit model with no limb darkening, after Seager & Mallén-Ornelas (2003), to which we added random noise at the level of the stated photometric errors. In the models, we assumed that the planet and star had the parameters listed in the best available literature (Santos et al., 2006; Konacki et al., 2004; Moutou et al., 2004; Torres et al., 2004). We also assumed that we acquired data of the desired precision every 100 s for nine hours, with baselines evenly distributed before and after transit.

Since these calculations were done, simple scaling relations for the errors on important transit parameters have been calculated by Carter et al. (2008). Assuming uniform time sampling and independent Gaussian error, σ of the data, for a transit of depth δ , total duration T_{14} , and ingress/egress duration τ , with N data points, the error on the depth is

$$\sigma_{\delta}/\delta \approx \sigma/(\sqrt{N}\delta), \quad (\text{B.2})$$

while the error on the transit midtime, T_C , is

$$\sigma_{T_C} \approx (T_{14} - \tau) * \sqrt{\tau/2(T_{14} - \tau)} * \sigma/(\sqrt{N}\delta). \quad (\text{B.3})$$

For OGLE-TR-113b, the estimated error on the midtime using this method and assuming 0.6 mmag in 2 min (our best achieved photometric precision) is 4 s, similar to the error we estimated as described above and shown in Table B.1 and about half

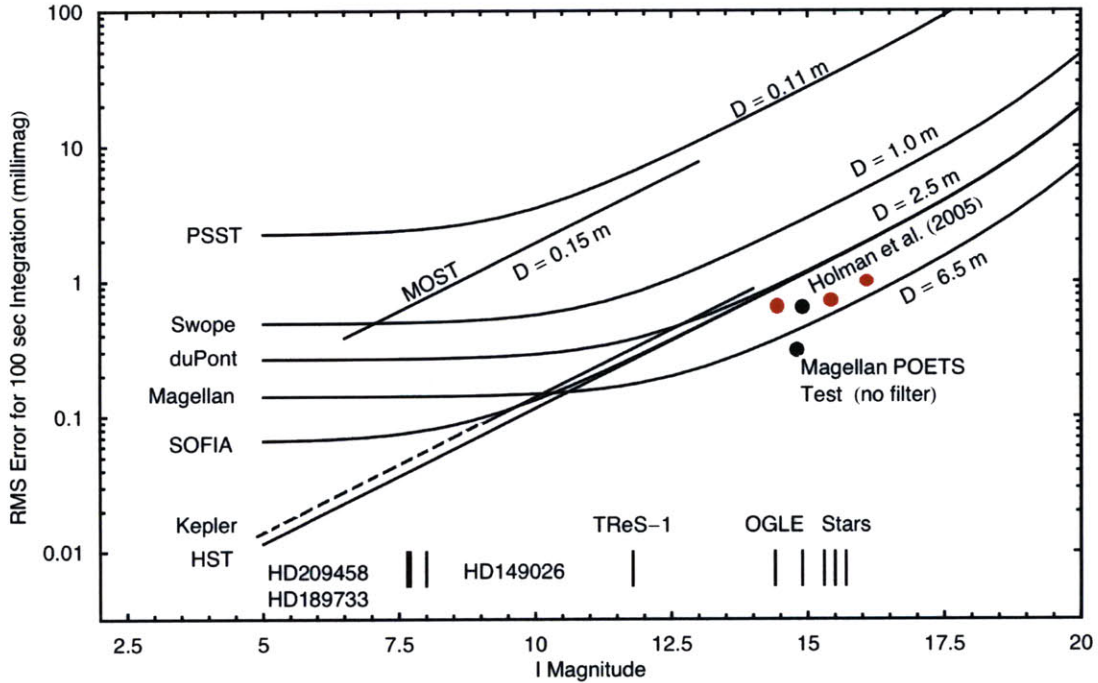


Figure B-1 Predicted RMS error vs. I magnitude for 100 s integrations. The rms error in millimag is plotted versus I magnitude for a 100-sec integration for several telescopes. The only noise sources considered are photon noise and scintillation noise caused by the Earth's atmosphere. For bright sources, scintillation noise dominates for ground-based telescopes, but it does not affect photometry from space. For faint sources, photon noise dominates, so that a large, ground-based telescope can potentially yield lower noise than the HST. The plotted points on the right both refer to Magellan data. One is for a transit light curve for OGLE-TR-10 obtained with MagIC by Holman et al. (2007), and the other is from a POETS test on Magellan (3 mmag in 1 sec and $R = 14.8$). The POETS test had better performance due to better duty cycle, more throughput (no filter), and a shorter time interval for the data. The projected Kepler performance (dashed for sources brighter than the mission design limit) is better than for a 1.0 m telescope (even in the photon-noise limit) because the bandpass of the Kepler filter is much greater than that for the projections for the I filter displayed here. For sources fainter than about $I = 11$, transit photometry from ground-based telescopes 6.5m and larger will provide more accurate data than from current and near-term air and space telescopes. (The preceding text was from a figure for a funding proposal by PI J. Elliot in 2006; the red points have been added to show the measured residuals in 100 s on our best light curves for three planets, from brightest to faintest, OGLE-TR-113b, OGLE-TR-56b, and OGLE-TR-132b.)

Table B.1. Predicted vs. actual performance for three planets

Planet	Error in 100 s (mmag)	σ_k	σ_{T_C} (s)
<i>Predicted</i>			
OGLE-TR-113b	0.37	0.0011	3.3
OGLE-TR-56b	0.53	0.0026	10
OGLE-TR-132b	0.64	0.0047	18
<i>Achieved</i>			
OGLE-TR-113b	0.74	0.0004	6 ^a
OGLE-TR-56b	0.67	0.0011	23 ^a
OGLE-TR-132b	1.0	0.0016	32 ^a

^aFormal MCMC fit errors; after accounting for correlated errors these values are increased to 9s, 34 s, and 57 s.

our actual precision (after accounting for systematic errors, which were not included in any of the noise estimates).

B.2 Actual achieved precision

We examined our best light curves for the same three planets: 20080514 for OGLE-TR-113b, 20080514 for OGLE-TR-56b, and 20090511 for OGLE-TR-132b. In Table B.1 we show the actual achieved residuals in 100 s, along with the formal errors on the radius ratio and the midtime taken from the independent MCMC fit (2850000 links) for each transit.

Comparing the two, we find that our achieved errors were 1.3 to 2 times the calculated photon noise limit, and the errors on the transit midtimes were likewise estimated at about half what we actually measured. On the other hand, we overestimated the error on the radius ratio, with the predicted errors about 3 times larger than we actually measured on our best light curves. (Note that we are comparing formal errors only, since no attempt was made in our predictions to quantify systematic sources of error.)

Appendix C

Accurate timing

C.1 Accurate UTC times

Transit timing depends on being able to compare multiple transits with a precision of a few seconds, so it is important to make sure that the times are also as accurate as possible. The appendix presents a brief explanation of different time systems in use. All of the start times for our original data frames were recorded in UTC (Coordinated Universal Time). The UTC time stamp either came directly from a GPS (in the case of triggered images, such as those taken by POETS, with an error of microseconds), or else was taken from a network time server which was regularly synchronized to a GPS (e.g. for MagIC-e2v, with errors of no more than 1 s in a few cases, and usually smaller). The errors on the UTC times in both cases are smaller than our midtime errors by at least an order of magnitude. As photometric precision improves and transit midtimes are known to greater precision, the accuracy of the times on the source files will become more important, favoring systems that use GPS times.

C.2 BJD and HJD

The UTC time system should be used to record data, but for astrophysical calculations a more continuous, uniformly increasing time scale is required. There are three main effects to consider when precision of seconds or better is required: the offset

between UTC and terrestrial time (TT), where the latter time scale accounts for leap seconds; the light-travel time between the Earth and the Sun, which varies seasonally; and relativistic effects, the highest-order of which are included despite being only important at the millisecond level. This combined set of corrections translates the UTC time into a Barycentric Julian Date (BJD) if the correction is to the barycenter of the solar system; if the center of the sun is used instead, it is a Heliocentric Julian Date (HJD). The two times are used more or less interchangeably in the transit literature, and the difference between them is at most a second or two, well below most current midtime precisions, although it will become more important in the future. We calculated the times in BJD for all of the transits we took ourselves and any literature transits which were provided with UTC times.

C.3 Converting UTC to BJD

I describe below the method I implemented in Mathematica to convert UTC times to BJD, based largely on the one implemented in the IDL routine `barycen.pro`, by E. Goehler¹. Thanks are due to J. Eastman for clarifying the UTC-TT conversion step, which led to the discovery of a bug in my Mathematica-based conversion code about how the UTC-TT conversion was being applied. Most such routines use solar system ephemerides provided by JPL (currently the DE405), which use TT as their time coordinate. Although the routine `barycen.pro` is designed to be used on times that have already been converted from UTC to TT, this is not immediately obvious, and some times reported in the literature have used the code incorrectly. To first order, these times can be corrected by adding the UTC to TT conversion, since the difference in positions of solar system bodies results in very slight (much less than 1 s) changes to the BJD correction.

We first convert from UTC to TT (which has been formerly known as TDT, or Terrestrial Dynamical Time; ET, or Ephemeris Time; and CT, or Coordinate Time). For dates since 1972, the conversion follows the form

¹<http://astro.uni-tuebingen.de/software/idl/aitlib/astro/barycen.pro>

$$t_{TT} = t_{UTC} + 32.184 + N_L, \quad (\text{C.1})$$

where 32.184 is the difference between TT and TAI, the international atomic time scale, and N_L is the number of leap seconds to date. Leap seconds are added irregularly based on the observed rotation rate for the Earth, which is not uniform, and must be updated periodically; the most recent leap second was on January 1, 2009. (For a list of all leap seconds, see: <ftp://maia.usno.navy.mil/ser7/tai-utc.dat>)

We next calculate the geometric effect of the Earth traveling around the sun, which means that the observed arrival time of the light from a fixed star may vary by up to 16 minutes. To correct for this, we convert all light arrival times into the time they would have arrived at the barycenter of the solar system. To find the locations of the Earth and Sun relative to the solar system barycenter, we used the DE405 ephemeris provided by JPL's Horizons query system; a sample email query is reproduced below.

```
!$$$SOF (ssd) JPL/Horizons Execution Control VARLIST
!Oct 30,2002
!ftp://ssd.jpl.nasa.gov/pub/ssd/horizons_batch_example.brief
!!+++++
!NOTE:First line in this file must start!$$$SOF
!Last line in this file must start!$$EOF
!Assigned values should be in quotes
!+++++
EMAIL_ADDR='era@mit.edu'
COMMAND='399'
OBJ_DATA='YES'
MAKE_EPHEM='YES'
TABLE_TYPE='VECTORS'
CENTER='500@0'
REF_PLANE='FRAME'
START_TIME='2006-Jan-01 00:00'
```

```

STOP_TIME='2007-Jan-01 00:00'
STEP_SIZE='1 day'
REF_SYSTEM='J2000'
OUT_UNITS='KM-S'
VECT_TABLE='3'
VECT_CORR='NONE'
TIME_ZONE='+00:00'
TIME_DIGITS='FRACSEC'
RANGE_UNITS='AU'
CSV_FORMAT='YES'
VEC_LABELS='NO'
R_T_S_ONLY='NO'
!$$EOF~~~~~

```

When sent as the text of an email to horizons@ssd.jpl.nasa.gov with the subject JOB, the above command will result in a return email with daily rectangular coordinates and velocities relative to the solar system barycenter, for the object specified by the line `COMMAND='X'`. We request files for both the Earth (399) and the Sun (10). These coordinates are interpolated to the desired date using Mathematica's built-in interpolation functions; note that the argument for the interpolation function is the date in TT, not UTC, with the correction in Equation C.1 having already been applied.

For a given star at RA ρ and declination δ , we calculate the geometric correction for light travel time, T_G , as

$$T_G = (x * x_E + y * y_E + z * z_E)/c, \tag{C.2}$$

where the subscript E refers to the coordinates of the Earth, and where the coordinates of the star around found using:

$$x = \cos(\delta) * \cos(\rho), \tag{C.3}$$

$$y = \cos(\delta) * \sin(\rho), \quad (\text{C.4})$$

$$z = \sin(\delta). \quad (\text{C.5})$$

Finally, although they are below the currently required level of precision, we include two relativistic corrections. The first takes into account the velocity of the observatory with respect to the solar center barycenter and the gravitational potential of the sun and planet, and is known variously as the Einstein correction or the conversion from TT to TDB (Barycentric Dynamic Time); its value is never more than 2 ms. Because we do not care about inaccuracies at the microsecond level, we use the approximate functions provided by the Astronomical Almanac for 2009, which yield a correction of

$$T_E = 0.001657 * \sin(g) + 0.000022 * \sin(L - L_J), \quad (\text{C.6})$$

where the mean anomaly of the Earth in orbit around the sun, g , is given by

$$g = 357.53 + 0.98560028 * (t - 2451545.0), \quad (\text{C.7})$$

and where $L - L_J$, the difference in the mean ecliptic longitudes of the Sun and Jupiter, is approximated by

$$L - L_J = 246.11 + 0.90251792 * (t - 2451545.0), \quad (\text{C.8})$$

with the input time, t , in TT. (The stated accuracy on this formula is $\pm 30 \mu s$ during 1980-2050.)

The second correction accounts for the Shapiro delay, or the time dilation caused passage through the curved spacetime around the Sun (Shapiro, 1964). The equation we use is

$$T_S = 2GM_{\odot}/c^3 * \ln(1 + \cos(\theta)), \quad (\text{C.9})$$

using

$$\cos(\theta) = ((x_E - x_S) * x + (y_E - y_S) * y + (z_E - z_S) * z) / d_{ES}, \quad (\text{C.10})$$

$$d_{ES} = \sqrt{(x_S - x_E)^2 + (y_S - y_E)^2 + (z_S - z_E)^2}. \quad (\text{C.11})$$

where the coordinate subscripts refer to the Earth and Sun and d_{ES} the distance between the Earth and the Sun.

The total correction from TT to BJD is a linear sum of these four terms, so that

$$t_{BJD} = t_{TT} + T_G + T_E + T_S. \quad (\text{C.12})$$

Bibliography

- Adams, E. R., López-Morales, M., Elliot, J. L., Seager, S., & Osip, D. J. 2010, *ApJ*, 714, 13
- Adams, E. R., Seager, S., & Elkins-Tanton, L. 2008, *ApJ*, 673, 1160
- Agol, E., Steffen, J., Sari, R., & Clarkson, W. 2005, *MNRAS*, 359, 567
- Agol, E. & Steffen, J. H. 2007, *MNRAS*, 374, 941
- Alonso, R., Auvergne, M., Baglin, A., Ollivier, M., Moutou, C., Rouan, D., Deeg, H. J., Aigrain, S., Almenara, J. M., Barbieri, M., Barge, P., Benz, W., Bordé, P., Bouchy, F., de La Reza, R., Deleuil, M., Dvorak, R., Erikson, A., Fridlund, M., Gillon, M., Gondoin, P., Guillot, T., Hatzes, A., Hébrard, G., Kabath, P., Jorda, L., Lammer, H., Léger, A., Llebaria, A., Loeillet, B., Magain, P., Mayor, M., Mazeh, T., Pätzold, M., Pepe, F., Pont, F., Queloz, D., Rauer, H., Shporer, A., Schneider, J., Stecklum, B., Udry, S., & Wuchterl, G. 2008, *A&A*, 482, L21
- Ammler-von Eiff, M. & Santos, N. C. 2008, *Astronomische Nachrichten*, 329, 573
- Bakos, G., Afonso, C., Henning, T., Jordán, A., Holman, M., Noyes, R. W., Sackett, P. D., Sasselov, D., Kovács, G., Csubry, Z., & Pál, A. 2009, in *IAU Symposium*, Vol. 253, *IAU Symposium*, 354–357
- Ballard, S., Christiansen, J. L., Charbonneau, D., Deming, D., Holman, M. J., Fabrycky, D., A’Hearn, M. F., Wellnitz, D. D., Barry, R. K., Kuchner, M. J., Liveness, T. A., Hewagama, T., Sunshine, J. M., Hampton, D. L., Lisse, C. M., Seager, S., & Veverka, J. F. 2009, *ArXiv e-prints*
- Barge, P., Baglin, A., Auvergne, M., Rauer, H., Léger, A., Schneider, J., Pont, F., Aigrain, S., Almenara, J., Alonso, R., Barbieri, M., Bordé, P., Bouchy, F., Deeg, H. J., La Reza, D., Deleuil, M., Dvorak, R., Erikson, A., Fridlund, M., Gillon, M., Gondoin, P., Guillot, T., Hatzes, A., Hébrard, G., Jorda, L., Kabath, P., Lammer, H., Llebaria, A., Loeillet, B., Magain, P., Mazeh, T., Moutou, C., Ollivier, M., Pätzold, M., Queloz, D., Rouan, D., Shporer, A., & Wuchterl, G. 2008, *A&A*, 482, L17
- Barnes, R. & Greenberg, R. 2006, *ApJ*, 647, L163
- Bean, J. L. 2009, *A&A*, 506, 369

- Bean, J. L. & Seifahrt, A. 2008, *A&A*, 487, L25
- Bean, J. L., Seifahrt, A., Hartman, H., Nilsson, H., Reiners, A., Dreizler, S., Henry, T. J., & Wiedemann, G. 2010, *ApJ*, 711, L19
- Benedict, G. F., McArthur, B. E., Gatewood, G., Nelan, E., Cochran, W. D., Hatzes, A., Endl, M., Wittenmyer, R., Baliunas, S. L., Walker, G. A. H., Yang, S., Kürster, M., Els, S., & Paulson, D. B. 2006, *AJ*, 132, 2206
- Bentley, S. J., Hellier, C., Maxted, P. F. L., Dhillon, V. S., Marsh, T. R., Copperwheat, C. M., & Littlefair, S. P. 2009, *A&A*, 505, 901
- Bond, I. A., Udalski, A., Jaroszyński, M., Rattenbury, N. J., Paczyński, B., Soszyński, I., Wyrzykowski, L., Szymański, M. K., Kubiak, M., Szewczyk, O., Żebruń, K., Pietrzyński, G., Abe, F., Bennett, D. P., Eguchi, S., Furuta, Y., Hearnshaw, J. B., Kamiya, K., Kilmartin, P. M., Kurata, Y., Masuda, K., Matsubara, Y., Muraki, Y., Noda, S., Okajima, K., Sako, T., Sekiguchi, T., Sullivan, D. J., Sumi, T., Tristram, P. J., Yanagisawa, T., & Yock, P. C. M. 2004, *ApJ*, 606, L155
- Bouchy, F., Pont, F., Melo, C., Santos, N. C., Mayor, M., Queloz, D., & Udry, S. 2005, *A&A*, 431, 1105
- Bouchy, F., Pont, F., Santos, N. C., Melo, C., Mayor, M., Queloz, D., & Udry, S. 2004, *A&A*, 421, L13
- Burke, C. J., McCullough, P. R., Valenti, J. A., Johns-Krull, C. M., Janes, K. A., Heasley, J. N., Summers, F. J., Stys, J. E., Bissinger, R., Fleenor, M. L., Foote, C. N., García-Melendo, E., Gary, B. L., Howell, P. J., Mallia, F., Masi, G., Taylor, B., & Vanmunster, T. 2007, *ApJ*, 671, 2115
- Cameron, A. C., Bouchy, F., Hébrard, G., Maxted, P., Pollacco, D., Pont, F., Skillen, I., Smalley, B., Street, R. A., West, R. G., Wilson, D. M., Aigrain, S., Christian, D. J., Clarkson, W. I., Enoch, B., Evans, A., Fitzsimmons, A., Fleenor, M., Gillon, M., Haswell, C. A., Hebb, L., Hellier, C., Hodgkin, S. T., Horne, K., Irwin, J., Kane, S. R., Keenan, F. P., Loeillet, B., Lister, T. A., Mayor, M., Moutou, C., Norton, A. J., Osborne, J., Parley, N., Queloz, D., Ryans, R., Triaud, A. H. M. J., Udry, S., & Wheatley, P. J. 2007, *MNRAS*, 375, 951
- Carone, L. & Pätzold, M. 2007, *Planet. Space Sci.*, 55, 643
- Carter, J. A. & Winn, J. N. 2009, *ApJ*, 704, 51
- Carter, J. A., Yee, J. C., Eastman, J., Gaudi, B. S., & Winn, J. N. 2008, *ApJ*, 689, 499
- Charbonneau, D., Allen, L. E., Megeath, S. T., Torres, G., Alonso, R., Brown, T. M., Gilliland, R. L., Latham, D. W., Mandushev, G., O'Donovan, F. T., & Sozzetti, A. 2005, *ApJ*, 626, 523

- Charbonneau, D., Brown, T. M., Latham, D. W., & Mayor, M. 2000, *ApJ*, 529, L45
- Charbonneau, D., Brown, T. M., Noyes, R. W., & Gilliland, R. L. 2002, *ApJ*, 568, 377
- Chauvin, G., Lagrange, A., Dumas, C., Zuckerman, B., Mouillet, D., Song, I., Beuzit, J., & Lowrance, P. 2005, *A&A*, 438, L25
- Claret, A. 2000, *A&A*, 363, 1081
- . 2004, *A&A*, 428, 1001
- Coughlin, J. L., Stringfellow, G. S., Becker, A. C., López-Morales, M., Mezzalana, F., & Krajci, T. 2008, *ApJ*, 689, L149
- Csizmadia, S., Renner, S., Barge, P., Agol, E., Aigrain, S., Alonso, R., Almenara, J. M., Bonomo, A. S., Borde, P., Bouchy, F., Cabrera, J., Deeg, H. J., De la Reza, R., Deleuil, M., Dvorak, R., Erikson, A., Guenther, E. W., Fridlund, M., Gondoin, P., Guillot, T., Hatzes, A., Jorda, L., Lammer, H., Lázaro, C., Leger, A., Llebaria, A., Magain, P., Moutou, C., Ollivier, M., Paetzold, M., Queloz, D., Rauer, H., Rouan, D., Schneider, J., Wuchterl, G., & Gandolfi, D. 2009, *ArXiv e-prints*
- Czesla, S., Huber, K. F., Wolter, U., Schröter, S., & Schmitt, J. H. M. M. 2009, *A&A*, 505, 1277
- Deming, D., Seager, S., Richardson, L. J., & Harrington, J. 2005, *Nature*, 434, 740
- Díaz, R. F., Ramírez, S., Fernández, J. M., Gallardo, J., Gieren, W., Ivanov, V. D., Mauas, P., Minniti, D., Pietrzynski, G., Pérez, F., Ruíz, M. T., Udalski, A., & Zoccali, M. 2007, *ApJ*, 660, 850
- Díaz, R. F., Rojo, P., Melita, M., Hoyer, S., Minniti, D., Mauas, P. J. D., & Ruíz, M. T. 2008, *ApJ*, 682, L49
- Dravins, D., Lindegren, L., Mezey, E., & Young, A. T. 1998, *PASP*, 110, 610
- Dressler, A., Hare, T., Bigelow, B. C., & Osip, D. J. 2006, in *Society of Photo-Optical Instrumentation Engineers (SPIE) Conference Series*, Vol. 6269, *Society of Photo-Optical Instrumentation Engineers (SPIE) Conference Series*
- Dunham, E. W., Elliot, J. L., Bida, T. A., & Taylor, B. W. 2004, in *Presented at the Society of Photo-Optical Instrumentation Engineers (SPIE) Conference*, Vol. 5492, *Society of Photo-Optical Instrumentation Engineers (SPIE) Conference Series*, ed. A. F. M. Moorwood & M. Iye, 592–603
- Elliot, J. L. 1978, *Icarus*, 35, 156
- Fernandez, J. M., Holman, M. J., Winn, J. N., Torres, G., Shporer, A., Mazeh, T., Esquerdo, G. A., & Everett, M. E. 2009, *AJ*, 137, 4911

- Fischer, D. A., Marcy, G. W., Butler, R. P., Vogt, S. S., Laughlin, G., Henry, G. W., Abouav, D., Peek, K. M. G., Wright, J. T., Johnson, J. A., McCarthy, C., & Isaacson, H. 2008, *ApJ*, 675, 790
- Ford, E. B. & Holman, M. J. 2007, *ApJ*, 664, L51
- Gallardo, J., Minniti, D., Valls-Gabaud, D., & Rejkuba, M. 2005, *A&A*, 431, 707
- Gatewood, G. & Eichhorn, H. 1973, *AJ*, 78, 769
- Gelman, A. & Rubin, D. B. 1992, *Statistical Science*, 7, 457
- Gibson, N. P., Pollacco, D., Simpson, E. K., Barros, S., Joshi, Y. C., Todd, I., Keenan, F. P., Skillen, I., Benn, C., Christian, D., Hrudková, M., & Steele, I. A. 2009, *ApJ*, 700, 1078
- Gibson, N. P., Pollacco, D. L., Barros, S., Benn, C., Christian, D., Hrudková, M., Joshi, Y. C., Keenan, F. P., Simpson, E. K., Skillen, I., Steele, I. A., & Todd, I. 2010, *MNRAS*, 401, 1917
- Gillon, M., Pont, F., Moutou, C., Bouchy, F., Courbin, F., Sohy, S., & Magain, P. 2006, *A&A*, 459, 249
- Gillon, M., Pont, F., Moutou, C., Santos, N. C., Bouchy, F., Hartman, J. D., Mayor, M., Melo, C., Queloz, D., Udry, S., & Magain, P. 2007, *A&A*, 466, 743
- Henry, G. W., Marcy, G. W., Butler, R. P., & Vogt, S. S. 2000, *ApJ*, 529, L41
- Heyl, J. S. & Gladman, B. J. 2007, *MNRAS*, 377, 1511
- Holman, M. J. & Murray, N. W. 2005, *Science*, 307, 1288
- Holman, M. J., Winn, J. N., Fuentes, C. I., Hartman, J. D., Stanek, K. Z., Torres, G., Sasselov, D. D., Gaudi, B. S., Jones, R. L., & Fraser, W. 2007, *ApJ*, 655, 1103
- Huber, K. F., Czesla, S., Wolter, U., & Schmitt, J. H. M. M. 2009, *A&A*, 508, 901
- Ibgui, L. & Burrows, A. 2009, *ApJ*, 700, 1921
- Johnson, J. A., Winn, J. N., Cabrera, N. E., & Carter, J. A. 2009, *ApJ*, 692, L100
- . 2010, *ApJ*, 712, L122
- Kalas, P., Graham, J. R., Chiang, E., Fitzgerald, M. P., Clampin, M., Kite, E. S., Stapelfeldt, K., Marois, C., & Krist, J. 2008, *Science*, 322, 1345
- Kashyap, V. L., Drake, J. J., & Saar, S. H. 2008, *ApJ*, 687, 1339
- Kipping, D. M. 2009, *MNRAS*, 396, 1797
- Kipping, D. M., Fossey, S. J., & Campanella, G. 2009, *MNRAS*, 400, 398

- Knutson, H. A., Charbonneau, D., Allen, L. E., Fortney, J. J., Agol, E., Cowan, N. B., Showman, A. P., Cooper, C. S., & Megeath, S. T. 2007a, *Nature*, 447, 183
- Knutson, H. A., Charbonneau, D., Noyes, R. W., Brown, T. M., & Gilliland, R. L. 2007b, *ApJ*, 655, 564
- Konacki, M., Torres, G., Jha, S., & Sasselov, D. D. 2003a, *Nature*, 421, 507
- Konacki, M., Torres, G., Sasselov, D. D., & Jha, S. 2003b, *ApJ*, 597, 1076
- . 2005, *ApJ*, 624, 372
- Konacki, M., Torres, G., Sasselov, D. D., Pietrzyński, G., Udalski, A., Jha, S., Ruiz, M. T., Gieren, W., & Minniti, D. 2004, *ApJ*, 609, L37
- Lanza, A. F., Pagano, I., Leto, G., Messina, S., Aigrain, S., Alonso, R., Auvergne, M., Baglin, A., Barge, P., Bonomo, A. S., Boumier, P., Collier Cameron, A., Comparato, M., Cutispoto, G., de Medeiros, J. R., Foing, B., Kaiser, A., Moutou, C., Parihar, P. S., Silva-Valio, A., & Weiss, W. W. 2009, *A&A*, 493, 193
- Latham, D. W., Stefanik, R. P., Mazeh, T., Mayor, M., & Burki, G. 1989, *Nature*, 339, 38
- Levrard, B., Winisdoerffer, C., & Chabrier, G. 2009, *ApJ*, 692, L9
- Mandel, K. & Agol, E. 2002, *ApJ*, 580, L171
- Mandushev, G., O'Donovan, F. T., Charbonneau, D., Torres, G., Latham, D. W., Bakos, G. Á., Dunham, E. W., Sozzetti, A., Fernández, J. M., Esquerdo, G. A., Everett, M. E., Brown, T. M., Rabus, M., Belmonte, J. A., & Hillenbrand, L. A. 2007, *ApJ*, 667, L195
- Marcy, G. W. & Butler, R. P. 1996, *ApJ*, 464, L147+
- Marois, C., Macintosh, B., Barman, T., Zuckerman, B., Song, I., Patience, J., Lafrenière, D., & Doyon, R. 2008, *Science*, 322, 1348
- Mayor, M., Bonfils, X., Forveille, T., Delfosse, X., Udry, S., Bertaux, J., Beust, H., Bouchy, F., Lovis, C., Pepe, F., Perrier, C., Queloz, D., & Santos, N. C. 2009, *A&A*, 507, 487
- Mayor, M. & Queloz, D. 1995, *Nature*, 378, 355
- Mayor, M., Udry, S., Naef, D., Pepe, F., Queloz, D., Santos, N. C., & Burnet, M. 2004, *A&A*, 415, 391
- McLaughlin, D. B. 1924, *ApJ*, 60, 22
- Miller-Ricci, E., Rowe, J. F., Sasselov, D., Matthews, J. M., Guenther, D. B., Kuschnig, R., Moffat, A. F. J., Rucinski, S. M., Walker, G. A. H., & Weiss, W. W. 2008a, *ApJ*, 682, 586

- Miller-Ricci, E., Rowe, J. F., Sasselov, D., Matthews, J. M., Kuschnig, R., Croll, B., Guenther, D. B., Moffat, A. F. J., Rucinski, S. M., Walker, G. A. H., & Weiss, W. W. 2008b, *ApJ*, 682, 593
- Minniti, D., Fernández, J. M., Díaz, R. F., Udalski, A., Pietrzynski, G., Gieren, W., Rojo, P., Ruíz, M. T., & Zoccali, M. 2007, *ApJ*, 660, 858
- Miralda-Escudé, J. 2002, *ApJ*, 564, 1019
- Moutou, C., Pont, F., Bouchy, F., & Mayor, M. 2004, *A&A*, 424, L31
- Mugrauer, M., Neuhaeuser, R., Mazeh, T., & Guenther, E. W. 2007, in *IAU Symposium*, Vol. 240, *IAU Symposium*, ed. W. I. Hartkopf, E. F. Guinan, & P. Harmanec, 329–+
- Narita, N., Sato, B., Hirano, T., & Tamura, M. 2009, *PASJ*, 61, L35
- Ohta, Y., Taruya, A., & Suto, Y. 2005, *ApJ*, 622, 1118
- Osip, D. J., Floyd, D., & Covarrubias, R. 2008, in *Presented at the Society of Photo-Optical Instrumentation Engineers (SPIE) Conference*, Vol. 7014, *Society of Photo-Optical Instrumentation Engineers (SPIE) Conference Series*, 9
- Pätzold, M., Carone, L., & Rauer, H. 2004, *A&A*, 427, 1075
- Pietrukowicz, P., Minniti, D., Díaz, R. F., Fernández, J. M., Zoccali, M., Gieren, W., Pietrzyński, G., Ruíz, M. T., Udalski, A., Szeifert, T., & Hempel, M. 2010, *A&A*, 509, A260000+
- Pont, F., Bouchy, F., Queloz, D., Santos, N. C., Melo, C., Mayor, M., & Udry, S. 2004, *A&A*, 426, L15
- Pont, F., Knutson, H., Gilliland, R. L., Moutou, C., & Charbonneau, D. 2008, *MNRAS*, 385, 109
- Pont, F., Moutou, C., Gillon, M., Udalski, A., Bouchy, F., Fernandes, J. M., Gieren, W., Mayor, M., Mazeh, T., Minniti, D., Melo, C., Naef, D., Pietrzynski, G., Queloz, D., Ruiz, M. T., Santos, N. C., & Udry, S. 2007, *A&A*, 465, 1069
- Pont, F., Zucker, S., & Queloz, D. 2006, *MNRAS*, 373, 231
- Pravdo, S. H. & Shaklan, S. B. 2009, *ApJ*, 700, 623
- Queloz, D., Eggenberger, A., Mayor, M., Perrier, C., Beuzit, J. L., Naef, D., Sivan, J. P., & Udry, S. 2000, *A&A*, 359, L13
- Rabus, M., Deeg, H. J., Alonso, R., Belmonte, J. A., & Almenara, J. M. 2009, *A&A*, 508, 1011

- Rauer, H., Erikson, A., Kabath, P., Hedelt, P., Boer, M., Carone, L., Csizmadia, S., Eigmüller, P., Paris, P. v., Renner, S., Tournois, G., Titz, R., & Voss, H. 2010, *AJ*, 139, 53
- Rossiter, R. A. 1924, *ApJ*, 60, 15
- Santos, N. C., Ecuivillon, A., Israelian, G., Mayor, M., Melo, C., Queloz, D., Udry, S., Ribeiro, J. P., & Jorge, S. 2006, *A&A*, 458, 997
- Sasselov, D. D. 2003, *ApJ*, 596, 1327
- Seager, S., Kuchner, M., Hier-Majumder, C. A., & Militzer, B. 2007, *ApJ*, 669, 1279
- Seager, S. & Mallén-Ornelas, G. 2003, *ApJ*, 585, 1038
- Shapiro, I. I. 1964, *Physical Review Letters*, 13, 789
- Silva, A. V. R. & Cruz, P. C. 2006, *ApJ*, 642, 488
- Silva-Valio, A., Lanza, A. F., Alonso, R., & Barge, P. 2010, *A&A*, 510, A260000+
- Silvotti, R., Schuh, S., Janulis, R., Solheim, J., Bernabei, S., Østensen, R., Oswald, T. D., Bruni, I., Gualandi, R., Bonanno, A., Vauclair, G., Reed, M., Chen, C., Leibowitz, E., Paparo, M., Baran, A., Charpinet, S., Dolez, N., Kawaler, S., Kurtz, D., Moskalik, P., Riddle, R., & Zola, S. 2007, *Nature*, 449, 189
- Simon, A., Szatmáry, K., & Szabó, G. M. 2007, *A&A*, 470, 727
- Sing, D. K. & López-Morales, M. 2009, *A&A*, 493, L31
- Snellen, I. A. G. & Covino, E. 2007, *MNRAS*, 375, 307
- Southworth, J. 2008, *MNRAS*, 386, 1644
- Souza, S. P., Babcock, B. A., Pasachoff, J. M., Gulbis, A. A. S., Elliot, J. L., Person, M. J., & Gangestad, J. W. 2006, *PASP*, 118, 1550
- Steffen, J. H. & Agol, E. 2005, *MNRAS*, 364, L96
- Taylor, B. W., Dunham, E. W., & Elliot, J. L. 2004, in Presented at the Society of Photo-Optical Instrumentation Engineers (SPIE) Conference, Vol. 5496, Society of Photo-Optical Instrumentation Engineers (SPIE) Conference Series, ed. H. Lewis & G. Raffi, 446–454
- Torres, G., Konacki, M., Sasselov, D. D., & Jha, S. 2004, *ApJ*, 609, 1071
- Udalski, A., Paczynski, B., Zebrun, K., Szymanski, M., Kubiak, M., Soszynski, I., Szewczyk, O., Wyrzykowski, L., & Pietrzynski, G. 2002a, *Acta Astronomica*, 52, 1
- Udalski, A., Pietrzynski, G., Szymanski, M., Kubiak, M., Zebrun, K., Soszynski, I., Szewczyk, O., & Wyrzykowski, L. 2003, *Acta Astronomica*, 53, 133

- Udalski, A., Szewczyk, O., Zebrun, K., Pietrzynski, G., Szymanski, M., Kubiak, M., Soszynski, I., & Wyrzykowski, L. 2002b, *Acta Astronomica*, 52, 317
- Udalski, A., Zebrun, K., Szymanski, M., Kubiak, M., Soszynski, I., Szewczyk, O., Wyrzykowski, L., & Pietrzynski, G. 2002c, *Acta Astronomica*, 52, 115
- van de Kamp, P. 1963, *AJ*, 68, 295
- Vereš, P., Budaj, J., Világi, J., Galád, A., & Kornoš, L. 2009, *Contributions of the Astronomical Observatory Skalnaté Pleso*, 39, 34
- Winn, J. N., Holman, M. J., & Fuentes, C. I. 2007, *AJ*, 133, 11
- Winn, J. N., Howard, A. W., Johnson, J. A., Marcy, G. W., Gazak, J. Z., Starkey, D., Ford, E. B., Colón, K. D., Reyes, F., Nortmann, L., Dreizler, S., Odewahn, S., Welsh, W. F., Kadakia, S., Vanderbei, R. J., Adams, E. R., Lockhart, M., Crossfield, I. J., Valenti, J. A., Dantowitz, R., & Carter, J. A. 2009a, *ApJ*, 703, 2091
- Winn, J. N., Johnson, J. A., Albrecht, S., Howard, A. W., Marcy, G. W., Crossfield, I. J., & Holman, M. J. 2009b, *ApJ*, 703, L99
- Wolszczan, A. 1994, *Science*, 264, 538
- Wolszczan, A. & Frail, D. A. 1992, *Nature*, 355, 145
- Wolter, U., Schmitt, J. H. M. M., Huber, K. F., Czesla, S., Müller, H. M., Guenther, E. W., & Hatzes, A. P. 2009, *A&A*, 504, 561
- Xie, J. & Zhou, J. 2009, *ApJ*, 698, 2066
- Yamamoto, K., Matsuo, T., McElwain, M., Tamura, M., Morishita, H., Nakashima, A., Shibai, H., Fukagawa, M., Kato, E., Kanoh, T., Itoh, Y., Kaneko, Y., Shimoura, M., Itoh, Y., Funayama, H., & Hashiguchi, T. 2009, in *American Institute of Physics Conference Series*, Vol. 1158, American Institute of Physics Conference Series, ed. T. Usuda, M. Tamura, & M. Ishii, 273–274
- Zapolsky, H. S. & Salpeter, E. E. 1969, *ApJ*, 158, 809